

APPLICATIONS OF A NEW THEORY EXTENDING CONTINUUM
MECHANICS TO THE NANOSCALE

A Dissertation

by

KAIBIN FU

Submitted to the Office of Graduate Studies of
Texas A&M University
in partial fulfillment of the requirements for the degree of

DOCTOR OF PHILOSOPHY

August 2005

Major Subject: Aerospace Engineering

APPLICATIONS OF A NEW THEORY EXTENDING CONTINUUM
MECHANICS TO THE NANOSCALE

A Dissertation

by

KAIBIN FU

Submitted to the Office of Graduate Studies of
Texas A&M University
in partial fulfillment of the requirements for the degree of

DOCTOR OF PHILOSOPHY

Approved by:

Chair of Committee,	John C. Slattery
Committee Members,	Malcolm Andrews
	Dimitris C. Lagoudas
	Jay R. Walton
Head of Department,	Helen L. Reed

August 2005

Major Subject: Aerospace Engineering

ABSTRACT

Applications of a New Theory Extending Continuum Mechanics to the Nanoscale.

(August 2005)

Kaibin Fu, B.En., Tsinghua University;

B.A., Tsinghua University

Chair of Advisory Committee: Dr. John C. Slattery

In this dissertation, we present the Slattery-Oh-Fu theory extending continuum mechanics to the nanoscale and its applications.

We begin with an analysis of supercritical adsorption of argon, krypton, and methane on Graphon before we fully develop the theory. We compare our results both with existing experimental data and with prior molecular-based theories.

Then, we present the general theory, which is based upon a long history of important developments beginning with Hamaker (1937). In the context of continuum mechanics, nanoscale problems always involve the immediate neighborhood of a phase interface or the immediate neighborhood of a three-phase line of contact or common line. We test this theory by using it to predict both the surface tensions of the n-alkanes and the static contact angles for the n-alkanes on PTFE and for several liquids on PDMS. For the contact angle predictions, the results are compatible with previously published experimental data. The results for the contact angle analysis also provide a successful test of a previously derived form of Young's equation for the true, rather than apparent, common line.

We also studied Mode I fracture at nanoscale. While we don't have experimental data to compare, we get reasonable crack configuration and avoid stress singularity at the crack tip. Coalescence problems are revisited to explore the retardation effects in

the computation of intermolecular forces. We get good agreement with experimental results.

We conclude with a confidence that this theory can be used as a bridge between continuum mechanics and other molecular-based methods.

To my parents and my wife Jihong

ACKNOWLEDGMENTS

I would like to show my gratitude to my advisor, Professor John C. Slattery, for his support, guidance and constant encouragement during these years of my studies. He has been acting like a father for a foreign student. Under his guidance, I have learned not only his professional knowledge in transport phenomena and continuum mechanics but also the integrity of being a researcher.

I would like to thank Professor Jay Walton for many insightful discussions on my research and Professors Dimitris Lagoudas and Malcolm Andrews for serving on my committee. Without their help, my work could not be completed. Also, Eun-Suok Oh, Xiuhua Si, Kuang-Yao Peng, Yongzhe Tian gave me lots of help through the years.

Especially, I need to give thanks to my parents and my wife for their love and patience. My wife Jihong has been a student's wife without any complaints for years. She has been bearing my difficulties and burden in all aspects.

Finally, I thank my Lord, Jesus Christ, who helps me to overcome all my frustrations. He gives me hope, faith, love and compassion.

TABLE OF CONTENTS

CHAPTER		Page
I	INTRODUCTION AND RESEARCH BACKGROUND	1
	A. Continuum mechanics	1
	B. The history of intermolecular forces	3
	C. Nanoscale science and engineering	4
	D. Nanomechanics	5
II	AN ANALYSIS OF SUPERCRITICAL ADSORPTION IN THE CONTEXT OF CONTINUUM MECHANICS	9
	A. Introduction	9
	B. Corrections for intermolecular forces	11
	1. Estimating the two-point potential	14
	2. Estimating $\mathbf{b}^{(f,corr)}$	15
	C. Density distribution	16
	D. Comparison with experimental data	17
	E. Comparison with previous theories	19
	F. Discussion	23
III	GENERALIZED THEORY AND APPLICATION ON CON- TACT ANGLE	27
	A. Introduction	27
	B. The correction	30
	C. One dividing surface	35
	1. One dividing surface: with interfacial energy or tension	36
	a. Computation of surface tensions	38
	D. One thin film	41
	1. One thin film: with interfacial energy or tension in both interfaces	43
	a. Parallel plane interfaces	45
	2. A discontinuous thin film	47
	E. One thin lens or fracture	47
	1. One thin lens or fracture, phase C is a vacuum	48
	2. One thin lens or fracture, phase C is a vacuum: with interfacial energy or tension	49

CHAPTER	Page
F. Application on static contact angle	50
1. Problem statement	51
2. Correction for long-range intermolecular forces	52
3. Solving procedure	53
4. Prediction of $\Theta^{(\text{stat})}$	57
5. Young's equation	59
IV THE APPLICATION ON A MODE I NANOSCALE FRACTURE PROBLEM	61
A. Introduction	61
B. A modified version of the theory	63
C. Problem statement	66
D. Solution	70
1. Singular perturbation method	71
a. Outer solution	72
b. Inner solution	73
E. Discussion	78
V DISCUSSION OF RETARDED DISPERSION FORCES AND ITS APPLICATION TO THE COALESCENCE PROBLEM	80
A. Retarded dispersion forces	80
B. A review of coalescence	82
C. Coalescence time	87
D. Comparison with experimental results	99
E. Discussion	100
VI CONCLUSION	102
NOTATION	104
REFERENCES	108
VITA	124

LIST OF TABLES

TABLE		Page
I	Comparisons of calculated and measured values of surface tensions for n-alkanes.	40
II	Comparison of calculation and experimental data of static contact angle $\Theta^{(stat)}$ for n-Alkanes on PTFE.	58
III	Comparison of calculation and experimental data of static contact angle $\Theta^{(stat)}$ for dispersive liquids on PDMS.	60
IV	Experimental results for three different sizes of the bubble.	100
V	Computational results from Equation (5.60).	100

LIST OF FIGURES

FIGURE	Page
1	A material body consisting of two adjoining phases, <i>A</i> and <i>B</i> 13
2	Two semi-infinite phases <i>A</i> and <i>B</i> separated by a phase interface or dividing surface. 14
3	Γ^σ (μ mol/m ²) as a function of <i>P</i> (MPa) for argon on Graphon at 0°C predicted by (2.11) (the solid curve). The experimental observations are from Specovius and Findenegg (1978). The dashed-dot curve represents the computations of Sokolowski (1982). 19
4	Γ^σ (μ mol/m ²) as a function of <i>P</i> (MPa) for argon on Graphon at 25°C predicted by (2.11) (the solid curve). The experimental observations are from Specovius and Findenegg (1978). 20
5	Γ^σ (μ mol/m ²) as a function of <i>P</i> (MPa) for argon on Graphon at 50°C predicted by (2.11) (the solid curve). The experimental observations are from Specovius and Findenegg (1978). The dashed-dot curve represents the computations of Fischer (1978). 20
6	Γ^σ (μ mol/m ²) as a function of <i>c</i> (mol L ⁻¹) for argon on Graphon at 25°C predicted by (2.11) (the solid curve). The experimental observations are from Specovius and Findenegg (1978). The dashed line represents the computations of Egorov (2001). 21
7	Γ^σ (μ mol/m ²) as a function of <i>P</i> (MPa) for krypton on Graphon at 25°C and at 100°C predicted by (2.11) (the solid curves). The experimental observations are from Blumel et al. (1982). The dashed-dot curve represents the computations of Rangarajan et al. (1995) for 25°C; the dashed curve for 100°C. 21
8	Γ^σ (μ mol/m ²) as a function of <i>P</i> (MPa) for krypton on Graphon at 50°C predicted by (2.11) (the solid curves). The experimental observations are from Blumel et al. (1982). The dashed-dot curve represents the computations of Rangarajan et al. (1995). 22

FIGURE	Page
9	Γ^σ (μ mol/m ²) as a function of P (MPa) for krypton on Graphon at 0°C and at 75°C predicted by (2.11) (the solid curves). The experimental observations are from Blumel et al. (1982). The dashed-dot curve represents the computations of Rangarajan et al. (1995) for 0°C; the dashed curve for 75°C. 22
10	Γ^σ (μ mol/m ²) as a function of c (mol L ⁻¹) for krypton on Graphon at 25°C predicted by (2.11) (the solid curves). The experimental observations are from Blumel et al. (1982). The dashed curve represents the computations of Egorov (2001). 23
11	Γ^σ (μ mol/m ²) as a function of P (MPa) for methane on Graphon at 0°C and at 50°C predicted by (2.11) (the solid curves). The experimental observations are from Specovius and Findenegg (1978). The dashed curve represents the computations of Sokolowski (1982) for 0°C; the dashed-dot curve for 50°C. 24
12	Γ^σ (μ mol/m ²) as a function of P (MPa) for methane on Graphon at 25°C predicted by (2.11) (the solid curves). The experimental observations are from Specovius and Findenegg (1978). The dashed curve represents the computations of Sokolowski (1982). . . . 24
13	A material body consisting of two adjoining phases, A and B 32
14	For simplicity, the dividing surfaces and the two singular surfaces for each interface are shown as a single curve. Two cases are illustrated. (a) Two semi-infinite phases A and B . (b) Two semi-infinite phases A and B separated by a thin film of phase C 34
15	A thin discontinuous film C forms a common line. 42
16	A thin film bounded by two parallel, plane interfaces. 45
17	A thin lens (or fracture) of phase C in phase A 48
18	A thin discontinuous film C forms a common line. 52
19	Schematic of Mode I fracture of phase C in phase A 67

FIGURE	Page	
20	<p>δ is the distance separating the two phases A and C, corresponding physically to the sum of the effective radii of the A and C molecules or the effective distance between molecules of A and C (Slattery et al., 2004, p. 4623). The dividing surface $h(x)$ is located halfway between the two phases.</p>	69
21	<p>Dimensionless crack configurations h^* (the solid curve) for $\delta^* = 0.02$ and $\delta^{**} = 2.50$. Here we have used $E = 100$ GPa, $\delta = 0.2$ nm (Israelachvili, 1973, 1991; Slattery et al., 2004), $a = 10$ nm, and $\mathcal{A} = 2\pi \times 10^{-20}$ J (Hough and White, 1980; Israelachvili, 1991; Slattery et al., 2004). The dash lines represent results from classical linear elastic fracture mechanics.</p>	76
22	<p>Dimensionless stress distribution T_{22}^* on the fracture axis for $\delta^* = 0.02$ and $\delta^{**} = 2.50$. Here we have used $E = 100$ GPa, $\delta = 0.2$ nm (Israelachvili, 1973, 1991; Slattery et al., 2004), $a = 10$ nm, and $\mathcal{A} = 2\pi \times 10^{-20}$ J (Hough and White, 1980; Israelachvili, 1991; Slattery et al., 2004);</p>	77
23	<p>A symmetric bubble (phase D) moves through a liquid (phase C) as it approaches a fluid–fluid interface (between phases C and B). The configuration of the bubble–fluid interface is given by $z = h_2(r, t)$; that of the fluid–gas interface by $z = h_1(r, t)$</p>	87
24	<p>Dependence of t_c^* on B^*</p>	98

CHAPTER I

INTRODUCTION AND RESEARCH BACKGROUND

A. Continuum mechanics

Mechanics is one of the most important areas in natural science. I will not spend too much time discussing the evolution of mechanics, simply because there are too many stories involving big names such as Archimedes, Kepler, Galileo, Huygens, da Vinci, Hooke, Newton, Bernoulli, Euler, D'Alembert, Lagrange, Fourier, Poisson, Cauchy, Taylor, MacLaurin, Clairaut, Navier, Green, Saint-Venant, Stokes, Kelvin, Helmholtz, Kirchhoff, Maxwell, Gibbs. Instead we will only mention the fundamental principles as Euler described:

- The total force acting upon the body equals the rate of change of the total momentum.
- The total torque acting upon the body equals the rate of change of the total moment of momentum, where both the torque and the moment are taken with respect to the same fixed point.

These principles are developed along Newton's Law. As used in almost every mechanics problem, we also use these principles in our analysis. We recommend these three books for the reader who has interest in the history of mechanics. (Timoshenko, 1953; Dugas, 1955; Truesdell, 1968)

In reality, matter is formed of separate molecules or atoms. Yet, people didn't realize the micro details of matter in the early years of science. When Newton, Euler or other people used mathematical tools to solve mechanics problems, they treated

This dissertation follows the style and format of Chemical Engineering Science.

every matter as a continuous body. We could state the assumptions of those important mechanics theories before 1900 in today's terminology: describing relationships between gross phenomena, neglecting the structure of material on a smaller scale. For example, the theory of elasticity is based upon this understanding. (Love, 1944)

The foundations of the continuum theory are matured in 1960s (Truesdell, 1966). The continuum theory regards matter as indefinitely divisible so that we can define stress and strain at each point. The theory is justified in many macro scale circumstances and it is used widely in today's engineering field. The subjects of continuum mechanics are simple:

- General principles applicable to all continuous media
- Constitutive equations defining the particular idealized material

We will not repeat the historical information and details here, but recommend further readings. (Truesdell and Toupin, 1960; Truesdell and Noll, 1965; Truesdell, 1966; Eringen, 1967)

While continuum mechanics is largely successful applying to macro scale bodies, it encounters tremendous difficulties dealing with tiny bodies, especially involving the interfacial surfaces. We can either use the continuum theory in combination with empirical information or with information derived from a physical theory based on the molecular structure of the matter. Quantum theory tells us the importance of two types of interaction between elementary particles: long-range and short-range. In chemistry and biology, the emphasis is placed on the short-range force fields around atoms and molecules. In mechanics, the emphasis is placed on the long-range forces which are given several names for different situations. In this work, we call it long-range intermolecular forces.

B. The history of intermolecular forces

Intermolecular forces has been a very important subject in science and engineering for a long time. It plays a key role in various phenomena: adhesion, adsorption, surface tension, wetting, densification and so on. The simplest question involving intermolecular forces will be “why two bodies attract or repulse each other when they are getting close”

More than 300 years ago, Isaac Newton showed some interest on the strong attractions between two bodies. (Rowlinson, 2002) When Laplace solved the capillarity problem, he is the first one to calculate the attractive force between a spherical liquid drop and a thin vertical ‘canal’ of liquid outside it. Van der Waals’ milestone doctoral thesis “On the continuity of gases and liquids” in 1873 and his later work brought a breakthrough to phenomena involving interfacial surfaces. In his well-known equation of state for gases and liquids, he took account for the attractive intermolecular forces which are known as Van der Waals forces. In the early years of 20th century, quantum mechanics has changed the way scientists think about materials in atomic level and high speed. But for those objects which are much larger than atomic scale and much slower than the speed of light, classical mechanics still does an excellent job. And also, classical mechanics can use results of quantum and statistical mechanics. After we know the forces as a function of intermolecular separation and orientation, we can use this information in a purely classical way to calculate the properties of materials. This is the reason of proposing a new theory of intermolecular force correction and seek its application.

There are many researchers working in the field of intermolecular forces. Here I will only present those work which are mostly related to my research. Lennard-Jones and Dent (1928) proposed an intermolecular potential energy function for non-

polar molecules in 1928. Steele (1973) computed the energy of a single gas atom interacting with a solid phase based on Lennard-Jones potential in 1973. Hamaker (1937) calculate attractive London-Van der Waals forces between macrobodies by using pairwise summation of intermolecular forces in 1937. Lifshitz (1956) developed a macroscopic theory for the interaction of bodies which is considered to come through the medium of fluctuating electromagnetic field in 1956. Hough and White (1980) calculated Hamaker constant based on Lifshitz theory in 1980. Readers can find more review and detail in the books by Hirschfelder et al. (1954) and Israelachvili (1991).

Material behavior is different in the interfacial region. When two different materials are put together, the behaviors of the two materials change as the dividing surface is approached. We will focus on the changes within three-dimensional interfacial region and propose to incorporate the effect of intermolecular forces from adjacent phases as a body force in the standard developments of continuum mechanics. In contrast with the developments of Hamaker and Lifshitz, our focus is the body force at a point in a continuum rather than the force between two macroscopic bodies. However, we will use their ideas in this work, using pairwise additivity of intermolecular forces and an effective, Lifshitz type, Hamaker constant.

C. Nanoscale science and engineering

Nanoscale science and engineering activities are flourishing in the U.S. since 1997. It gives us the ability to understand and manipulate things at the level of single molecules and clusters of molecules. We realize that we could build a bright future from tiny things. According to the National Nanotechnology Initiative, nanotechnology includes three elements (Roco et al., 2000)

- Exploiting the new phenomena and processes at the intermediate length scale

between single atom or molecule and about 100 molecular diameters, in the range of about 1 to 100 nanometers. ($1nm = 10^{-9}m$)

- With the same principles and tools to establish a unifying platform for science and engineering at the nanoscale.
- Using the atomic and molecular interactions to develop efficient manufacturing methods.

There are several reasons for the interest in nanotechnology. First, it holds the promise of radically new applications and more precise products. Many advanced materials and manufacturing process for industry, new devices and medicines for human health care are on the way.

Second, it helps us fill a major gap in our fundamental knowledge of matter. We already know many details at the molecular scale with quantum physics and chemistry. In the other end, classical physics and chemistry, biology and engineering have taught us about the bulk behavior of materials and systems. Yet, we have known much less about the intermediate nanoscale, where all living systems and man-made systems work. Based upon scientific knowledge, there are two major strategies to attack nanoscale problems: Bottom-up which starts from molecular scale and Top-down which starts from macroscale or microscale.

Finally and most important, it ignites the interdisciplinary research and educational opportunities. We have already seen the coalition of academe, industry and government to seek the full potential of this new technology.

D. Nanomechanics

Understanding the mechanics of nanomaterials is crucial. Many traditional methods used for testing of mechanical behavior of materials are only applicable to nanomateri-

als in some cases. So new experimental methods are introduced. Among them, atomic force microscopy, scanning tunneling microscopy and instrumented nanoindentation are most important techniques.

Atomic force microscope (AFM) uses a ceramic or semiconductor tip one atom wide positioned at the end of a cantilevered bar. As the tip is moved over the material, it either continuously touches or periodically taps the surface and bends as it is repelled or attracted to the structure. A laser picks up the deflections. Scanning tunneling microscope (STM) uses a piezoelectric tube with a tiny sharp tip at the end that is moved within nanometers of the object being sampled. As the tip is moved and bumps into an obstruction, the “tunneling” current changes. In order to maintain a certain constant current, the tip is raised and lowered accordingly, and this movement pattern is magnified and displayed on screen.

Both AFM and STM can be used to get detailed images of nanomaterials and determine the mechanical properties of the investigated surface. For example, AFM was used to measure the Young’s modulus of a carbon nanotube by first positioning it in a proper suspended configuration and then by bending the tube with a fixed force and measuring the tube deflection. (Salvetat et al., 1999)

While indentation is a traditional method, the idea of ultra low-load indentation was first proposed by Pethica et al. (1983). Researchers found its important application in the case of studying nanomaterials and call it nanoindentation. Nanoindentation has been used to determine elastic modulus, hardness, stress relaxation and more. The interpretation of nanoindentation experiments is also complicated.

Various modelling methods have been used for materials at nanoscale: atomistic simulation, molecular dynamics, Monte Carlo method, dislocation dynamics, statistical mechanics, continuum mechanics.

The combination of finite element method and molecular dynamics is widely used.

(Smith et al., 2001) The atomistic simulation provides better insight into atomistic processes yet sometimes is not accurate on the size of the simulated cluster. (Miller and Shenoy, 2000; Astala et al., 2000)

We should not be surprised with doubts on the possibility of solving nanoscale problems with continuum mechanics because their scales fall far beyond the frames of continuum mechanics. The confidence comes from the incorporation of many-body intermolecular potentials which is based upon quantum mechanics.

The analysis of supercritical adsorption of argon, krypton, and methane on Graphon is the first successful application before we fully develop the theory. We compare the results both with existing experimental data and with prior molecular-based theories. The conclusion is that our computation is superior. We have made more progress on the theory, but what I present in Chapter II is in its original article form. I want to show as much as possible of the evolution of our development in this dissertation.

In Chapter III, we present the entire theory which is based upon a long history of important developments beginning with Hamaker (1937). This work is taken out from Slattery et al. (2004). We also present another application in this chapter predicting the static contact angle for the n -alkanes on PTFE (polytetrafluoroethylene) and for several liquids on PDMS (polydimethylsiloxane). It successfully matches published experimental data.

In Chapter V, we study Mode I fracture at nanoscale. While we don't have experimental data to compare, we get reasonable crack configuration and avoid stress singularity at the crack tip.

In Chapter VI, we review the literature on retarded intermolecular forces and incorporate retarded intermolecular forces into the analysis of coalescence between air and hexadecane. We compare the computational results with experiments.

With several successful applications, we could visualize more efforts and prospects in the future.

CHAPTER II

AN ANALYSIS OF SUPERCRITICAL ADSORPTION IN THE CONTEXT OF
CONTINUUM MECHANICS

A. Introduction

Far from a solid-fluid interface on a molecular scale, the density of a gas, either subcritical or supercritical, approaches the bulk density. Within a few molecular diameters of the interface, the gas is subjected to intense attractive intermolecular forces attributable to the solid. The magnitudes of these forces increase as the distance to the interface decreases. With a subcritical gas or vapor, condensation occurs. With a supercritical fluid, the density increases as the interface is approached, becoming similar to that of a liquid. We will confine our attention here to the case of a supercritical fluid. We explore the “adsorption” or densification of three supercritical gases on Graphon: argon, krypton, and methane.

Specovius and Findenegg (1978) used a gravimetric method for the determination of surface excess isotherms of argon and methane on Graphon (a graphitized carbon black) for temperatures from -20°C to 50°C and pressures up to 150 bar. This corresponded to bulk densities up to the critical density for methane and more than half the critical density for argon. Blumel et al. (1982) did a similar study for krypton on Graphon but for temperatures up to 100°C .

Five analyses of these data starting from a molecular point of view have been published.

- Egorov (2001) presented a microscopic statistical mechanical theory of adsorption of supercritical fluids. The theory is in excellent agreement with experimental observations of Specovius and Findenegg (1978) and Blumel et al. (1982)

for argon and krypton, although the error increases at higher densities as the temperature approaches the critical temperature.

- Rangarajan et al. (1995) developed a mean-field model that superimposes the fluid-solid potential on a fluid equation of state to predict adsorption on a flat wall. Their paper shows some predicted adsorption isotherms for krypton but none for argon or methane.
- Sokolowski (1982) used the Percus-Yevick equation for the local density of a gas in contact with a flat solid surface to calculate the adsorption characteristics of argon and of methane on graphite. The calculations used the Boltzmann-averaged potential (Abraham and Singh, 1978), which is calculated from the particle-graphite basal-plane potential (Steele, 1973), for the gas-surface interaction and used the Lennard-Jones (12,6) potential for the gas-gas interactions.
- Fischer (1978) used a model for high temperature and high pressure adsorption that was the same as the one introduced in previous papers (Fischer, 1977; Findenegg and Fischer, 1975) for moderate pressures. He assumed that a hard sphere gas was in contact with a structureless plane wall and that a Lennard-Jones potential described the wall-particle interaction.
- Aranovich and Donohue (1996) used two adjustable parameters in comparing the Ono and Kondo (1960) theory to the data reported by Specovius and Findenegg (1978).

The first four of these analyses will be discussed further in Section E.

There have been a number of studies of supercritical adsorption on activated carbons, both theoretical and experimental (Gusev et al., 1997; Neimark and Ravikovitch, 1997; Miyawaki et al., 1998; Zhou et al., 2000; Murata and Kaneko, 2001; Cao et al.,

2002; Lozano-Castelló et al., 2002; Ohkubo et al., 2002). While activated carbons are of immense practical importance, they are not well-suited to test theories, because they are porous and the effects of intermolecular forces are more complex. For this reason, they will not be discussed here.

The purpose of this paper is to present the first and simplest application of a new extension of continuum mechanics to the nanoscale (not the molecular scale). Specifically, in the immediate neighborhood of phase interfaces, we introduce a body force representing a correction for intermolecular forces attributable to the adjoining phase.

Our intention here is not to find fault with prior analyses. Nor are we arguing that continuum mechanics is superior to a molecular point of view. To the extent that our approach may appear to have some advantages in describing experimental data, it must be kept in mind that we will be taking advantage of empirical equations of state for bulk behavior that the molecular-based theories do not use.

B. Corrections for intermolecular forces

Surface excess variables such as the surface mass density, surface velocity, surface stress tensor, . . . account for changes in the corresponding quantities in the adjoining phases within the immediate neighborhood of the dividing surface (Slattery, 1990, secs. 1.3.2 and 2.1.8). These changes occur, because the behaviors of the two materials change as the dividing surface is approached.

Why is material behavior different in the interfacial region? All descriptions of material behavior at some distance from the interface are based upon the assumption that the material extends to “infinity” (perhaps 100 nm) in all directions. Material points outside the immediate neighborhood of the interface are subjected to inter-

molecular forces only from one phase. Material points within the interfacial region are subjected to intermolecular forces from both phases.

Our premise is that material behavior within the interfacial region can be represented as bulk material behavior corrected for the intermolecular forces from the adjoining phase. In particular, we recognize the equivalence of stresses and body forces (Truesdell and Toupin, 1960, p. 549).

There are three descriptions of the interfacial region of a single interface (as opposed to a thin film), each view having its own somewhat different notation.

- a) Material behavior is a function of position within the interfacial region. No excess quantities are associated with any dividing surface. The problem with this view is that in general we will not know the appropriate descriptions of behavior in the interfacial regions.
- b) In the second view, we use the descriptions of material behavior appropriate outside the interfacial region (bulk material behavior). The effects of the interfacial region are taken into account by the excess quantities assigned to the corresponding dividing surface (Slattery, 1990, secs. 1.3.5 and 2.1.6).
- c) In the third view described in Figure 1, we again use the descriptions of material behavior appropriate outside the interfacial region (bulk material behavior), corrected for intermolecular forces from the adjoining phase as described below. No excess properties are assigned to the dividing surface.

In the context of view (c), the differential and jump mass balances as well as the jump momentum balance take the usual forms (Slattery, 1999, pp. 51 and 59). It is only the differential momentum balance that is changed, which for a static fluid becomes

$$-\nabla P^{(A)} + \mathbf{b}^{(A,corr)} = 0 \quad (2.1)$$

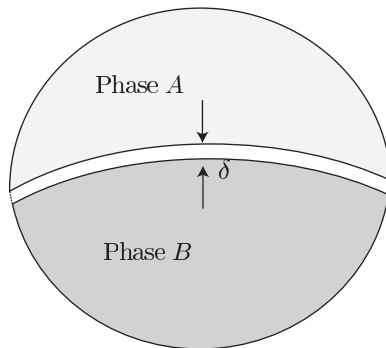


Fig. 1. A material body consisting of two adjoining phases, A and B .

Here P is thermodynamic pressure and $\mathbf{b}^{(corr)}$ is the body force per unit volume attributable to the adjoining phase. Here and in what follows, we will neglect the effects of gravity.

Referring to Figure 2, we reason that $\mathbf{b}^{(corr)}$ represents the force per unit volume that results from

- subtracting the force per unit volume at a point in phase A attributable to that portion of phase A that has been replaced by phase B , and
- adding the force per unit volume at this same point in phase A attributable to phase B .

In other words, for each point in the gas phase A

$$\mathbf{b}^{(A,corr)} \equiv - \int_{R^{(B)}} \mathbf{f}^{(A,A)} dV + \int_{R^{(B)}} \mathbf{f}^{(A,B)} dV \quad (2.2)$$

Here $R^{(B)}$ is the region occupied by phase B , $\mathbf{f}^{(A,B)}(\mathbf{r}^{(A)}, \mathbf{r}^{(B)})$ is the force per unit volume of phase A per unit volume of phase B at a point $\mathbf{r}^{(A)}$ in phase A attributable to the material at point $\mathbf{r}^{(B)}$ in phase B , and dV indicates that a volume integration is to be performed.

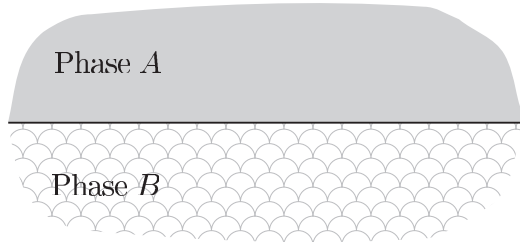


Fig. 2. Two semi-infinite phases A and B separated by a phase interface or dividing surface.

In reality, the effective replacement region $R^{(B)}$ may be no more than 100 nm thick, since outside this region the intermolecular forces between phases A and B go to zero.

1. Estimating the two-point potential

The Lennard-Jones (6-12) potential is commonly recommended for non-polar dilute gases (Hirschfelder et al., 1954, p. 22)

$$\phi^{(A,B)} = 4\epsilon^{(A,B)} \left[\left(\frac{\sigma^{(A,B)}}{r} \right)^{12} - \left(\frac{\sigma^{(A,B)}}{r} \right)^6 \right] \quad (2.3)$$

Here $\phi^{(A,B)}$ is the potential energy for two molecules A and B separated by a distance r ; the parameters $\sigma^{(A,B)}$, $\epsilon^{(A,B)}$ represent the collision diameter and depth of the energy well. The r^{-6} term describes attractive forces: the dispersion forces (London forces or induced-dipole–induced dipole forces) (Israelachvili, 1991, p. 83). The r^{-12} contribution represents short-range repulsive forces. The corresponding expression for $\mathbf{f}^{(A,B)}$ is

$$\mathbf{f}^{(AB)} = -\nabla (n^{(A)}n^{(B)}\phi^{(A,B)}) \quad (2.4)$$

where $n^{(A)}$ and $n^{(B)}$ are the number densities at the specified points in phases A and B . For a gas, intermolecular forces attributable to a Lennard-Jones potential are

pairwise additive (Hirschfelder et al., 1954, p. 148).

2. Estimating $\mathbf{b}^{(f,corr)}$

In the following section, we will use (2.3) to find the density distribution in a supercritical fluid f within the immediate neighborhood of a crystalline solid s . We will find shortly that we will require $\mathbf{b}^{(f,corr)}$, the correction for intermolecular forces at any point in the supercritical fluid attributable to the presence of the crystalline solid.

From (2.2) and (2.4), at each point in the gas or fluid phase

$$\begin{aligned} \mathbf{b}^{(f,corr)} &= n^{(f)} \left[- \int_{R^{(s)}} \nabla (n^{(s)} \phi^{(f,s)}) dV + \int_{R^{(s)}} \nabla (n^{(f,bulk)} \phi^{(f,f)}) dV \right] \\ &= -n^{(f)} \left[\nabla \int_{R^{(s)}} n^{(s)} \phi^{(f,s)} dV - \nabla \int_{R^{(s)}} n^{(f,bulk)} \phi^{(f,f)} dV \right] \\ &= -n^{(f)} \nabla \Phi^{(f,corr)} \end{aligned} \quad (2.5)$$

Here

$$\Phi^{(f,corr)} \equiv \int_{R^{(s)}} n^{(s)} \phi^{(f,s)} dV - \int_{R^{(s)}} n^{(f,bulk)} \phi^{(f,f)} dV \quad (2.6)$$

and $n^{(f,bulk)}$ is the number density in the fluid that would exist, if the solid were not present.

In discussing the intermolecular forces between a gas and a crystalline solid such as graphite, Steele (1973, 1974, 1978) assumed that the Lennard-Jones potential was also applicable. He recognized that pairwise additivity of intermolecular forces could be expected to be in error, but he argued that he “at least partially by-passed this problem by using semi-empirical pair-wise potentials that are reasonably closely related to the bulk properties” of the crystalline solid (Steele, 1974, p. 52). For this reason, he assumed that the crystalline solid was not continuously distributed in space, but instead discretely distributed in a layered lattice, each layer being laterally

continuous. As a result, Steele (1974, 1978) computed

$$\int_{R^{(s)}} n^{(s)} \phi^{(f,s)} dV = \frac{2\pi n_c \sigma^{(f,s)^2} \epsilon^{(f,s)}}{a_c} \left\{ \frac{2}{5} \left[\left(\frac{\sigma^{(f,s)}}{z} \right)^{10} + \frac{\sigma^{(f,s)^{10}}}{9\Delta(z + 0.72\Delta)^9} \right] - \left(\frac{\sigma^{(f,s)}}{z} \right)^4 - \frac{\sigma^{(f,s)^4}}{3\Delta(z + 0.61\Delta)^3} \right\} \quad (2.7)$$

Here z is the coordinate measured into the fluid f , perpendicular to the lattice planes (and therefore perpendicular to the surface) of the solid s ; $z = 0$ can be interpreted either as the surface of the solid or as the center of the atoms in the first lattice plane. The Lennard-Jones parameters $\epsilon^{(f,s)}$ and $\sigma^{(f,s)}$ between fluid and solid are taken from Steele (1974, p. 56), n_c is the number of atoms in the unit surface cell, Δ is the distance between lattice planes, a_c is the area of the unit cell in the lattice plane. The number density for the solid $n^{(s)} = n_c / (a_c \Delta)$. We will use the values of $n^{(s)}$ and Δ given by Tan and Gubbins (1990). To our knowledge, Steele's argument justifying the use of additivity has never been tested. We will say more about this in Section D.

Similarly, we find

$$\int_{R^{(s)}} n^{(f,bulk)} \phi^{(f,f)} dV = -\frac{4\pi n^{(f,bulk)} \epsilon^{(f,f)} (\sigma^{(f,f)})^{12}}{45z^9} + \frac{4\pi n^{(f,bulk)} \epsilon^{(f,f)} (\sigma^{(f,f)})^6}{6z^3} \quad (2.8)$$

in which $n^{(f,bulk)}$ is the number density of the fluid that would be observed in the absence of the solid; $\epsilon^{(f,f)}$ and $\sigma^{(f,f)}$ are the Lennard-Jones parameters for the fluid given by Bird et al. (2002, p. 864).

C. Density distribution

In one dimension, (2.1) becomes with the help of (2.5) and the chain rule

$$\frac{1}{c^{(f)}} \left(\frac{dP^{(f)}}{dc^{(f)}} \right)_T \frac{dc^{(f)}}{dz} + N \frac{d\Phi^{(f,corr)}}{dz} = 0 \quad (2.9)$$

Here $(dP^{(f)}/dc^{(f)})_T$ will be evaluated using an empirical equations of state for argon (Michels et al., 1949), for krypton (Trappeniers et al., 1966), and for methane (Trappeniers et al., 1979, 1980); N is Avogadro's number; $c^{(f)} = n^{(f)}/N$ is the molar density in the interfacial region. The solution of this differential equation with the boundary condition

$$\text{as } z \rightarrow \infty : c^{(f)} \rightarrow c^{(f,bulk)} \quad (2.10)$$

gives a density distribution.

The surface excess or the apparent adsorption

$$\Gamma^{(\sigma)} \equiv \int_{\delta}^{\infty} (c^{(f)} - c^{(f,bulk)}) dz \quad (2.11)$$

Since δ is not a known parameter, it must be defined. From (2.6) and (2.9), there are two values of z at which $\Phi^{(f,corr)} = 0$ and $c^{(f)} = c^{(f,bulk)}$. One is as $z \rightarrow \infty$; the other we will define to be $z = \delta$. The graphite is assumed to be impermeable to the fluid.

D. Comparison with experimental data

Before comparing (2.11) with experimental data, let us consider the sources of experimental error. For graphitized carbon blacks, the uncertainty in the measured surface area is approximately 10% (Specovius and Findenegg, 1978; Steele, 1974), which translates to 10% uncertainty in the surface excess mass. Specovius and Findenegg (1978) and Blumel et al. (1982) found that the maximum relative error in their buoyancy correction to be 3% and 4% respectively, the values of which could be expected to increase as the critical point was approached. Other errors such as base-line drift were reported to be $< 1\%$. Precluding any random or systematic error, the uncertainty of the results should be less than 15%.

In the comparisons of (2.11) with experimental data in Figures 3 through 12,

we would like to emphasize that no adjustable parameters have been used. Equation (2.11) describes these data within the uncertainty range for argon and krypton as well as for methane at 50°C.

It is clear that, for both the krypton and for the methane, (2.11) underestimates the data, the error becoming progressively larger as the temperature decreases. There are at least two possible explanations.

As noted earlier in Section 2, Steele (1974, p. 52) expressed some doubt about the assumption of additivity of intermolecular forces in using his semi-empirical extension of the Lennard-Jones potential to the interactions between a crystalline solid and a gas. He proposed that this problem could be at least partially avoided by using a more realistic description of the solid. For this reason, he described the solid as being discretely rather than continuously distributed in space. While this proposal has not been previously tested experimentally to our knowledge, we believe that the excellent agreement between the predictions of our theory and the experimental observations for argon does support the use of pairwise additivity, at least when temperature is sufficiently above the critical temperature T_c . Notice that for argon $T_c = 150.8$ K. For krypton, $T_c = 209.4$ K, and we have excellent agreement between our predictions and the experimental observations at 100°C, but errors increase as the temperature decreases, the density increases, and the interference of neighboring of krypton increases. In summary, we believe that pairwise additivity can be used as suggested by Steele (1974, p. 52), so long as the temperature is sufficiently above the critical temperature.

The poor agreement between our predictions and the experimental observations for methane is due in part to the same failure of pairwise additivity as the critical temperature $T_c = 190.4$ K is approached. But the errors are larger than those seen with krypton, which has a higher T_c . We do see the errors decrease as the temperature

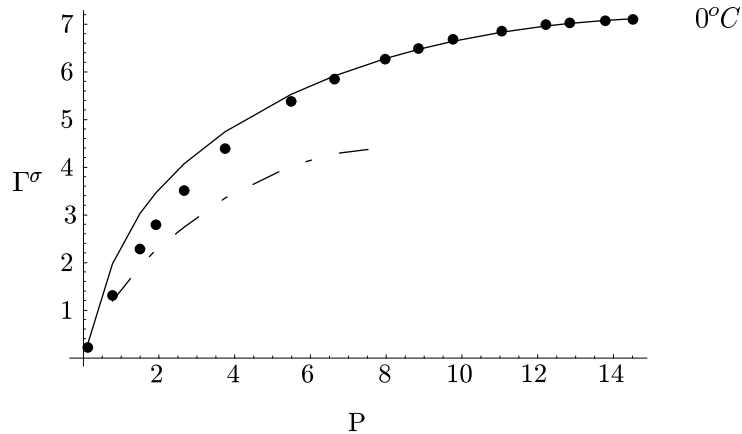


Fig. 3. Γ^σ ($\mu\text{ mol/m}^2$) as a function of P (MPa) for argon on Graphon at 0°C predicted by (2.11) (the solid curve). The experimental observations are from Specovius and Findenegg (1978). The dashed-dot curve represents the computations of Sokolowski (1982).

is raised, but we don't have measurements at high temperatures. However, we are also concerned that the Lennard-Jones potential may not be appropriate, particularly in denser fluids, because the methane molecule is not spherical.

E. Comparison with previous theories

As mentioned in the introduction, there are four analysis based upon statistical mechanics which have been compared with these same data: Egorov (2001), Rangarajan et al. (1995), Sokolowski (1982), and Fischer (1978). In all cases, we have used their results from their figures without repeating their computations.

Figure 6 compares the computations of Egorov (2001) with (2.11) for the argon data of Specovius and Findenegg (1978) at 25°C ; figure 10 compares the two theories for the krypton data of Blumel et al. (1982). The computations of Egorov (2001) are excellent, although, as he notes, they begin to fail at higher densities. Unfortunately, he did not report computations for higher temperatures.

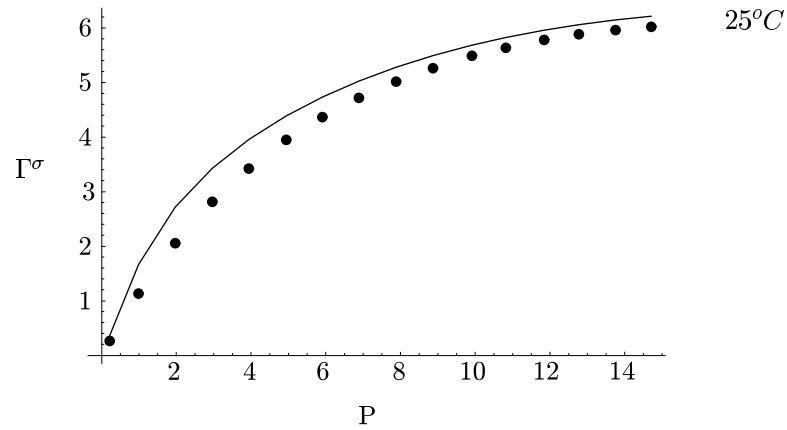


Fig. 4. Γ^σ ($\mu\text{ mol/m}^2$) as a function of P (MPa) for argon on Graphon at 25°C predicted by (2.11) (the solid curve). The experimental observations are from Specovius and Findenegg (1978).

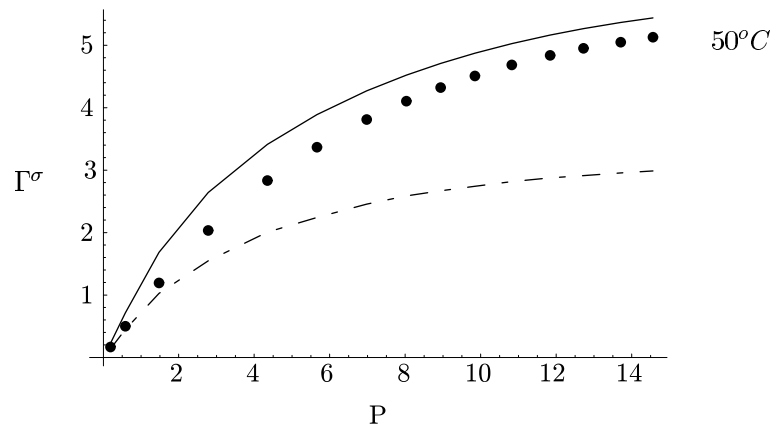


Fig. 5. Γ^σ ($\mu\text{ mol/m}^2$) as a function of P (MPa) for argon on Graphon at 50°C predicted by (2.11) (the solid curve). The experimental observations are from Specovius and Findenegg (1978). The dashed-dot curve represents the computations of Fischer (1978).

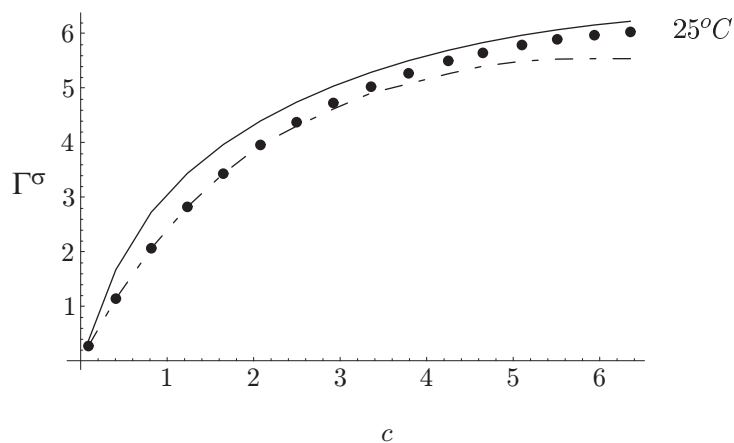


Fig. 6. Γ^σ ($\mu \text{ mol/m}^2$) as a function of c (mol L^{-1}) for argon on Graphon at 25°C predicted by (2.11) (the solid curve). The experimental observations are from Specovius and Findenegg (1978). The dashed line represents the computations of Egorov (2001).

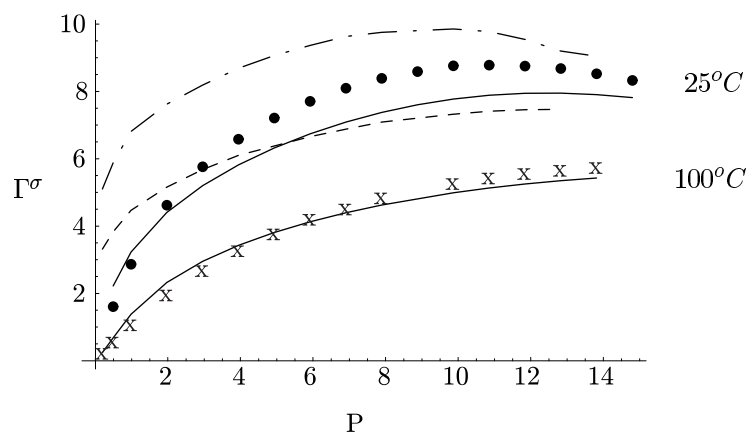


Fig. 7. Γ^σ ($\mu \text{ mol/m}^2$) as a function of P (MPa) for krypton on Graphon at 25°C and at 100°C predicted by (2.11) (the solid curves). The experimental observations are from Blumel et al. (1982). The dashed-dot curve represents the computations of Rangarajan et al. (1995) for 25°C ; the dashed curve for 100°C .

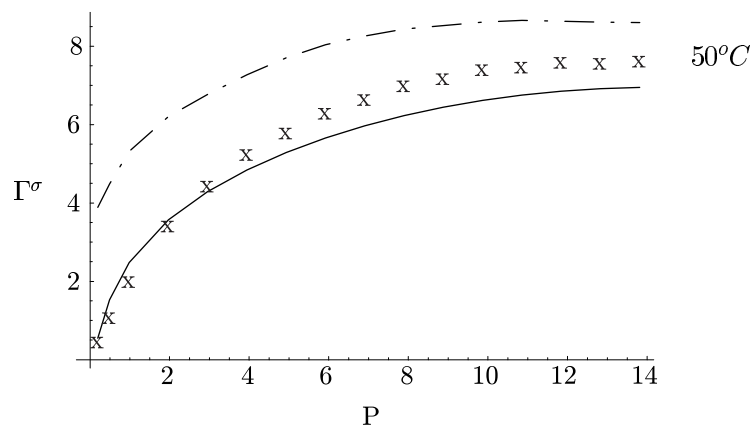


Fig. 8. Γ^σ ($\mu\text{ mol/m}^2$) as a function of P (MPa) for krypton on Graphon at 50°C predicted by (2.11) (the solid curves). The experimental observations are from Blumel et al. (1982). The dashed-dot curve represents the computations of Rangarajan et al. (1995).

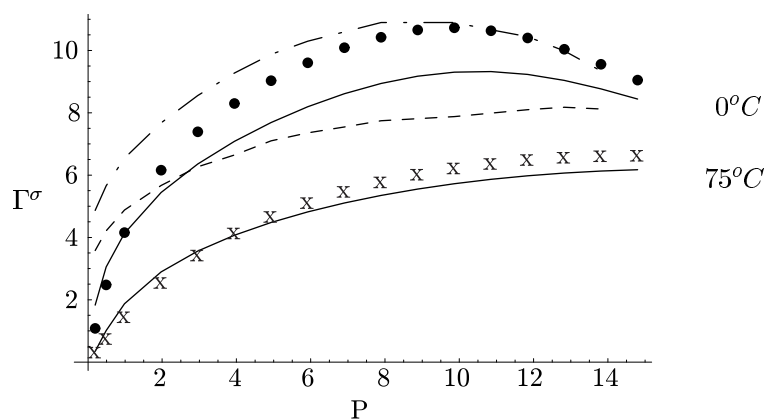


Fig. 9. Γ^σ ($\mu\text{ mol/m}^2$) as a function of P (MPa) for krypton on Graphon at 0°C and at 75°C predicted by (2.11) (the solid curves). The experimental observations are from Blumel et al. (1982). The dashed-dot curve represents the computations of Rangarajan et al. (1995) for 0°C ; the dashed curve for 75°C .

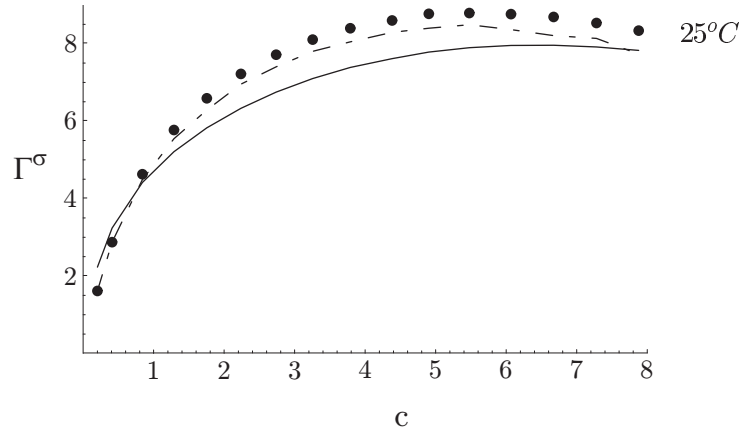


Fig. 10. Γ^σ ($\mu \text{ mol/m}^2$) as a function of c (mol L^{-1}) for krypton on Graphon at 25°C predicted by (2.11) (the solid curves). The experimental observations are from Blumel et al. (1982). The dashed curve represents the computations of Egorov (2001).

Figures 7 through 9 compare the model of Rangarajan et al. (1995) with (2.11) for the krypton data of Blumel et al. (1982). Figures 3, 11, and 12 compare the Sokolowski (1982) model with both (2.11) and the argon and methane data of Specovius and Findenegg (1978). Fischer (1978) presented a plot of his results compared with the data of Specovius and Findenegg (1978) for argon at only one temperature 50°C . Figure 5 compares his results with (2.11). In all cases, (2.11) was superior.

F. Discussion

The purpose of this chapter is to present a first application of a new idea—extension of continuum mechanics to the nanoscale (not the molecular scale) in which a correction for intermolecular forces from the adjoining phase is introduced in the differential momentum balance. We feel that we have successfully demonstrated this theory for supercritical adsorption of argon on Graphon (a graphitized carbon black) using no adjustable parameters.

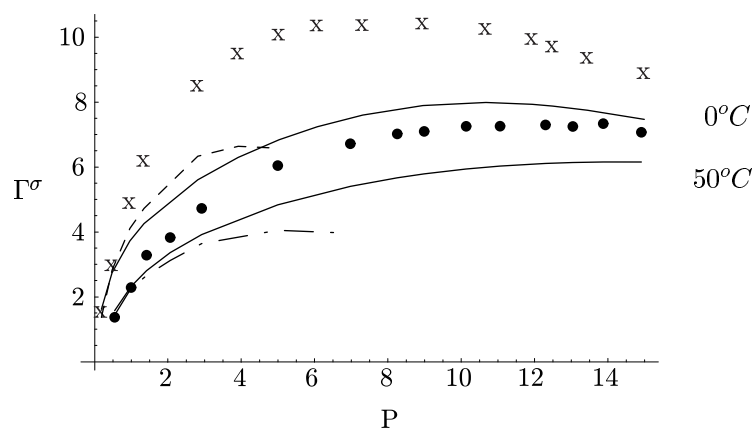


Fig. 11. Γ^σ ($\mu \text{ mol/m}^2$) as a function of P (MPa) for methane on Graphon at 0°C and at 50°C predicted by (2.11) (the solid curves). The experimental observations are from Specovius and Findenegg (1978). The dashed curve represents the computations of Sokolowski (1982) for 0°C ; the dashed-dot curve for 50°C .

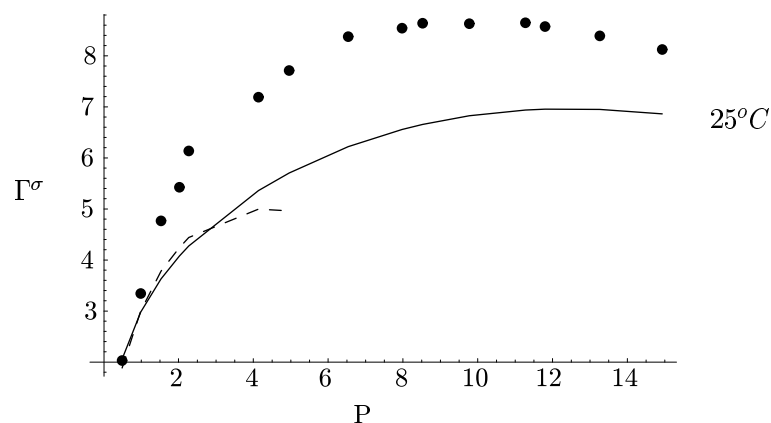


Fig. 12. Γ^σ ($\mu \text{ mol/m}^2$) as a function of P (MPa) for methane on Graphon at 25°C predicted by (2.11) (the solid curves). The experimental observations are from Specovius and Findenegg (1978). The dashed curve represents the computations of Sokolowski (1982).

Our theory does not do as well in describing the supercritical adsorption of krypton or of methane as the critical point is approached. We do not feel that this indicates a failure or limitation of the theory, but rather a limitation in the way that the theory was executed. Following Steele (1973, 1974, 1978), we have assumed the Lennard-Jones potential can be used to describe the carbon-fluid as well as the fluid-fluid interactions, and we have assumed that long-range intermolecular forces are pairwise additive.

We believe that the poorer agreement between our predictions and the experimental observations for krypton at lower temperatures is attributable to the assumption of pairwise additivity beginning to fail. The critical temperature for argon $T_c = 150.8$ K; for krypton, $T_c = 209.4$ K. Since the assumption of pairwise additivity would begin to fail as $T \rightarrow T_c$ and the fluid became denser, we could expect to see these effects at higher temperatures with krypton than with argon.

The poor agreement between our predictions and experimental observations for methane is certainly due in large measure to this same failure of the assumption of pairwise additivity. For methane, $T_c = 190.4$ K, and the error in our predictions decreases as the temperature is increased. However, we are also concerned that the Lennard-Jones potential may not be appropriate, particularly in the denser fluids as T_c is approached, because the methane molecule is not spherical.

Steele (1974, p. 52) clearly recognized that pairwise additivity of intermolecular forces could not be justified in condensed materials. He proposed that this problem could be at least partially avoided by using a more realistic description of the solid, one in which the crystalline solid was distributed discretely rather than continuously in space. We believe that the excellent agreement between the predictions of our theory and the experimental observations for argon and krypton, particularly at higher temperatures, supports his proposal.

We wish to emphasize that the use of pairwise additivity is not an inherent limitation in the use of this theory. For example, in describing the interactions between two condensed media, the limitations of pairwise additivity can be avoided by describing the two-point interactions using an effective, Lifshitz type, Hamaker constant that is both screened and retarded (Bowen and Jenner, 1995).

Based upon this success, we developed the theory which includes the computation of the correction for intermolecular forces in many different situations.

CHAPTER III

GENERALIZED THEORY AND APPLICATION ON CONTACT ANGLE

A. Introduction

By *nanoscale* we mean the immediate neighborhood of a phase interface, where the behavior of each phase is altered by the intermolecular forces from the adjoining phase. We are generally talking about more than the effect of interfacial tension or energy, which is a correction for long-range intermolecular forces between two “semi-infinite” phases. But we are not talking about the interaction between molecules within a single phase. We assume that such molecular-scale interactions are taken into account with an appropriate bulk description for material behavior.

In the immediate neighborhood of a phase interface, material behavior differs from that observed at some distance from the interface. All (local) descriptions of material behavior at some distance from the interface are based upon the assumption that the material extends to “infinity” (perhaps 100 nm) in all directions. Material points outside the immediate neighborhood of the interface are subjected to intermolecular forces only from one phase. Material points within the immediate neighborhood of a phase interface are subjected to intermolecular forces from both phases.

There is a large literature describing intermolecular forces and how they should be represented, and it is not our intention to review it here. We suggest as starting points for understanding this subject in more detail the books by Israelachvili (1991) and by Hirschfelder et al. (1954). But it will be helpful to note that the Lennard-Jones (6-12) potential is commonly recommended for non-polar dilute gases (Hirschfelder

et al., 1954, p. 22)

$$\phi^{(A,B)} = 4\epsilon^{(A,B)} \left[\left(\frac{\sigma^{(A,B)}}{r} \right)^{12} - \left(\frac{\sigma^{(A,B)}}{r} \right)^6 \right] \quad (3.1)$$

Here $\phi^{(A,B)}$ is the potential energy for two molecules A and B separated by a distance r ; the parameters $\sigma^{(A,B)}$, $\epsilon^{(A,B)}$ represent the collision diameter and well depth. The r^{-6} term describes attractive forces: the dispersion forces (London forces or induced-dipole-induced dipole forces) (Israelachvili, 1991, p. 83). The r^{-12} contribution represents short-range repulsive forces. The only caution necessary to observe here is that $\phi^{(A,B)}$ can not be allowed to become infinite; r can not be allowed to go to zero; it can be no smaller than the sum of the effective radii of molecules of A and B or the effective distance between molecules of A and B .

Israelachvili (1991, pp. 113, 176) argues that, due to a fortuitous cancellation of errors, the r^{-12} repulsive potential can be successfully replaced by a hard-sphere repulsive potential, reducing (3.1) for $r > \sigma$ to

$$\begin{aligned} \phi^{(A,B)} &= -\frac{C^{(AB)}}{r^6} && \text{for } r > \sigma^{(A,B)} \\ &= \infty && \text{for } r \leq \sigma^{(A,B)} \end{aligned} \quad (3.2)$$

There is also a large literature in which the effects of intermolecular forces are discussed at the continuum scale.

Hamaker (1937) adopted (3.2) in discussing the force between macroscopic bodies of condensed matter, writing (Israelachvili, 1991, p. 176)

$$C^{(AB)} = \frac{A^{(AB)}}{\pi^2 n^{(A)} n^{(B)}} \quad (3.3)$$

where $A^{(AB)}$ is the Hamaker constant, $n^{(A)}$ and $n^{(B)}$ are the number densities at the concerned points in phases A and B . There are at least three drawbacks to the

Hamaker relation that should be noted. First, in calculating the force between two macroscopic bodies, he assumed that the intermolecular forces could be added pairwise. Second, $A^{(AB)}$ is assumed to be geometry independent. Third, with increasing r , the attractive force decays even faster than r^{-6} , approaching r^{-7} . This is referred to as the *retardation* effect (Casimir and Polder, 1948).

To avoid these limitations, Lifshitz (1956) developed what we now refer to as *Lifshitz theory* by describing the multibody interaction in the fluctuating electromagnetic field created by the material. Dzyaloshinskii et al. (1961) generalized Lifshitz theory, using quantum field theory. The results have the same form as those obtained using pairwise additivity as suggested by Hamaker (1937), but the value of the effective Hamaker constant is dependent on a number of effects. Mahanty and Ninham (1976) discussed the dependence of the effective Hamaker constant upon the macroscopic geometry. Hough and White (1980) employed Lifshitz theory to calculate non-retarded Hamaker constants. Russel et al. (1989) gave an expression for the effective Hamaker constant that includes the effects of retardation and properly reduces to the results of Hough and White (1980) when the effects of retardation are absent. Bowen and Jenner (1995) have examined all of these issues, and they recommend a calculation for an effective, Lifshitz type, Hamaker constant that is both screened and retarded and that is geometry independent.

In what follows, we propose to incorporate the effect of intermolecular forces from adjacent phases as a body force in the standard developments of continuum mechanics. Following the developments described above, we can completely avoid the difficulties of pairwise additivity by employing effective, Lifshitz-type, Hamaker constants (Israelachvili, 1991, p. 180; Bowen and Jenner, 1995).

In particular, using (3.2) and (3.3), we will express the potential energy per unit

volume of A per unit volume of B as

$$\begin{aligned} n^{(A)}n^{(B)}\phi^{(ACB)} &= -\frac{C^{(AB)}n^{(A)}n^{(B)}}{r^6} \\ &= -\frac{A^{(ACB)}}{\pi^2r^6} \end{aligned} \quad (3.4)$$

Here $A^{(ACB)}$ denotes the effective, Lifshitz-type, Hamaker constant for species A and B interacting across an intermediate phase C . If there is no intermediate phase or the intermediate phase is a vacuum, we will use the notation $A^{(AB)}$. The corresponding force $\mathbf{f}^{(A,B)}(\mathbf{r}^{(A)}, \mathbf{r}^{(B)})$ per unit volume of phase A per unit volume of phase B at a point $\mathbf{r}^{(A)}$ in phase A attributable to the material at point $\mathbf{r}^{(B)}$ in phase B is

$$\begin{aligned} \mathbf{f}^{(A,B)} &= -\nabla(n^{(A)}n^{(B)}\phi^{(A,B)}) \\ &= \nabla\left(\frac{A^{(ACB)}}{\pi^2r^6}\right) \end{aligned} \quad (3.5)$$

As explained above, because we propose to use an effective, Lifshitz type, Hamaker constant $A^{(ACB)}$ such as that recommended by Bowen and Jenner (1995), we will assume that these two-point forces are pairwise additive and therefore that they can be integrated.

B. The correction

Our premise is that material behavior within the interfacial region can be represented as bulk material behavior corrected for the intermolecular forces from the adjoining phase. In particular, we recognize the equivalence of stresses and body forces (Truesdell and Toupin, 1960, p. 549).

There are four descriptions of the interfacial region, each view having its own somewhat different notation.

- a) Ideally, we would wish to use the true descriptions of material behavior appro-

priate everywhere, including the interfacial region. Using these descriptions, we would refer to $\mathbf{v}^{(I)}$, $\mathbf{T}^{(I)}$ and $\rho^{(I)}$ as the velocity, stress tensor and density. No excess quantities would be associated with any dividing surface. The problem with this view is that in general we will not know the appropriate descriptions of behavior in the interfacial regions.

- b) In the second view, we use everywhere the descriptions of material behavior appropriate outside the interfacial region (bulk material behavior). The effects of the interfacial region are taken into account by the excess quantities assigned to the corresponding dividing surface (Slattery, 1990, secs. 1.3.5 and 2.1.6). By $\mathbf{v}^{(\sigma)}$, $\mathbf{T}^{(\sigma)}$ and $\rho^{(\sigma)}$, we mean the corresponding surface velocity, surface stress tensor, and surface mass density.
- c) In the third view described in Figure 13, we again use the descriptions of material behavior appropriate outside the interfacial region (bulk material behavior), but no excess properties are assigned to the dividing surface. By $\mathbf{v}^{(I,bulk)}$, $\mathbf{T}^{(I,bulk)}$ and $\rho^{(I,bulk)}$, we indicate the velocity, stress tensor and density determined using the bulk descriptions of material behavior, corrected for intermolecular forces from the adjoining phase as described below. The two phases are separated by a distance δ , which physically corresponds to the sum of the effective radii of the A and B molecules or the effective distance between molecules of A and B .^a These surfaces should not be thought of as dividing surfaces, since there are no excess properties associated with them. If a dividing surface is introduced, it will be located in a standard manner (Slattery, 1990, secs. 1.3.6

^aFu et al. (2004), working in the context of supercritical adsorption on Graphon and representing $\phi^{(AA)}$ and $\phi^{(AB)}$, determines $\delta^{(AB)}$ by requiring $\Phi^{(A)} = 0$. We believe that this can be done only with the Lennard-Jones potential which accounts for both repulsive and attractive forces.

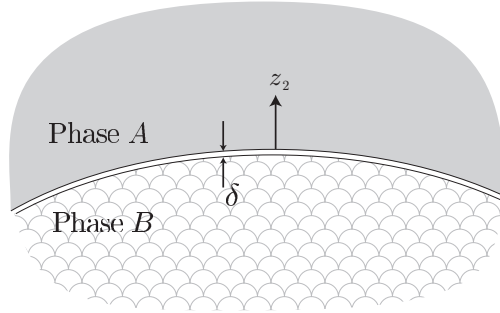


Fig. 13. A material body consisting of two adjoining phases, A and B .

and 5.2.3).

Conservation of mass tells us

$$\frac{d}{dt} \int_{R(m)} \rho^{(I,bulk)} dV = 0 \quad (3.6)$$

By the transport theorem for a region containing a dividing surface given in Slattery (1999, Sec. 1.3.5), (3.6) maybe written as

$$\begin{aligned} \frac{d}{dt} \int_{R(m)} \rho^{(I,bulk)} dV &= \int_{R(m)} \left(\frac{d_{(m)}\rho^{(I,bulk)}}{dt} + \rho^{(I,bulk)} \operatorname{div} \mathbf{v}^{(I,bulk)} \right) dV \\ &+ \int_{\Sigma} \left[\rho^{(I,bulk)} (\mathbf{v}^{(I,bulk)} - \mathbf{v}^{(\sigma)}) \cdot \boldsymbol{\xi} \right] dA \end{aligned} \quad (3.7)$$

Since $R(m)$ and Σ could be arbitrary, we get differential mass balance and jump mass balance from (3.7):

$$\frac{d_{(m)}\rho^{(I,bulk)}}{dt} + \rho^{(I,bulk)} \operatorname{div} \mathbf{v}^{(I,bulk)} = 0 \quad (3.8)$$

$$\left[\rho^{(I,bulk)} (\mathbf{v}^{(I,bulk)} - \mathbf{v}^{(\sigma)}) \cdot \boldsymbol{\xi} \right] = 0 \quad (3.9)$$

In Figure 13, we introduce that the jump is now over both singular surfaces. The boldface brackets denote the jump of the quantity enclosed across the interface

between phase A and phase B :

$$[\mathbf{S}\boldsymbol{\xi}] \equiv \mathbf{S}^{(A)}\boldsymbol{\xi}^{(A)} + \mathbf{S}^{(B)}\boldsymbol{\xi}^{(B)} \quad (3.10)$$

where $\boldsymbol{\xi}^{(\alpha)}$ is the unit normal to the interface pointing into phase α .

In the same way, we can write the differential and jump momentum balances in the standard forms (Slattery, 1990, sec. 5.4.1 and 5.4.2):

$$\rho^{(I,bulk)} \frac{d_{(m)} \mathbf{v}^{(I,bulk)}}{dt} = \text{div } \mathbf{T}^{(I,bulk)} + \rho^{(I,bulk)} \mathbf{b} + \mathbf{b}^{(corr)} \quad (3.11)$$

$$\left[\rho^{(I,bulk)} \left(\mathbf{v}^{(I,bulk)} \cdot \boldsymbol{\xi} - v_{(\boldsymbol{\xi})}^{(\sigma)} \right)^2 \boldsymbol{\xi} - \mathbf{T}^{(I,bulk)} \cdot \boldsymbol{\xi} \right] = 0 \quad (3.12)$$

Here \mathbf{b} is the body force per unit mass, typically gravity; $\mathbf{b}^{(corr)}$ is a body force per unit volume introduced to correct for the use of bulk material behavior in the interfacial region.

- d) The fourth view is a variation on view (b) above, and it is used only in the case of a thin film. The only difference is that we add a body force $\mathbf{b}^{(corr)\infty}$ that corrects for overlapping intermolecular forces. The excess properties in (b) are those attributable to a single, isolated interface. In the case of a thin film, the two interfaces are not isolated, and each phase is subjected to long-range intermolecular forces from the other two.

In order to illustrate the estimation of $\mathbf{b}^{(corr)}$, consider the two cases shown in Figure 14.

1. For the two phases shown in Figure 14(a), in estimating $\mathbf{b}^{(A,corr)}$ we will
 - subtract the force per unit volume at a point in phase A attributable to that portion of phase A that has been replaced by phase B , and

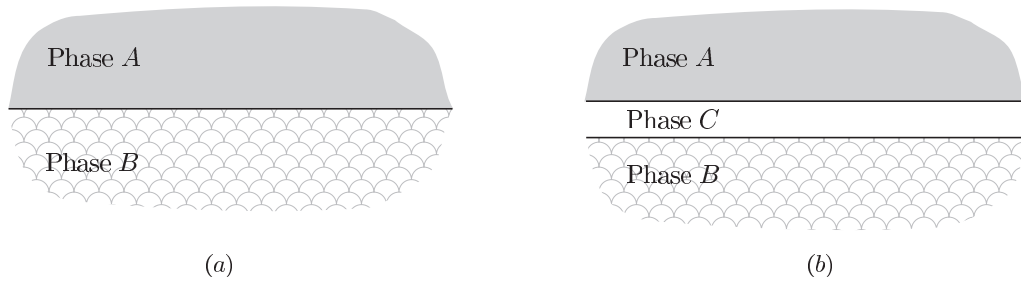


Fig. 14. For simplicity, the dividing surfaces and the two singular surfaces for each interface are shown as a single curve. Two cases are illustrated. (a) Two semi-infinite phases A and B . (b) Two semi-infinite phases A and B separated by a thin film of phase C .

- add the force per unit volume at this same point in phase A attributable to phase B .

In reality, the effective replacement region $R^{(B)}$ may be no more than 100 nm thick, since outside this region the intermolecular forces between phases A and B go to zero.

2. Let us now consider the thin film as shown in Figure 14(b). In order to estimate $\mathbf{b}^{(A,corr)}$, we will

- subtract the force per unit volume at a point in phase A attributable to that portion of phase A that has been replaced by phase C and phase B ,
- add force per unit volume at this same point in phase A attributable to phase C , and
- add force per unit volume at this point in phase A attributable to phase B .

C. One dividing surface

Consider two semi-infinite phases A and B shown in Figure 14(a), although it will not be necessary to make any assumption about the configuration of the interface. In particular, it is not necessary to assume that the dividing surface is a plane. As suggested in the assumptions above, the net correction for intermolecular forces $\mathbf{b}^{(A,corr)}$ at each point in phase A within the immediate neighborhood of the dividing surface is

$$\begin{aligned}\mathbf{b}^{(A,corr)} &\equiv - \int_{R^{(B)}} \mathbf{f}^{(A,A)} d\mathbf{r} + \int_{R^{(B)}} \mathbf{f}^{(A,B)} d\mathbf{r} \\ &= \int_{R^{(B)}} \nabla \left(n^{(A)2} \phi^{(A,A)} \right) d\mathbf{r} - \int_{R^{(B)}} \nabla \left(n^{(A)} n^{(B)} \phi^{(A,B)} \right) d\mathbf{r} \\ &= -\nabla \Phi^{(A,corr)}\end{aligned}\tag{3.13}$$

where

$$\Phi^{(A,corr)} \equiv - \int_{R^{(B)}} n^{(A)2} \phi^{(A,A)} d\mathbf{r} + \int_{R^{(B)}} n^{(A)} n^{(B)} \phi^{(A,B)} d\mathbf{r}\tag{3.14}$$

In a similar manner,

$$\begin{aligned}\mathbf{b}^{(B,corr)} &\equiv - \int_{R^{(A)}} \mathbf{f}^{(B,B)} d\mathbf{r} + \int_{R^{(A)}} \mathbf{f}^{(A,B)} d\mathbf{r} \\ &= \int_{R^{(A)}} \nabla \left(n^{(B)2} \phi^{(B,B)} \right) d\mathbf{r} - \int_{R^{(A)}} \nabla \left(n^{(A)} n^{(B)} \phi^{(A,B)} \right) d\mathbf{r} \\ &= -\nabla \Phi^{(B,corr)}\end{aligned}\tag{3.15}$$

in which

$$\Phi^{(B,corr)} \equiv - \int_{R^{(A)}} n^{(B)2} \phi^{(B,B)} d\mathbf{r} + \int_{R^{(A)}} n^{(A)} n^{(B)} \phi^{(A,B)} d\mathbf{r}\tag{3.16}$$

Fu et al. (2004) employed (3.13), (3.14), and the differential momentum balance to discuss supercritical adsorption or local densification of a supercritical gas on an impermeable Graphon. Following Steele (1973; 1974; 1978), they used the Lennard-

Jones potential with standard parameters for $\phi^{(AA)}$ (Bird et al., 2002, p. 804) and for $\phi^{(AB)}$ (Steele, 1974, p. 56). Using no adjustable parameters, they presented favorable comparisons with experimental data and alternative theories from several groups.

1. One dividing surface: with interfacial energy or tension

Let us now adopt view (b) of the interfacial region, in which bulk descriptions of material behavior are used, but excess properties are assigned to the dividing surface. It is not necessary to make any assumption about the configuration of the dividing surface, but for the sake of simplifying the argument, we will neglect the effects of any external force such as gravity.

It has been shown that (Slattery, 1990, p. 164)

$$\mathbf{T}^{(\sigma)} \equiv \left\{ \int_0^{\lambda^+} (\mathbf{T}^{(I)} - \mathbf{T}) d\lambda \right\} \cdot \mathbf{P} + \left\{ \int_{\lambda^-}^{-\delta} (\mathbf{T}^{(I)} - \mathbf{T}) d\lambda \right\} \cdot \mathbf{P} \quad (3.17)$$

where \mathbf{P} is the projection tensor (Slattery, 1990, p. 1085), λ is the distance measured along the normal to the dividing surface, and δ is the distance separating the two phases.

Let us use the results above to compute $\mathbf{T}^{(\sigma)}$.

We will approximate (since we have no way of knowing the true description of behavior in the interfacial region)

$$\mathbf{T}^{(I)} \doteq \mathbf{T}^{(I,bulk)} \quad (3.18)$$

In view of (3.13), equations (3.11) reduces to

$$\rho^{(I,bulk)} \frac{d_{(m)} \mathbf{V}^{(I,bulk)}}{dt} = \text{div} \left(\mathbf{T}^{(I,bulk)} - \Phi^{(corr)} \mathbf{I} \right) + \rho^{(I,bulk)} \mathbf{b} \quad (3.19)$$

Comparing this with the usual form of the differential momentum balance (Slattery,

1999, p. 34), we can identify

$$\mathbf{T} = \mathbf{T}^{(I,bulk)} - \Phi^{(corr)} \mathbf{I} \quad (3.20)$$

Given (3.18) and (3.20), equation (3.17) reduces to

$$\begin{aligned} \mathbf{T}^{(\sigma)} &= \left\{ \int_0^{\lambda^+} \Phi^{(A,corr)} \mathbf{I} d\lambda + \int_{\lambda^-}^{-\delta^{(AB)}} \Phi^{(B,corr)} \mathbf{I} d\lambda \right\} \cdot \mathbf{P} \\ &= \int_0^{\lambda^+} \Phi^{(A,corr)} d\lambda \mathbf{P} + \int_{\lambda^-}^{-\delta^{(AB)}} \Phi^{(B,corr)} d\lambda \mathbf{P} \end{aligned} \quad (3.21)$$

or

$$\mathbf{T}^{(\sigma)} = \gamma \mathbf{P} \quad (3.22)$$

where

$$\begin{aligned} \gamma &\equiv \int_0^{\lambda^+} \Phi^{(A,corr)} d\lambda + \int_{\lambda^-}^{-\delta^{(AB)}} \Phi^{(B,corr)} d\lambda \\ &= \int_0^{\infty} \Phi^{(A,corr)} d\lambda + \int_{-\infty}^{-\delta^{(AB)}} \Phi^{(B,corr)} d\lambda \end{aligned} \quad (3.23)$$

is interfacial tension or interfacial energy.

It is important to realize that γ represents the correction of intermolecular forces in the immediate neighborhood of a single dividing surface. But (3.22) also tells us that we should not expect to see surface viscous effects with clean interfaces such as we are considering in these first four chapters, which is in agreement with common observations.

Just to emphasize the point, since we are employing interfacial energy or tension, the stresses that appear in the jump momentum balance are the bulk stresses rather than the interfacial stresses.

a. Computation of surface tensions

Starting with (3.2) and (3.3), we can compute from (3.14) and (3.16)

$$\Phi^{(A,corr)} = \frac{A^{(AA)}}{6\pi (\delta^{(AA)} + z_2)^3} - \frac{A^{(AB)}}{6\pi (\delta^{(AB)} + z_2)^3} \quad (3.24)$$

and

$$\Phi^{(B,corr)} = \frac{A^{(AB)}}{6\pi z_2^3} - \frac{A^{(BB)}}{6\pi (\delta^{(AB)} - \delta^{(BB)} + z_2)^3} \quad (3.25)$$

where $\delta^{(\alpha\beta)}$ is the effective distance between molecules of α and β . Following (Fu et al., 2004), we will require

$$\text{at } z_2 = 0 : \quad \Phi^{(A,corr)} = 0 \quad (3.26)$$

or

$$\frac{A^{(AA)}}{\delta^{(AA)^3} = \frac{A^{(AB)}}{\delta^{(AB)^3}} \quad (3.27)$$

and

$$\text{at } z_2 = -\delta^{(AB)} : \quad \Phi^{(B,corr)} = 0 \quad (3.28)$$

or

$$\frac{A^{(AB)}}{\delta^{(AB)^3} = \frac{A^{(BB)}}{\delta^{(BB)^3}} \quad (3.29)$$

These together with (3.23) give us

$$\begin{aligned} \gamma &= \frac{A^{(AA)}}{12\pi\delta^{(AA)^2} - \frac{A^{(AB)}}{6\pi\delta^{(AB)^2} + \frac{A^{(BB)}}{12\pi\delta^{(BB)^2}} \\ &= \frac{\delta^{(AA)} A^{(BB)}}{12\pi \delta^{(BB)^3} - \frac{\delta^{(AB)} A^{(BB)}}{6\pi \delta^{(BB)^3} + \frac{A^{(BB)}}{12\pi\delta^{(BB)^3}} \\ &= \left(\frac{\delta^{(AA)}}{\delta^{(BB)}} - 2 \frac{\delta^{(AB)}}{\delta^{(BB)}} + 1 \right) \frac{A^{(BB)}}{12\pi\delta^{(BB)^3} \\ &= \left[\left(\frac{A^{(AA)}}{A^{(BB)}} \right)^{1/3} - 2 \left(\frac{A^{(AB)}}{A^{(BB)}} \right)^{1/3} + 1 \right] \frac{A^{(BB)}}{12\pi\delta^{(BB)^3} \end{aligned} \quad (3.30)$$

Note that (3.30) should not be expected to represent very well the surface or interfacial

tensions for liquids with strong hydrogen bonding; our simple representation of point-to-point forces (3.2) only attempts to take into account dispersion or van der Waals forces (Israelachvili, 1991, p. 204).

If we assume that phase A is a gas, we can neglect $A^{(AA)}$ and $A^{(AB)}$ with respect to $A^{(BB)}$ and (3.35) reduces to ^b

$$\gamma = \frac{A^{(BB)}}{12\pi\delta^{(BB)^2}} \quad (3.35)$$

^bIsraelachvili (1991, pp. 202-203, 313) arrived at a similar expression

$$\gamma = \frac{A^{(BB)}}{24\pi\delta^{(BB)^2}} \quad (3.31)$$

using a much different argument, in which a body was ruptured by tensile forces to form two pieces and two interfaces. Deformation of the body prior to rupture was not taken into account. In order to fit experimental data for a variety of system, he recommended $\delta^{(BB)} = 0.165$ nm. In the context of (3.35), we would say

$$\begin{aligned} \delta^{(BB)} &= 0.165 \times \sqrt{2} \\ &= 0.233 \text{ nm} \end{aligned} \quad (3.32)$$

Israelachvili (1973) suggests that, within phase A , $\delta^{(AA)}$ be viewed as the mean distance between the centers of individual molecules, units of molecules, or atoms and that it be estimated as

$$\delta^{(AA)} = 0.916 [M^{(A)} / (\rho^{(A)} n_a N)]^{1/3} \quad (3.33)$$

Here $M^{(A)}$ is the molecular weight of phase A , n_a is the number of atoms per molecule, N is Avogadro's constant ($6.023 \times 10^{23} \text{ mol}^{-1}$), and $\rho^{(A)}$ the mass density of phase A . In arriving at (3.33), the atoms have been assumed to be in a close packing arrangement.

For a molecule consisting of a repeating unit, such as a n-alkane with $-CH_2-$ being the repeating unit, we suggest a simple picture in which the molecules are arranged in such a manner that the *repeating units* are in a close packing arrangement. Retracing the argument of Israelachvili (1973), we have instead

$$\delta^{(AA)} = 0.916 [M^{(A)} / (\rho^{(A)} n_u N)]^{1/3} \quad (3.34)$$

where n_u is the number of repeating units in the molecule. This last is similar to the suggestion of Padday and Uffindell (1968), who replaced M/n_a by the $-CH_2-$ group weight and took the coefficient to be unity.

Table I.: Comparisons of calculated and measured values of surface tensions for n-alkanes.

n	$A^{(BB)^a}$ ($10^{-20} J$)	$\delta^{(BB)^b}$ nm	$\delta^{(BB)^c}$ nm	$\gamma_{\text{meas.}}^d$ (mJ m^{-2})	γ_{calc}^e (mJ m^{-2})	$\gamma_{\text{calc.}}^f$ (mJ m^{-2})
5	3.74	0.205	0.309	16.0	18.2	16.6
6	4.06	0.203	0.303	18.4	19.8	18.8
7	4.31	0.201	0.299	20.3	21.0	20.5
8	4.49	0.200	0.296	21.8	21.9	21.8
9	4.66	0.199	0.294	22.9	22.7	22.9
10	4.81	0.198	0.292	23.9	23.4	23.9
11	4.87	0.198	0.291	24.7	23.7	24.4
12	5.03	0.197	0.289	25.4	24.5	25.6
14	5.09	0.196	0.287	26.7	24.8	26.2
16	5.22	0.196	0.286	27.6	25.4	27.1

a) Calculated by Hough and White (1980).

b) Calculated using (3.33).

c) Calculated using (3.34).

d) Measured by Jasper and Kring (1955).

e) Calculated by Israelachvili (1991) using (3.31) and (3.32).

f) Calculated using (3.35) and $\delta^{(BB)} = 0.79 \times (3.34)$.

In preparing Table I to test the validity of (3.35), we have used $\delta^{(BB)} = 0.79 \times (3.34)$, a one-parameter fit of the experimental data similar to (3.32), essentially the one-parameter fit of experimental data recommended by Israelachvili (1991, pp. 202-203, 313). For broader variety of systems, Israelachvili (1991, p. 204) presents an

interesting comparison of (3.31) using $\delta^{(BB)} = 0.165$ nm, which is equivalent to (3.35) with (3.32).

D. One thin film

Consider now the thin film shown in Figure 14(b). It is not necessary that the dividing surfaces be planes or equidistant surfaces.

As suggested in the assumptions above, the net correction for intermolecular forces at each point in phase A is

$$\begin{aligned}
\mathbf{b}^{(A,corr)} &\equiv - \int_{R^{(B+C)}} \mathbf{f}^{(A,A)} d\mathbf{r} + \int_{R^{(C)}} \mathbf{f}^{(A,C)} d\mathbf{r} + \int_{R^{(B)}} \mathbf{f}^{(A,B)} d\mathbf{r} \\
&= \nabla \int_{R^{(B+C)}} n^{(A)2} \phi^{(A,A)} d\mathbf{r} - \nabla \int_{R^{(C)}} n^{(A)} n^{(C)} \phi^{(A,C)} d\mathbf{r} \\
&\quad - \nabla \int_{R^{(B)}} n^{(A)} n^{(B)} \phi^{(A,B)} d\mathbf{r} \\
&= -\nabla \Phi^{(A,corr)}
\end{aligned} \tag{3.36}$$

where

$$\begin{aligned}
\Phi^{(A,corr)} &\equiv - \int_{R^{(B+C)}} n^{(A)2} \phi^{(A,A)} d\mathbf{r} + \int_{R^{(C)}} n^{(A)} n^{(C)} \phi^{(A,C)} d\mathbf{r} \\
&\quad + \int_{R^{(B)}} n^{(A)} n^{(B)} \phi^{(A,B)} d\mathbf{r}
\end{aligned} \tag{3.37}$$

In a similar way, we conclude that

$$\begin{aligned}
\mathbf{b}^{(B,corr)} &\equiv - \int_{R^{(A+C)}} \mathbf{f}^{(B,B)} d\mathbf{r} + \int_{R^{(C)}} \mathbf{f}^{(B,C)} d\mathbf{r} + \int_{R^{(A)}} \mathbf{f}^{(A,B)} d\mathbf{r} \\
&= \nabla \int_{R^{(A+C)}} n^{(B)2} \phi^{(B,B)} d\mathbf{r} - \nabla \int_{R^{(C)}} n^{(B)} n^{(C)} \phi^{(B,C)} d\mathbf{r} \\
&\quad - \nabla \int_{R^{(A)}} n^{(A)} n^{(B)} \phi^{(A,B)} d\mathbf{r} \\
&= -\nabla \Phi^{(B,corr)}
\end{aligned} \tag{3.38}$$

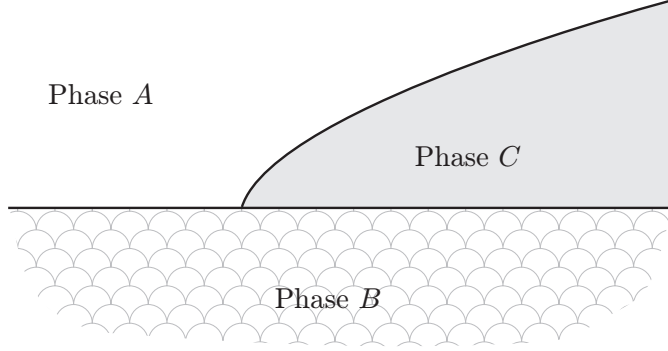


Fig. 15. A thin discontinuous film C forms a common line.

$$\begin{aligned}
\mathbf{b}^{(C,corr)} &\equiv - \int_{R^{(A+B)}} \mathbf{f}^{(C,C)} d\mathbf{r} + \int_{R^{(A)}} \mathbf{f}^{(A,C)} d\mathbf{r} + \int_{R^{(B)}} \mathbf{f}^{(B,C)} d\mathbf{r} \\
&= \nabla \int_{R^{(A+B)}} n^{(C)2} \phi^{(C,C)} d\mathbf{r} - \nabla \int_{R^{(A)}} n^{(A)} n^{(C)} \phi^{(A,C)} d\mathbf{r} \\
&\quad - \nabla \int_{R^{(B)}} n^{(B)} n^{(C)} \phi^{(B,C)} d\mathbf{r} \\
&= -\nabla \Phi^{(C,corr)}
\end{aligned} \tag{3.39}$$

Here

$$\begin{aligned}
\Phi^{(B,corr)} &\equiv - \int_{R^{(A+C)}} n^{(B)2} \phi^{(B,B)} d\mathbf{r} + \int_{R^{(C)}} n^{(B)} n^{(C)} \phi^{(B,C)} d\mathbf{r} \\
&\quad + \int_{R^{(A)}} n^{(A)} n^{(B)} \phi^{(A,B)} d\mathbf{r}
\end{aligned} \tag{3.40}$$

and

$$\begin{aligned}
\Phi^{(C,corr)} &\equiv - \int_{R^{(A+B)}} n^{(C)2} \phi^{(C,C)} d\mathbf{r} + \int_{R^{(A)}} n^{(A)} n^{(C)} \phi^{(A,C)} d\mathbf{r} \\
&\quad + \int_{R^{(B)}} n^{(B)} n^{(C)} \phi^{(B,C)} d\mathbf{r}
\end{aligned} \tag{3.41}$$

Note that these results also apply to a discontinuous film forming a common line as shown in Figure 15.

1. One thin film: with interfacial energy or tension in both interfaces

Let us now adopt view (d) of the interfacial region as outlined in the introduction to this section.

For the case considered in Section D, let us specifically assume that phase A is a gas, phase B a liquid, and phase C a solid. We will now adopt view (b) of the interfacial region, in which interfacial energies or tensions are introduced in both dividing surface.

This means that, in contrast with the discussion in Sec. B, $\gamma^{(AC)}$ and $\gamma^{(BC)}$ can not fully account for the correction that must be made to the intermolecular forces. There is an additional correction to be made, which we will develop here. As an example, for phase A we will name this correction $\mathbf{b}^{(A,corr)\infty}$, in order to distinguish it from $\mathbf{b}^{(A,corr)}$ developed above.

In particular, the correction for intermolecular forces at any point in phase A now becomes (3.36) minus (3.13) and (3.15), both of which have to be suitably modified:

$$\begin{aligned}
\mathbf{b}^{(A,corr)\infty} &\equiv \mathbf{b}^{(A,corr)} - \nabla \int_{R^{(B+C)}} n^{(A)2} \phi^{(A,A)} d\mathbf{r} + \nabla \int_{R^{(B+C)}} n^{(A)} n^{(C)} \phi^{(A,C)} d\mathbf{r} \\
&\quad - \nabla \int_{R^{(B)}} n^{(C)2} \phi^{(C,C)} d\mathbf{r} + \nabla \int_{R^{(B)}} n^{(B)} n^{(C)} \phi^{(B,C)} d\mathbf{r} \\
&= \nabla \int_{R^{(B)}} \left[n^{(A)} n^{(C)} \phi^{(A,C)} - n^{(A)} n^{(B)} \phi^{(A,B)} - n^{(C)2} \phi^{(C,C)} \right. \\
&\quad \left. + n^{(B)} n^{(C)} \phi^{(B,C)} \right] d\mathbf{r} \\
&= -\nabla \Phi^{(A,corr)\infty}
\end{aligned} \tag{3.42}$$

where

$$\begin{aligned}
\Phi^{(A,corr)\infty} &\equiv - \int_{R^{(B)}} \left[n^{(A)} n^{(C)} \phi^{(A,C)} - n^{(A)} n^{(B)} \phi^{(A,B)} \right. \\
&\quad \left. - n^{(C)2} \phi^{(C,C)} + n^{(B)} n^{(C)} \phi^{(B,C)} \right] d\mathbf{r}
\end{aligned} \tag{3.43}$$

In a similar manner, we find

$$\begin{aligned}
& \mathbf{b}^{(B,corr)\infty} \\
& \equiv \mathbf{b}^{(B,corr)} - \nabla \int_{R^{(A+C)}} n^{(B)2} \phi^{(B,B)} d\mathbf{r} + \nabla \int_{R^{(A+C)}} n^{(B)} n^{(C)} \phi^{(B,C)} d\mathbf{r} \\
& \quad + \nabla \int_{R^{(A+C)}} n^{(B)} n^{(C)} \phi^{(B,C)} d\mathbf{r} - \nabla \int_{R^{(A)}} n^{(C)2} \phi^{(C,C)} d\mathbf{r} \\
& \quad \quad + \nabla \int_{R^{(A)}} n^{(A)} n^{(C)} \phi^{(A,C)} d\mathbf{r} \\
& = \nabla \int_{R^{(A)}} \left[n^{(B)} n^{(C)} \phi^{(B,C)} - n^{(A)} n^{(B)} \phi^{(A,B)} - n^{(C)2} \phi^{(C,C)} \right. \\
& \quad \quad \left. + n^{(A)} n^{(C)} \phi^{(A,C)} \right] d\mathbf{r} \\
& = -\nabla \Phi^{(B,corr)\infty}
\end{aligned} \tag{3.44}$$

and

$$\begin{aligned}
& \mathbf{b}^{(C,corr)\infty} \\
& \equiv \mathbf{b}^{(C,corr)} - \nabla \int_{R^{(A)}} n^{(C)2} \phi^{(C,C)} d\mathbf{r} + \nabla \int_{R^{(A)}} n^{(A)} n^{(C)} \phi^{(A,C)} d\mathbf{r} \\
& \quad - \nabla \int_{R^{(B)}} n^{(C)2} \phi^{(C,C)} d\mathbf{r} + \nabla \int_{R^{(B)}} n^{(B)} n^{(C)} \phi^{(B,C)} d\mathbf{r} \\
& = -\nabla \Phi^{(C,corr)\infty} \\
& = 0
\end{aligned} \tag{3.45}$$

in which

$$\begin{aligned}
\Phi^{(B,corr)\infty} \equiv & - \int_{R^{(A)}} \left[n^{(B)} n^{(C)} \phi^{(B,C)} - n^{(A)} n^{(B)} \phi^{(A,B)} \right. \\
& \quad \left. - n^{(C)2} \phi^{(C,C)} + n^{(A)} n^{(C)} \phi^{(A,C)} \right] d\mathbf{r}
\end{aligned} \tag{3.46}$$

and

$$\Phi^{(C,corr)\infty} = 0 \tag{3.47}$$

No assumption is made here about the configuration of the thin film C , and they are immediately applicable to the discontinuous film shown in Figure 15 as explained

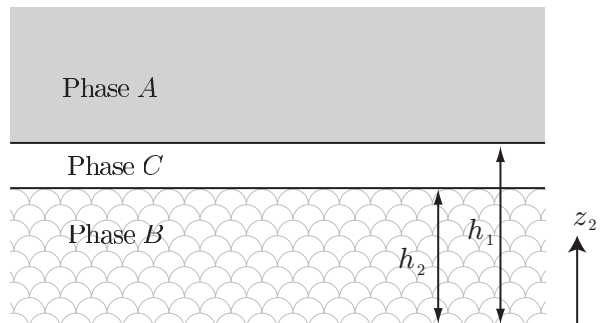


Fig. 16. A thin film bounded by two parallel, plane interfaces.

in Section 2.

a. Parallel plane interfaces

In order to illustrate the results derived here, consider a thin film of phase C bounded by parallel, plane interfaces in which interfacial tensions or energies have been introduced. The film is unbounded in z_1 and z_3 directions; its thickness is the difference between h_1 and h_2 as illustrated in Figure 16. Using (3.43) and (3.46), we can show in region A

$$\Phi^{(A,corr)\infty} = -\frac{A^{(ACB)} - A^{(AC)} + A^{(CC)} - A^{(BC)}}{6\pi(z_2 - h_2)^3}$$

and in region B

$$\Phi^{(B,corr)\infty} = \frac{A^{(BC)} - A^{(ACB)} - A^{(CC)} + A^{(AC)}}{6\pi(h_1 - z_2)^3}$$

For simplicity, let us neglect any effect of gravity within the interfacial region. It is common to introduce an extra stress

$$\mathbf{S} \equiv \mathbf{T} + P\mathbf{I} \tag{3.48}$$

and a modified pressure

$$\mathcal{P} \equiv P + \Phi^{(corr)\infty} \quad (3.49)$$

The physical significance of \mathcal{P} is that this is the thermodynamic pressure that would exist in the absence of the correction for intermolecular forces. This has the advantage that, if we are willing to assume $\rho^{(I,bulk)}$ is a constant within the interfacial region, the corrections for intermolecular forces drop out of the differential momentum balance (3.11)

$$\rho^{(I,bulk)} \frac{d_{(m)} \mathbf{v}^{(I,bulk)}}{dt} = -\nabla \mathcal{P} + \text{div } \mathbf{S}^{(I,bulk)} \quad (3.50)$$

and appear only in the jump momentum balance (3.12)

$$\left[\rho^{(I,bulk)} \left(\mathbf{v}^{(I,bulk)} \cdot \boldsymbol{\xi} - v_{(\boldsymbol{\xi})}^{(\sigma)} \right)^2 \boldsymbol{\xi} + \mathcal{P} \boldsymbol{\xi} - \Phi^{(corr)\infty} \boldsymbol{\xi} - \mathbf{S}^{(I,bulk)} \cdot \boldsymbol{\xi} \right] = 0 \quad (3.51)$$

Consider the interface between phases A and C in Figure 16. Referring to (3.47), (3.49) and (3.51), we see that

$$\begin{aligned} \left[\mathcal{P} \boldsymbol{\xi} - \Phi \boldsymbol{\xi} \right] &= (\mathcal{P}^{(A)} - P^{(C)} - \Phi^{(A,corr)\infty}) \boldsymbol{\xi}^{(A)} \\ &= \left(\mathcal{P}^{(A)} - P^{(C)} - \frac{A^{(AC)} + A^{(BC)} - A^{(ACB)} - A^{(CC)}}{6\pi (h_1 - h_2)^3} \right) \boldsymbol{\xi}^{(A)} \end{aligned} \quad (3.52)$$

Here $\boldsymbol{\xi}^{(A)}$ is the unit normal to the interface pointing into phase A . In this context $\Phi^{(A,corr)\infty}$ may be referred to as the *disjoining pressure*, in the sense that it has the effect of changing $P^{(C)}$. A *positive disjoining pressure* or $A^{(AC)} + A^{(BC)} > A^{(ACB)} + A^{(CC)}$ means that phases A and B would prefer to be in contact with phase C rather than each other, and the thickness of the film will tend to increase or *disjoin*. A *negative disjoining pressure* or $A^{(AC)} + A^{(BC)} < A^{(ACB)} + A^{(CC)}$ means that phases A and B would prefer to be in contact with each other rather than phase C , and the thickness of the film will tend to decrease.

Here we have introduced the disjoining pressure only in the context of the cor-

rection for intermolecular forces. More generally, the disjoining pressure is introduced to describe both electrostatic forces and the correction for intermolecular forces. It is necessary only that the body force be representable in terms of a potential and that the density in the interfacial region be assumed to be a constant.

2. A discontinuous thin film

The most important point to reemphasize is that Section D applies to the discontinuous film shown in Figure 15.

Section 1 also applies to discontinuous films, with the understanding that the interfacial tensions or energies are those attributable to dividing surfaces separating semi-infinite regions; they are independent of position, in the absence of temperature or concentration gradients. These are the interfacial tensions or energies that are commonly used in the literature. The “true” interfacial tensions would be functions of distance to the common line.

E. One thin lens or fracture

Returning to view (c) of the interfacial region, consider the thin lens or fracture shown in Figure 17, but no excess properties are associated with the dividing surface.

As suggested in the assumptions above, the net correction for intermolecular forces at each point in phase A is

$$\begin{aligned}
 \mathbf{b}^{(A,corr)} &\equiv - \int_{R^{(C)}} \mathbf{f}^{(A,A)} d\mathbf{r} + \int_{R^{(C)}} \mathbf{f}^{(A,C)} d\mathbf{r} \\
 &= \nabla \int_{R^{(C)}} n^{(A)2} \phi^{(A,A)} d\mathbf{r} - \nabla \int_{R^{(C)}} n^{(A)} n^{(C)} \phi^{(A,C)} d\mathbf{r} \\
 &= -\nabla \Phi^{(A,corr)}
 \end{aligned} \tag{3.53}$$

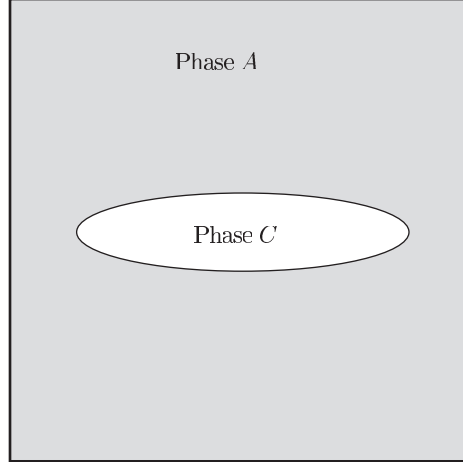


Fig. 17. A thin lens (or fracture) of phase C in phase A .

where

$$\Phi^{(A,corr)} \equiv - \int_{R^{(C)}} n^{(A)2} \phi^{(A,A)} d\mathbf{r} + \int_{R^{(C)}} n^{(A)} n^{(C)} \phi^{(A,C)} d\mathbf{r} \quad (3.54)$$

In a similar way, we conclude that

$$\begin{aligned} \mathbf{b}^{(C,corr)} &\equiv - \int_{R^{(A)}} \mathbf{f}^{(C,C)} d\mathbf{r} + \int_{R^{(A)}} \mathbf{f}^{(A,C)} d\mathbf{r} \\ &= \nabla \int_{R^{(A)}} n^{(C)2} \phi^{(C,C)} d\mathbf{r} - \nabla \int_{R^{(A)}} n^{(A)} n^{(C)} \phi^{(A,C)} d\mathbf{r} \\ &= -\nabla \Phi^{(C,corr)} \end{aligned} \quad (3.55)$$

Here

$$\Phi^{(C,corr)} \equiv - \int_{R^{(A)}} n^{(C)2} \phi^{(C,C)} d\mathbf{r} + \int_{R^{(A)}} n^{(A)} n^{(C)} \phi^{(A,C)} d\mathbf{r} \quad (3.56)$$

1. One thin lens or fracture, phase C is a vacuum

Let us assume that phase C is a vacuum, but let us now adopt view (b) of the interfacial region, in which bulk descriptions of material behavior is used, and interfacial energies or tensions is introduced in the dividing surface.

If in Section E phase C is a vacuum, those results become

$$\begin{aligned}
\mathbf{b}^{(A)} &\equiv - \int_{R^{(C)}} \mathbf{f}^{(A,A)} d\mathbf{r} \\
&= \nabla \int_{R^{(C)}} n^{(A)2} \phi^{(A,A)} d\mathbf{r} \\
&= -\nabla \Phi^{(A,corr)}
\end{aligned} \tag{3.57}$$

where

$$\Phi^{(A,corr)} \equiv - \int_{R^{(C)}} n^{(A)2} \phi^{(A,A)} d\mathbf{r} \tag{3.58}$$

2. One thin lens or fracture, phase C is a vacuum: with interfacial energy or tension

The introduction of interfacial energy or tension in section C can be immediately extended to this case to conclude that

$$\mathbf{b}^{(C,corr)\infty} = 0 \tag{3.59}$$

It is important to realize that, in contrast with Section C, equation (3.22) in this context requires

$$\gamma \equiv \int_0^{\lambda^+} \Phi^{(A,corr)} d\lambda \tag{3.60}$$

Since $\Phi^{(A,corr)}$ is a function of lateral position with respect to the lens as well as distance from the lens, γ will be a function of position on the surface of the lens. Since the configuration of the lens or fracture will in general not be known and the computation of $\Phi^{(A,corr)}$ and γ require the configuration of the lens, this would result in an awkward computation. It is for this reason that we recommend that view (b) of the interfacial region and surface tension not be used in analyzing these problems.

F. Application on static contact angle

Contact angle measurement has various application in science and technology. Yet theoretical prediction of contact angle is still unclear. Young's Equation (Young, 1805) interrelates the contact angle and surface tensions of the liquid and solid phases which has been used for almost 200 years. In this section we will consider the intermolecular forces into the study and also propose a different approach than the traditional way of using Young's equation.

It has been recognized for a long time that the molecular interactions play an important role within the immediate neighborhood of a three-phase common line where the meniscal film is very thin. The knowledge of bulk properties of liquid and solid is not enough for the theoretical prediction. The configuration of the fluid-fluid interface in the common line region and static contact angle depend on the correction for intermolecular forces.

Rayleigh (1890) recognized that, in two dimensions sufficiently far away from the common line, the fluid-fluid interface approaches a plane inclined at a angle $\Theta^{(\text{stat})}$ to the solid surface. As the common line is approached, the curvature of the interface is determined by a force balance to form a different angle Θ_0 with the solid surface. More recently, the configuration of the interface near the common line has been investigated in the context of statistical mechanics (Berry, 1974; Benner Jr. et al., 1982) and by molecular dynamics simulations (Saville, 1978). See Dussan V (1979) for a further review.

Fox and Zisman (1950) did a series of experiment on contact angles and liquid-liquid surface tension which is considered one of the most successful experimental work in this field. Also, contact angle problem has been discussed theoretically by many investigators (Dzyaloshinskii et al., 1960; Padday and Uffindell, 1968; Israelachvili,

1973; Miller and Ruckenstein, 1974; Jameson and del Cerro, 1976; Martynov et al., 1977; Hough and White, 1980; Wayner, 1980, 1982; Joanny and deGennes, 1984, 1986).

Figure 18 shows in two dimensions the three-phase common line formed at equilibrium between phases A , C , and a solid B . The static contact angle $\Theta^{(\text{stat})}$ might be measured by an experimentalist at some distance from the common line, using perhaps $10\times$ magnification. Hough and White (1980) calculated Hamaker constants from Lifshitz theory and applied them to describe contact angles of alkanes on Polytetrafluoroethylene. They did well for predicting contact angles of large alkane carbon number but failed for small alkane carbon number comparing with Zisman's experimental data. In this section we predict contact angles for all Alkanes on PTFE very well and have good agreements with experimental values of contact angles for other dispersive liquids on PDMS.

1. Problem statement

The objective is to determine the experimentally measured static contact angle $\Theta^{(\text{stat})}$, which we will distinguish from Θ_0 shown in Fig 18, the contact angle at the true common line. We will focus on the thin (precursor) film (Slattery, 1990, Sec. 1.2.9) formed in the neighborhood of the true common line

Three assumptions are made.

i) The solid is rigid, and its surface is smooth and planar. Because the effect of gravity will be ignored with respect to the correction for intermolecular forces, its orientation with respect to gravity is arbitrary.

ii) The system is static, and equilibrium has been established. There are no interfacial tension gradients developed in the system.

iii) The correction for intermolecular forces will be introduced as described in

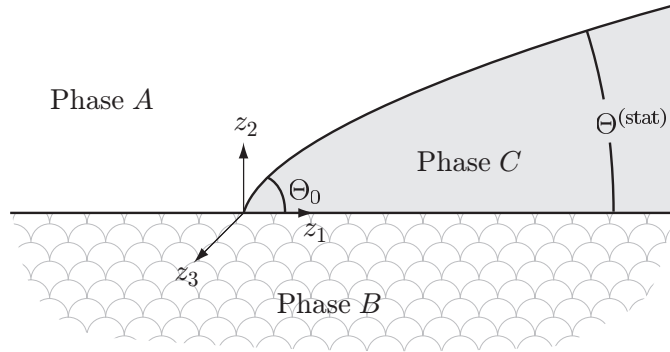


Fig. 18. A thin discontinuous film C forms a common line.

Section D.

In constructing this analysis, there are two important steps. First, how to compute intermolecular force correction term; Second, how might the correction term be taken into account in the context of continuum mechanics for this problem.

2. Correction for long-range intermolecular forces

From Figure 18, this problem are visualized as one thin film with interfacial tension in both interfaces. We will adopt view(d) from section B, because each phase of the thin film is subjected to long-range intermolecular forces from the other two. As discussed in Section D, we argue that the interfacial tension $\gamma^{(AC)}$ and $\gamma^{(BC)}$ cannot fully account for the correction that must be made to the intermolecular forces. There is an additional correction to be made.

From Equations (3.47) and (3.43), we have

$$\Phi^{(C,corr)\infty} \equiv 0 \quad (3.61)$$

$$\begin{aligned}
& \Phi^{(A,corr)\infty} \\
& \equiv - \int_{R^{(B)}} \left[n^{(A)} n^{(C)} \phi^{(A,C)} - n^{(A)} n^{(B)} \phi^{(A,B)} - n^{(C)^2} \phi^{(C,C)} \right. \\
& \quad \left. + n^{(B)} n^{(C)} \phi^{(B,C)} \right] d\mathbf{r} \\
& = \left[n^{(A)} n^{(C)} C^{(AC)} - n^{(A)} n^{(B)} C^{(AB)} - n^{(C)^2} C^{(CC)} + n^{(B)} n^{(C)} C^{(BC)} \right] \\
& \quad \times \int_{-\infty}^{\infty} \int_{-\infty}^0 \int_{-\infty}^{\infty} \left[\sqrt{(z_1 - x)^2 + (z_2 - y)^2 + z^2} \right]^{-6} dx dy dz \\
& = \frac{\pi}{6z_2^3} \left[n^{(A)} n^{(C)} C^{(AC)} - n^{(A)} n^{(B)} C^{(ACB)} - n^{(C)^2} C^{(CC)} + n^{(B)} n^{(C)} C^{(BC)} \right] \quad (3.62)
\end{aligned}$$

Superscript (ACB) represents for species A and B interacting across an intermediate phase C . The London dispersion force coefficient C is related to the Hamaker constant A by (Israelachvili, 1991, p. 176)

$$A^{(AC)} = \pi^2 C^{(AC)} n^{(A)} n^{(C)} \quad (3.63)$$

so that

$$\Phi^{(A,corr)\infty} = \frac{1}{6\pi z_2^3} \left[A^{(AC)} - A^{(ACB)} - A^{(CC)} + A^{(BC)} \right] \quad (3.64)$$

3. Solving procedure

Referring to Figure 18 and Slattery (1990, Table 2.4.2-6), the configuration of the A - C interface is unknown

$$z_2 = h(z_1) \quad (3.65)$$

assuming that the C - B interface is

$$z_2 = 0 \quad (3.66)$$

Both the z_1 and z_2 components of the jump momentum balance for the $A-C$ interface reduces to

$$\text{at } z_2 = h : p^{(A)} - p^{(C)} = \gamma \frac{d^2 h}{dz_1^2} \left[1 + \left(\frac{dh}{dz_1} \right)^2 \right]^{-3/2} \quad (3.67)$$

Here $p^{(A)}$ and $p^{(C)}$ are the pressures in these phases evaluated at the $A-C$ interface. To simplify the equation, we use γ instead of $\gamma^{(AC)}$ as the surface tension between A and C . The static differential momentum balances are from (3.11)

$$\begin{aligned} \mathcal{P}^{(A)} &\equiv p^{(A)} + \Phi^{(A,corr)\infty} \\ &= C_1 \end{aligned} \quad (3.68)$$

and

$$\begin{aligned} \mathcal{P}^{(C)} &\equiv p^{(C)} + \Phi^{(C,corr)\infty} \\ &= C_2 \end{aligned} \quad (3.69)$$

in which C_1 and C_2 are constants. This permits us to write (3.67) as

$$C_1 - C_2 + \Phi^{(C,corr)\infty} - \Phi^{(A,corr)\infty} = \gamma \frac{d^2 h}{dz_1^2} \left[1 + \left(\frac{dh}{dz_1} \right)^2 \right]^{-3/2} \quad (3.70)$$

or, in view of (3.61) and (3.62)

$$C_1 - C_2 + \frac{A^{(ACB)} - A^{(AC)} + A^{(CC)} - A^{(BC)}}{6\pi h^3} = \gamma \frac{d^2 h}{dz_1^2} \left[1 + \left(\frac{dh}{dz_1} \right)^2 \right]^{-3/2} \quad (3.71)$$

Let us introduce as dimensionless variables

$$\begin{aligned} h^* &\equiv \frac{h}{\delta^{(BC)}} & z_1^* &\equiv \frac{z_1}{\delta^{(BC)}} \\ B^* &\equiv \frac{A^{(ACB)} - A^{(AC)} + A^{(CC)} - A^{(BC)}}{6\pi\gamma\delta^{(BC)^2}} & C_i^* &\equiv \frac{C_i\delta^{(BC)}}{\gamma} \end{aligned} \quad (3.72)$$

where $\delta^{(BC)}$ is the interface separation distance between phases B and C . We will

explain how to get its value later. This permits us to express (3.71) as

$$C_1^* - C_2^* + \frac{B^*}{h^{*3}} = \frac{d^2 h^*}{dz_1^{*2}} \left[1 + \left(\frac{dh^*}{dz_1^*} \right)^2 \right]^{-3/2} \quad (3.73)$$

The quantity $C_1 - C_2$ represents the pressure difference across the interface as $z_1 \rightarrow \infty$.

We can safely estimate that

$$|C_1^* - C_2^*| \ll |B^*| \quad (3.74)$$

in which case (3.73) reduces to

$$\frac{B^*}{h^{*3}} = \frac{d^2 h^*}{dz_1^{*2}} \left[1 + \left(\frac{dh^*}{dz_1^*} \right)^2 \right]^{-3/2} \quad (3.75)$$

Our objective is to solve (3.75) consistent with the following conditions:

$$\text{at } z_1^* = 0 : h^* = 1 \quad (3.76)$$

$$\text{at } z_1^* = 0 : \frac{dh^*}{dz_1^*} = \tan \Theta_0 \quad (3.77)$$

where Θ_0 is the contact angle at the true common line.

Noting that

$$\begin{aligned} \frac{d^2 h^*}{dz_1^{*2}} &= \frac{dh^*}{dz_1^*} \frac{d^2 h^*}{dz_1^{*2}} \frac{dz_1^*}{dh^*} \\ &= \frac{1}{2} \frac{d}{dz_1^*} \left(\frac{dh^*}{dz_1^*} \right)^2 \frac{dz_1^*}{dh^*} \\ &= \frac{1}{2} \frac{d}{dh^*} \left(\frac{dh^*}{dz_1^*} \right)^2 \end{aligned} \quad (3.78)$$

we may write (3.75) as

$$\frac{B^*}{h^{*3}} = \frac{1}{2} \frac{d}{dh^*} \left(\frac{dh^*}{dz_1^*} \right)^2 \left[1 + \left(\frac{dh^*}{dz_1^*} \right)^2 \right]^{-3/2} \quad (3.79)$$

Integrating this once consistent with (3.76) and (3.77), we have

$$(1 + \tan^2 \Theta_0)^{-1/2} - \left[1 + \left(\frac{dh^*}{dz_1^*} \right)^2 \right]^{-1/2} = -\frac{B^*}{2} \left(\frac{1}{h^{*2}} - 1 \right) \quad (3.80)$$

In the limits

$$\text{as } z_1^* \rightarrow \infty : h^* \rightarrow \infty \quad (3.81)$$

and

$$\text{as } z_1^* \rightarrow \infty : \frac{dh^*}{dz_1^*} \rightarrow \Theta^{(\text{stat})} \quad (3.82)$$

equation (3.80) further reduces to

$$(1 + \tan^2 \Theta_0)^{-1/2} - (1 + \tan^2 \Theta^{(\text{stat})})^{-1/2} = \frac{B^*}{2} \quad (3.83)$$

or

$$|\cos \Theta_0| - |\cos \Theta^{(\text{stat})}| = \mp \frac{A^{(ACB)} - A^{(AC)} + A^{(CC)} - A^{(BC)}}{12\pi\gamma\delta^{(BC)^2}} \quad (3.84)$$

For the case in which phase A is a gas, this reduces in view of that Hamaker constants $A^{(AC)}$ and $A^{(AB)}$, which involve gas, are negligible to $A^{(CC)}$ and $A^{(BC)}$

$$|\cos \Theta_0| - |\cos \Theta^{(\text{stat})}| = \mp \frac{A^{(CC)} - A^{(BC)}}{12\pi\gamma\delta^{(BC)^2}} \quad (3.85)$$

The angle Θ_0 at the true common line should be determined using Young's equation. (Slattery, 1990, p. 169).

$$\gamma^{(AC)} \cos \Theta_0 = \gamma^{(AB)} - \gamma^{(BC)} \quad (3.86)$$

After some arrangement, we rewrite (3.85) as

$$\cos \Theta^{(\text{stat})} = \frac{\gamma^{(AB)} - \gamma^{(BC)}}{\gamma^{(AC)}} + \frac{A^{(CC)} - A^{(BC)}}{12\pi\gamma^{(AC)}\delta^{(BC)^2}} \quad (3.87)$$

4. Prediction of $\Theta^{(\text{stat})}$

We will validate (3.87) by predicting $\Theta^{(\text{stat})}$ for the n-alkanes against air on Polytetrafluoroethylene(PTFE) and various dispersive liquids against air on Polydimethylsiloxane(PDMS).

The Hamaker constants $A^{(BC)}$ and $A^{(CC)}$ were calculated by Hough and White (1980), and $\gamma^{(AC)}$ were measured by Fox and Zisman (1950).

Girifalco and Good (1957) [see also Adamson 1976, p. 360] proposed that $\gamma^{(BC)}$ could be estimated as

$$\begin{aligned}\gamma^{(BC)} &= \left(\sqrt{\gamma^{(AC)}} - \sqrt{\gamma^{(AB)}} \right)^2 \\ &= \gamma^{AB} + \gamma^{AC} - 2(\gamma^{AB}\gamma^{AC})^{1/2}\end{aligned}\quad (3.88)$$

It is important to recognize that the n-alkanes are volatile liquids and that the gas phase is dependent upon the specific n-alkane being considered. Fox and Zisman (1950) observed that there is no difference between contact angles measured in saturated air and those measured in unsaturated air. The conclusion is that $\gamma^{(AB)}$ is independent of the particular n-alkane being considered. From (3.86) and (3.88), we conclude that

$$\gamma^{(AC)} \cos \Theta_0 = \gamma^{(AB)} - [\gamma^{(AB)} + \gamma^{(AC)} - 2(\gamma^{(AB)}\gamma^{(AC)})^{1/2}] \quad (3.89)$$

or

$$\cos \Theta_0 = -1 + 2 \left(\frac{\gamma^{(AC)}}{\gamma^{(AB)}} \right)^{1/2} \quad (3.90)$$

As the alkane number n is decreased, there is a limiting value at which spontaneous wetting occurs, and $\Theta_0 = \Theta^{(\text{stat})} = 0$ and $\gamma^{(AB)} = \gamma^{(AC)}$. In this way, Zisman (1962, p. 190) [see also Zisman 1964, p. 20] concluded that

$$\gamma^{(AB)} = 18.5 \text{ mN/m} \quad (3.91)$$

Working with different liquids on PTFE, Owens and Wendt (1969) came to the same conclusion.

Table II.: Comparison of calculation and experimental data of static contact angle $\Theta^{(\text{stat})}$ for n-Alkanes on PTFE.

n-Alkanes	$\gamma^{(AC)}$	$\delta^{(BC)^a}$	$A^{(BC)^b}$	$A^{(CC)^b}$	$\Theta^{(\text{cal})^c}$	$\Theta^{(\text{cal})^d}$	$\Theta^{(\text{cal})^e}$	$\Theta^{(\text{exp})^f}$
	mN/m	\AA	$10^{-20} J$	$10^{-20} J$	$Deg.$	$Deg.$	$Deg.$	$Deg.$
Heptane	20.3	3.097	4.03	4.31	29.1	26.0	20.0	21.0
Octane	21.8	3.085	4.11	4.49	33.5	33.7	28.2	26.0
Nonane	22.9	3.073	4.18	4.66	36.9	38.0	32.3	32.0
Decane	23.9	3.067	4.25	4.81	39.8	41.4	35.5	35.0
Undecane	24.7	3.061	4.28	4.87	40.7	43.8	38.1	39.0
Dodecane	25.4	3.056	4.35	5.03	43.1	45.8	39.6	42.0
Tetradecane	26.7	3.050	4.38	5.09	44.1	49.0	43.3	44.0
Hexadecane	27.6	3.044	4.43	5.22	45.8	51.1	45.1	46.0

a) Calculated by (3.92).

b) Provided by Hough and White (1980).

c) Calculated by Hough and White (1980).

d) Calculated using Young's equation (3.86), replacing Θ_0 by $\Theta^{(\text{stat})}$ as in the common use of Young's equation.

e) Calculated by (3.87).

f) Measured by Fox and Zisman (1950).

In their analysis of supercritical adsorption of argon and krypton on impermeable

carbon spheres, Fu et al. (2004) chose δ as the position at which attractive and repulsive forces between the carbon and the gas, as described by a two-point Leonard-Jones potential, were balanced and $\Phi^{(f,corr)} = 0$. Here we can not do exactly the same thing, because our two-point potentials include only attractive forces. However, their approach inspires us to use a hard-sphere repulsion, estimating $\delta^{(BC)}$ as the apparent radius of the repeating $-CH_2-$ groups in the n -alkanes immediately adjacent to the PTFE (planar) surface. In estimating the apparent radius of the $-CH_2-$ groups, we will assume that they are spheres in hexagonal close packing on the PTFE plane:

$$\delta^{(BC)} = 1.062 [M^{(C)} / (\rho^{(C)} n_u N)]^{1/3} \quad (3.92)$$

Here $M^{(C)}$ is the molecular weight of phase C , $\rho^{(C)}$ is the mass density of phase C , n_u is the number of repeating units in the molecule, and N is Avogadro's number.

Table II compares our calculation with experimental data and a previous theory. We get excellent agreement for all the n -alkanes while Hough and White (1980) only did well for alkanes with large carbon number.

Table III shows the good results for another system: A is air, B is PDMS and C is one of the dispersive liquids. The calculated results are still from (3.87). The experimental data are from different sources (Chaudhury and Whitesides, 1991; Baier and Meyer, 1992; Bowers and Zisman, 1964).

5. Young's equation

Commonly in the literature, Young's equation is written as

$$\gamma^{(AC)} \cos \Theta^{(stat)} = \gamma^{(AB)} - \gamma^{(BC)} \quad (3.93)$$

and applied at the apparent common line (as seen with $10\times$ magnification). Tables II and III demonstrate that (3.93) does not represent the experimental measurements

of $\Theta^{(\text{stat})}$ well.

Slattery (1990, p. 169) derives Young's equation as (3.86), and applies it at the true common line as we do here. Equation (3.87), which was developed using (3.86), represents the experimental data in tables II and III much better than does (3.93). Our conclusion is that (3.86) is the preferred form of Young's equation.

Table III.: Comparison of calculation and experimental data of static contact angle $\Theta^{(\text{stat})}$ for dispersive liquids on PDMS.

liquids	$\gamma^{(AC)}$	$\delta^{(BC)^a}$	$A^{(BC)^b}$	$A^{(CC)^b}$	$\Theta^{(\text{cal})^c}$	$\Theta^{(\text{cal})^d}$	$\Theta^{(\text{exp})}$
	mN/m	\AA	$10^{-20}J$	$10^{-20}J$	<i>Deg.</i>	<i>Deg.</i>	<i>Deg.</i>
diiodomethane	50.8	3.178	5.57	7.18	71.9	66.8	70.0 ^e
bromonaphalene	44.4	2.497	5.05	5.93	66.4	61.0	62.0 ^f
methylnaphthalene	39.8	2.378	4.80	5.35	61.3	50.5	52.0 ^f
<i>tert</i> -butyl naphthalene	33.7	3.384	4.76	5.23	52.5	50.1	49.0 ^g
liq. paraffin	32.4	3.139	5.15	6.03	50.2	44.5	40.0 ^e
Hexadecane	27.6	3.044	4.80	5.22	38.6	34.4	36.0 ^g

a) Calculated by (3.92).

b) Provided by Drummond and Chan (1997).

c) Calculated using Young's equation (3.86), replacing Θ_0 by $\Theta^{(\text{stat})}$ as in the common use of Young's equation.

d) Calculated by (3.87).

e) Measured by Chaudhury and Whitesides (1991).

f) Measured by Baier and Meyer (1992).

g) Measured by Bowers and Zisman (1964).

CHAPTER IV

THE APPLICATION ON A MODE I NANOSCALE FRACTURE PROBLEM

A. Introduction

Understanding the fracture characteristics of semiconductor materials is crucial to modelling the mechanical response of them. The difficulties, both in experimental and theoretical fields, are obvious that the size of semiconductor materials are approaching nanoscale. There is a large and growing literature devoted to modelling and simulating fracture via atomistic simulation, molecular dynamics or lattice dynamics methods (Fineberg et al., 1991; Marder and Gross, 1995; Abraham et al., 1997, 1998; Holland and Marder, 1998; Slepyan et al., 1999; Abraham and Gao, 2000; Abraham, 2001; Swadener et al., 2002). Can continuum mechanics provide models capable of predicting or simulating nanoscale fracture problems? The work presented in this chapter is meant to answer this question. Usually linear elastic fracture mechanics (LEFM) is assumed to be only applicable to linear elastic materials under quasistatic conditions. This classical theory, which originates from works of Griffith (1921); Williams (1957); Westergaard (1939); Irwin (1958), predicts an infinite stress at the crack tip.

Barenblatt (1962) and Dugdale (1960) introduced so-called cohesive zone model. Compressional cohesive stresses are distributed over a small region near the crack tip. The cohesive zone has its own constitutive equations which is often determined arbitrarily. Gurtin (1979) introduced thermodynamics into the cohesive zone models. Since then, cohesive zone models have been developed and applied to a variety of fracture problems (Schapery, 1975; Knauss, 1993; Costanzo and Allen, 1995; Hui et al., 1987; Costanzo and Walton, 1997). Eringen (1972) developed the nonlocal continuum

theory and applied it to some crack problems (Eringen et al., 1977; Eringen, 1981; Ari and Eringen, 1983). In the approach of nonlocal continuum theory, the stress at a point is influenced by the strain field at all points of the body. By using proper nonlocal kernel and boundary conditions, stress singularities at the crack tip does not exist. Other non-elastic models have also been proposed to reduce stress singularities such as plastic zone (Irwin, 1961) in last several decades.

This continuum approach to nanoscale fracture modelling is based upon a new theory of extension of continuum mechanics to the nanoscale (Slattery et al., 2004). In the immediate neighborhood of a phase interface, material behavior differs from that observed at some distance from the interface. All (local) descriptions of material behavior at some distance from the interface are based upon the assumption that the material extends to “infinity” (perhaps 100 nm) in all directions. Material points outside the immediate neighborhood of the interface are subjected to intermolecular forces only from one phase. Material points within the immediate neighborhood of a phase interface are subjected to intermolecular forces from both phases. Intermolecular forces are taken into account with an appropriate bulk description for material behavior. An unusual aspect of this approach is that it proves more convenient to linearize the equations of elasticity about the deformed configuration in which the crack is open. This is in contrast to classical linear elastic fracture mechanics in which the linearization is relative to a reference configuration with the crack modelled as a virtual, unopened slit. In particular, it is more convenient to discuss the correction to bulk stress-deformation in the deformed frame than in the undeformed frame.

Oh et al. (2005) has presented an analysis by assigning variable surface energy γ to the interfaces which represents the correction of intermolecular forces in the immediate neighborhood of interfaces. Here we present a similar analysis with a crucial difference: constant surface energies are assigned to the interfaces. In the

discussion of results, we will not only compare this analysis with the work of Oh et al. (2005) but also show the perspective on the analogy of this analysis with cohesive zones model.

B. A modified version of the theory

Since the theory in Chapter III has been developed, we have understood more about interfacial surfaces. To explain things better, I put the modified version of the theory here. Five descriptions of a material interface are introduced:

- i) The most realistic view of an interface is as a thin, three-dimensional region. There is a smooth transition of the material's density and stress-deformation behavior through this interfacial region from one phase to the other. Because it is so thin, it is extremely difficult to study experimentally the material's behavior in the interfacial region, except as the critical point is approached (Hein, 1914; Winkler and Maass, 1933; Maass, 1938; McIntosh et al., 1939). With this point of view, $\rho^{(I)}$, $\mathbf{v}^{(I)}$ and $\mathbf{T}^{(I)}$ denote the true interfacial density, velocity and stress tensor in the interfacial region.
- ii) In the second view, we recognize that, since we have no way of knowing the true material behavior of the interfacial region, we will use bulk descriptions of material behavior corrected for the effects of long-range intermolecular forces from the adjacent phases. By $\rho^{(I,bulk)}$, $\mathbf{v}^{(I,bulk)}$ and $\mathbf{T}^{(I,bulk)}$, we indicate the density, velocity and stress tensor observed with this point of view.

Note that with this point of view, the interface is three-dimensional as in view (i). Consistent with view (i), one assumes that $\mathbf{T}^{(I,bulk)}$ is a continuous function of position, even though the description of stress-deformation behavior is discontinuous.

For the sake of simplicity and clarity, we focus on quasi-static systems and ignore effects of gravity. With this point of view, the differential momentum balance reduces to

$$\begin{aligned} \operatorname{div} \mathbf{T}^{(I,bulk)} + \mathbf{b}^{(corr)} &= \operatorname{div} (\mathbf{T}^{(I,bulk)} - \Phi^{(A,corr)}) \\ &= 0 \end{aligned} \quad (4.1)$$

where $\mathbf{T}^{(I,bulk)}$ is described by bulk material behavior and $\mathbf{b}^{(corr)}$ is the body force per unit volume introduced to correct for the use of bulk material behavior in the interfacial region. For a body containing a fracture as shown in Figure 19,

$$\begin{aligned} \mathbf{b}^{(A,corr)} &= \nabla \int_{R^{(C)}} n^{(A)2} \phi^{(A,A)} d\mathbf{r} \\ &= -\nabla \Phi^{(A,corr)} \end{aligned} \quad (4.2)$$

in which

$$\Phi^{(A,corr)} \equiv - \int_{R^{(C)}} n^{(A)2} \phi^{(A,A)} d\mathbf{r}. \quad (4.3)$$

Here $\phi^{(A,A)}$ is the potential energy between the point at which $\Phi^{(A,corr)}$ is defined and any point in the region $R^{(C)}$, and $n^{(A)}$ is the number density (number of molecules or atoms per unit volume).

- iii) In the third view, the interfacial region is described by a two-dimensional dividing surface. The effects of long-range intermolecular forces are taken into account by introducing *excess quantities*, such as a surface tension or energy γ , in the dividing surface (Slattery, 1990, Secs. 1.3.5 and 2.1.6). The dividing surface now becomes a two-dimensional representation of the interface.

Again ignoring inertial and gravitational effects, the differential and jump mo-

momentum balances become (Slattery, 1990, p. 152, 157)

$$\operatorname{div} \mathbf{T} = 0 \quad (4.4)$$

$$\nabla_{(\sigma)} \gamma + 2H\gamma \boldsymbol{\xi} + [\mathbf{T} \boldsymbol{\xi}] = 0 \quad (4.5)$$

where $\nabla_{(\sigma)}$ denotes a surface gradient, H is the mean curvature of the dividing surface, and $\boldsymbol{\xi}$ the unit normal to the dividing surface Σ . The boldface brackets denote the jump of the quantity enclosed across the interface between phases A and C :

$$[\mathbf{T} \boldsymbol{\xi}] \equiv A^{(A)} \boldsymbol{\xi}^{(A)} + A^{(C)} \boldsymbol{\xi}^{(C)}. \quad (4.6)$$

By ρ , \mathbf{v} and \mathbf{T} we mean the density, velocity, and stress tensor determined with this introduction of a dividing surface and excess properties.

- iv) The fourth point of view is a variation of view (ii) used only when there are two or more interfaces. In principle, view (ii) could be used for two or more interfaces. In reality, this would be difficult, because of the overlapping intermolecular forces.

We recommend as an approximation that dividing surfaces be introduced with constant values of surface tension or energy γ^∞ that correspond to static, unbounded dividing surfaces. These would be the surface tensions or energies commonly used. The correction potential $\Phi^{(A,corr)\infty}$ must of course be modified to account for these surface tensions or energies. With this point of view, the differential momentum balance becomes

$$\operatorname{div} \mathbf{T}^{(I,bulk)} - \nabla \Phi^{corr,\infty} = 0 \quad (4.7)$$

and jump momentum balance becomes

$$\nabla_{(\sigma)}\gamma + 2H\gamma\xi + [\mathbf{T}^{(I,bulk)}\xi] = 0 \quad (4.8)$$

- v) The fifth point of view is the one most commonly taken in the literature. It looks similar to view (iii), but no corrections for long-range intermolecular forces are introduced. With this point of view, $\mathbf{T} = \mathbf{T}^{(I,bulk)}$ is represented by bulk material behavior, and excess properties such as γ are determined empirically.

C. Problem statement

Figure 19 shows a static Mode I fracture with an applied stress σ_0 . The length of the fracture is specified to be a . Our objective is to solve the differential momentum balance (4.9) consistent with the jump momentum balance (4.10) and to determine both the crack configuration and the stress distribution in the solid, particularly within the immediate neighborhood of the fracture tip.

In the immediate neighborhood of a phase interface, material behavior differs from that observed at some distance from the interface. All (local) descriptions of material behavior at some distance from the interface are based upon the assumption that the material extends to “infinity” (perhaps 100 nm) in all directions. Material points outside the immediate neighborhood of the interface are subjected to intermolecular forces only from one phase. Material points within the immediate neighborhood of a phase interface are subjected to intermolecular forces from both phases. Our premise is that material behavior within the interfacial region can be represented as bulk material behavior corrected for the intermolecular forces from the adjoining phase. In particular, we recognize the equivalence of stresses and body forces (Truesdell and Toupin, 1960, p. 549).

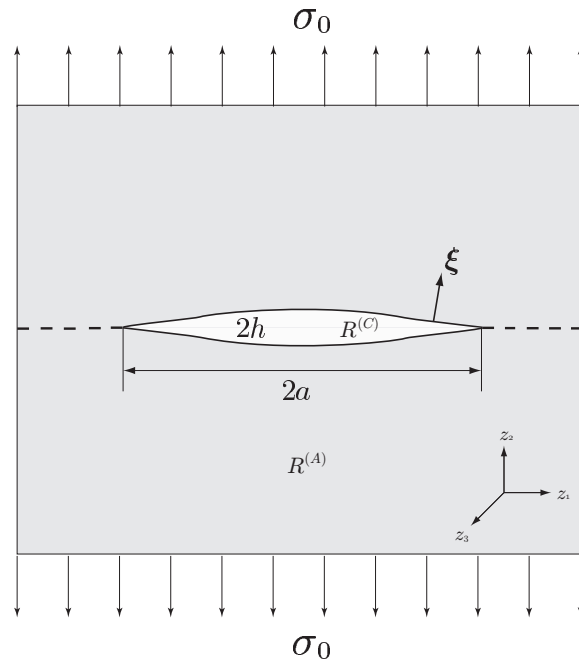


Fig. 19. Schematic of Mode I fracture of phase C in phase A .

We make several assumptions.

1. We have followed those descriptions of a material interface in Slattery et al. (2004) and Oh et al. (2005). While we will not repeat those descriptions, here we show more details of view (d) in Slattery et al. (2004)[view (v) in Oh et al. (2005)] which is used in this analysis.

We recommend as an approximation that dividing surfaces be introduced with constant values of surface tension or energy γ^∞ that correspond to static, unbounded dividing surfaces. These would be the surface tensions or energies commonly used. The correction potential $\Phi^{(A,corr)\infty}$ must of course be modified to account for these surface tensions or energies. With this point of view, the differential momentum balance becomes

$$\operatorname{div} \mathbf{T}^{(I,bulk)} - \nabla \Phi^{corr,\infty} = 0 \quad (4.9)$$

and jump momentum balance becomes

$$2H\gamma^\infty \boldsymbol{\xi} + [\mathbf{T}^{(I,bulk)} \boldsymbol{\xi}] = 0 \quad (4.10)$$

Here H is the mean curvature, $\boldsymbol{\xi}$ is the unit normal to the crack surface point into the solid.

2. We assume that the point-to-point intermolecular force potential can be represented as

$$\phi^{(A,C)} = -\frac{A^{(A,C)}}{\pi^2 n^{(A)^2 r^6} \gamma^6} \quad (4.11)$$

where $A^{(A,C)}$ is the effective, Lifshitz type, Hamaker constant (Bowen and Jenner, 1995; Lifshitz, 1956) between phases A and C . The Hamaker constants of most condensed phases are found to lie in the range of $0.4\text{--}4 \times 10^{-20}$ J (Israelachvili, 1991, p. 176).

3. The analysis is in the context of linear elasticity with assumption 1. Each crack face is regarded as a single dividing surface with a constant surface energy γ^∞ . As described in Slattery et al. (2004, Sec. 4.1), γ^∞ cannot fully account for the correction that must be made to the intermolecular forces. An additional correction $\Phi^{(A,corr)\infty}$ should be made. Two crack surfaces could be viewed as discontinuous thin films. Because a constant surface energy stands for the work to separate two materials from contact to infinity, we treat crack surfaces as

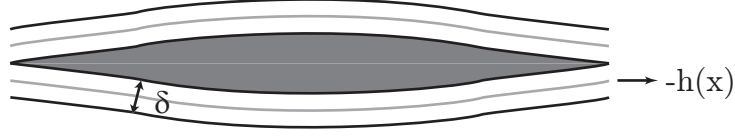


Fig. 20. δ is the distance separating the two phases A and C , corresponding physically to the sum of the effective radii of the A and C molecules or the effective distance between molecules of A and C (Slattery et al., 2004, p. 4623). The dividing surface $h(x)$ is located halfway between the two phases.

infinite continuous thin films in the computation of $\Phi^{(A,corr)\infty}$.

$$\begin{aligned} \Phi^{(A,corr)\infty} &= - \int_{R^{(A)}} \left\{ n^{(A)} n^{(C)} \phi^{(A,C)} - n^{(A)} n^{(A)} \phi^{(A,A)} \right. \\ &\quad \left. - n^{(C)^2} \phi^{(C,C)} + n^{(A)} n^{(C)} \phi^{(A,C)} \right\} d\mathbf{r} \\ &\simeq \frac{\mathcal{A}}{\pi^2} \int_{-a}^a \int_{-\infty}^{-h(x)-\delta/2} \int_{-\infty}^{\infty} \frac{1}{[(z_1 - x)^2 + (z_2 - y)^2 + z^2]^3} dz dy dx \end{aligned} \quad (4.12)$$

The first equation is derived from Slattery et al. (2004, Eq. 41). The second approximation is concluded from the asymptotic expansions executed later. Here we only write the significant contribution of $\Phi^{(A,corr)\infty}$ to simplify the expression. For the same reason, we define

$$\mathcal{A} \equiv -(2A^{(AC)} - A^{(AA)} - A^{(CC)}) \quad (4.13)$$

δ in Figure 20 is the distance separating the two phases A and C , corresponding physically to the sum of the effective radii of the A and C molecules or the effective distance between molecules of A and C (Slattery et al., 2004, p. 4623). The dividing surface $h(x)$ is located halfway between the two phases.

4. It is assumed that $T^{(I,bulk)}$ can be described by Hooke's law

$$\mathbf{T}^{(I,bulk)} = \lambda(\text{tr } \mathbf{e})\mathbf{I} + 2\mu \mathbf{e} \quad (4.14)$$

in which

$$\mathbf{e} \equiv \frac{1}{2}(\nabla \mathbf{u} + \nabla \mathbf{u}^T) \quad (4.15)$$

is the infinitesimal strain tensor, and λ and μ are Lamé constants independent of position.

5. Gravitational and inertial effects are neglected.

D. Solution

Let's introduce dimensionless variables:

$$\begin{aligned} \mathbf{u}^* &\equiv \frac{\mathbf{u}}{a}, & z_i^* &\equiv \frac{z_i}{a}, & h^* &\equiv \frac{h}{a}, & \delta^* &\equiv \frac{\delta}{a}, & \mu^* &\equiv \frac{\mu}{E}, & \lambda^* &\equiv \frac{\lambda}{E} \\ \mathcal{A}^* &\equiv \frac{\mathcal{A}}{\pi^2 E a^3} & H^* &\equiv H a & \gamma^* &\equiv \frac{\gamma^\infty}{E a} \end{aligned} \quad (4.16)$$

In terms of these dimensionless variables, the differential momentum balance (4.9) can be expressed as

$$\mu^* \Delta \mathbf{u}^* + (\lambda^* + \mu^*) \nabla \text{div } \mathbf{u}^* - \nabla \Phi^* = 0 \quad (4.17)$$

and the jump momentum balance (4.10) can be rewritten as

$$2H^* \gamma^* \boldsymbol{\xi} + \mu^* (\nabla \mathbf{u}^* + \nabla \mathbf{u}^{*T}) \boldsymbol{\xi} + \lambda^* (\text{div } \mathbf{u}^*) \boldsymbol{\xi} = 0 \quad (4.18)$$

where

$$\Phi^*(z_1^*, z_2^*) = \mathcal{A}^* \int_{-1}^1 \int_{-\infty}^{-h^*(x) - \delta^*/2} \int_{-\infty}^{\infty} \frac{1}{[(z_1^* - x^*)^2 + (z_2^* - y^*)^2 + z^{*2}]^3} dz^* dy^* dx^* \quad (4.19)$$

This expression depends upon the crack face profile $h(x)$ which is unknown á priori and must be determined as part of the problem's solution. However, two of the three iterated integrals can be evaluated in closed form using elementary techniques. In particular, one readily shows that

$$\Phi^*(z_1^*, z_2^*) = \frac{\mathcal{A}^* \pi}{4} \int_{-1}^1 \left\{ 1 - \frac{(2(h^*(x^*) + \delta^*/2) + 2z_2^*) [6(z_1^* - x^*)^2 + (2(h^*(x^*) + \delta^*/2) + 2z_2^*)^2]}{[4(z_1^* - x^*)^2 + (2(h^*(x^*) + \delta^*/2) + 2z_2^*)^2]^{3/2}} \right\} \frac{dx^*}{(z_1^* - x^*)^4} \quad (4.20)$$

We approximate the integral expression (4.20) with the assumption that $h(x)$ is locally constant. Mathematically it requires that $h(x)$ is slowly varying such that the magnitude of its derivative $|h'(x)|$ is small. Physically it means that we compute Φ^* for any point at the crack surfaces as a point at the parallel plane interfaces (Slatery et al., 2004, Sec. 4.1.1). This assumption will then be verified á posteriori for consistency. Therefore, we have the analytical expression for Φ^*

$$\Phi^*(z_1^*, z_2^*) = \mathcal{A}^* \left\{ \frac{1}{12(z_1^* - 1)^3} - \frac{1}{12(z_1^* + 1)^3} + \frac{2(z_1^* + 1)^4 + (z_1^* + 1)^2(z_2^* + h^* + \delta^*/2)^2 + 2(z_2^* + h^* + \delta^*/2)^4}{24(z_1^* + 1)^3(z_2^* + h^* + \delta^*/2)^3 \sqrt{(z_1^* + 1)^2 + (z_2^* + h^* + \delta^*/2)^2}} - \frac{2(z_1^* - 1)^4 + (z_1^* - 1)^2(z_2^* + h^* + \delta^*/2)^2 + 2(z_2^* + h^* + \delta^*/2)^4}{24(z_1^* - 1)^3(z_2^* + h^* + \delta^*/2)^3 \sqrt{(z_1^* - 1)^2 + (z_2^* + h^* + \delta^*/2)^2}} \right\} \quad (4.21)$$

1. Singular perturbation method

We seek a solution with the perturbation method. As we stated in assumption 2, Hamaker constant is very small. We choose the dimensionless Hamaker constant \mathcal{A}^* as the perturbation parameter.

When $\mathcal{A}^* = 0$, our theory demands that there must be no fracture. However, as $\mathcal{A}^* \rightarrow 0$, the solution does not approach this limit. For this reason, the perturbation

analysis performed for this problem is singular (Bush, 1992, p. 11).

Due to the singular nature of the problem, a single asymptotic expansion cannot be valid in the entire body. Thus, we develop two solutions: the *outer solution*, which represents the smoothly changing portion, and the *inner solution*, which represents the rapidly changing portion in the immediate neighborhood of crack surfaces. For the boundary conditions, we need to apply the method of matched asymptotic expansions. (Kevorkian and Cole, 1981) We force outer solution and inner solution to be identical at some point. In this analysis, it is when $y_2^{**} \rightarrow \infty$.

a. Outer solution

The outer solution corresponds to $\mathcal{A}^* = 0$, a uniaxial extension upon a body without a crack. (Soutas-Little, 1973, pp. 76, 101)

$$T_{22}^* = \sigma_0^* \quad (4.22)$$

$$u_1^* = -\frac{\lambda^*}{2\mu^*(3\lambda^* + 2\mu^*)} \sigma_0^* z_1^* \quad (4.23)$$

$$u_2^* = \frac{\lambda^* + \mu^*}{\mu^*(3\lambda^* + 2\mu^*)} \sigma_0^* z_2^* \quad (4.24)$$

where

$$T_{22}^{(I,bulk)*} \equiv \frac{T_{22}^{(I,bulk)}}{E}, \quad \sigma_0^* \equiv \frac{\sigma_0}{E}. \quad (4.25)$$

b. Inner solution

Within the immediate neighborhood of the crack surfaces (inner region), Φ^* must be preserved. This suggests that we introduce as expanded variables in this region

$$y_2^{**} \equiv \frac{z_2^* - h^*}{\mathcal{A}^{*n}} \quad (4.26)$$

$$v_2^{**} \equiv \frac{u_2^* - h^*}{\mathcal{A}^{*n}} \quad (4.27)$$

$$\delta^{**} \equiv \frac{\delta^*}{2\mathcal{A}^{*n}} \quad (4.28)$$

The exponent n is chosen in (4.35) so that the effect of the long-range intermolecular forces is retained as $\mathcal{A}^* \rightarrow 0$. Note that, with this value of n ,

$$\begin{aligned} \delta^{**} &= \frac{\delta \pi^{2/3} E^{1/3}}{2\mathcal{A}^{1/3}} \\ &= \text{constant} \end{aligned} \quad (4.29)$$

In terms of these scaled variables, the two components of the differential momentum balance (4.17) become

$$\begin{aligned} &\left\{ (\lambda^* + 2\mu^*) \frac{\partial^2 u_1^*}{\partial z_1^{*2}} + (\lambda^* + \mu^*) \frac{\partial^2 v_2^{**}}{\partial z_1^* \partial y_2^{**}} \right\} + \frac{1}{\mathcal{A}^{*2n}} \left\{ (\lambda^* + 2\mu^*) \left(\frac{dh^*}{dz_1^*} \right)^2 + \mu^* \right\} \frac{\partial^2 u_1^*}{\partial y_2^{**2}} \\ &- \frac{1}{\mathcal{A}^{*n}} \left\{ (\lambda^* + 2\mu^*) \frac{dh^*}{dz_1^*} \frac{\partial^2 u_1^*}{\partial z_1^* \partial y_2^{**}} - (\lambda^* + 2\mu^*) \frac{d^2 h^*}{dz_1^{*2}} \frac{\partial u_1^*}{\partial y_2^{**}} - (\lambda^* + \mu^*) \frac{dh^*}{dz_1^*} \frac{\partial^2 v_2^{**}}{\partial y_2^{**2}} \right\} \\ &= \frac{\partial \Phi^{**}}{\partial z_1^*} \end{aligned} \quad (4.30)$$

and

$$\begin{aligned} &\mathcal{A}^{*n} \mu^* \frac{\partial^2 v_2^{**}}{\partial z_1^{*2}} + \left\{ \mu^* \frac{d^2 h^*}{dz_1^{*2}} - \mu^* \frac{d^2 h^*}{dz_1^{*2}} \frac{\partial v_2^{**}}{\partial y_2^{**}} - 2\mu^* \frac{dh^*}{dz_1^*} \frac{\partial^2 v_2^{**}}{\partial z_1^* \partial y_2^{**}} \right\} \\ &\frac{1}{\mathcal{A}^{*n}} \left\{ (\lambda^* + 2\mu^*) \frac{\partial^2 v_2^{**}}{\partial y_2^{**2}} + \mu^* \frac{dh^*}{dz_1^*} \frac{\partial^2 v_2^{**}}{\partial y_2^{**2}} + (\lambda^* + \mu^*) \frac{\partial^2 u_1^*}{\partial z_1^* \partial y_2^{**}} \right\} \\ &- \frac{1}{\mathcal{A}^{*2n}} \left\{ (\lambda^* + \mu^*) \frac{dh^*}{dz_1^*} \frac{\partial^2 u_1^*}{\partial y_2^{**2}} \right\} = \frac{\partial \Phi^{**}}{\partial y_2^{**}} \end{aligned} \quad (4.31)$$

We have assumed that h^* is slowly varying, permitting us to neglect both the first and second derivatives of h^* over z_1^* . We can work on the simplified form of (4.30) and (4.31)

$$\mathcal{A}^{*-2n} \mu^* \frac{\partial^2 u_1^*}{\partial y_2^{**2}} + (\lambda^* + 2\mu^*) \frac{\partial^2 u_1^*}{\partial z_1^{*2}} + (\lambda^* + \mu^*) \frac{\partial^2 v_2^{**}}{\partial z_1^* \partial y_2^{**}} = \frac{\partial \Phi^{**}}{\partial z_1^*} \quad (4.32)$$

and

$$\mathcal{A}^{*2n} \mu^* \frac{\partial^2 v_2^{**}}{\partial z_1^{*2}} + \mathcal{A}^{*n} \mu^* \frac{\partial^2 h^*}{\partial z_1^{*2}} + (\lambda^* + 2\mu^*) \frac{\partial^2 v_2^{**}}{\partial y_2^{**2}} + (\lambda^* + \mu^*) \frac{\partial^2 u_1^*}{\partial z_1^* \partial y_2^{**}} = \frac{\partial \Phi^{**}}{\partial y_2^{**}}. \quad (4.33)$$

Here

$$\begin{aligned} \Phi^{**}(z_1^*, y_2^{**}) = & \mathcal{A}^{*1-3n} \left\{ \frac{(\mathcal{A}^*)^{3n}}{12(z_1^* - 1)^3} - \frac{(\mathcal{A}^*)^{3n}}{12(z_1^* + 1)^3} \right. \\ & + \frac{2(z_1^* + 1)^4 + (\mathcal{A}^*)^{2n}(z_1^* + 1)^2(y_2^{**} + 2h^{**} + \delta^{**})^2 + 2(\mathcal{A}^*)^{4n}(y_2^{**} + 2h^{**} + \delta^{**})^4}{24(z_1^* + 1)^3(y_2^{**} + 2h^{**} + \delta^{**})^3 \sqrt{(z_1^* + 1)^2 + (\mathcal{A}^*)^{2n}(y_2^{**} + 2h^{**} + \delta^{**})^2}} \\ & \left. - \frac{2(z_1^* - 1)^4 + (\mathcal{A}^*)^{2n}(z_1^* - 1)^2(y_2^{**} + 2h^{**} + \delta^{**})^2 + 2(\mathcal{A}^*)^{4n}(y_2^{**} + 2h^{**} + \delta^{**})^4}{24(z_1^* - 1)^3(y_2^{**} + 2h^{**} + \delta^{**})^3 \sqrt{(z_1^* - 1)^2 + (\mathcal{A}^*)^{2n}(y_2^{**} + 2h^{**} + \delta^{**})^2}} \right\} \end{aligned} \quad (4.34)$$

If the contribution of Φ^{**} in (4.32) and (4.33) is to be the same order of magnitude as the other terms when $\mathcal{A}^* \rightarrow 0$, we must identify

$$n = \frac{1}{3} \quad (4.35)$$

In view of (4.35), equations (4.32) and (4.33) reduce to

$$\frac{\partial^2 u_1^*}{\partial y_2^{**2}} = 0 \quad (4.36)$$

$$(\lambda^* + 2\mu^*) \frac{\partial^2 v_2^{**}}{\partial y_2^{**2}} + (\lambda^* + \mu^*) \frac{\partial^2 u_1^*}{\partial z_1^* \partial y_2^{**}} = \frac{\partial \Phi^{**}}{\partial y_2^{**}} \quad (4.37)$$

Equations (4.36) and (4.37) are satisfied with

$$u_1^* = a(z_1^*)y_2^{**} + b(z_1^*) \quad (4.38)$$

and

$$(\lambda^* + 2\mu^*)v_2^{**} = \int \Phi^{**} dy_2^{**} + f(z_1^*)y_2^{**} - \frac{\lambda^* + \mu^*}{2} \frac{\partial a(z_1^*)}{\partial z_1^*} y_2^{**2} + g(z_1^*) \quad (4.39)$$

Functions $a(z_1^*)$, $b(z_1^*)$, $f(z_1^*)$ and $g(z_1^*)$ can be obtained using the boundary conditions.

On the crack surfaces, the two components of (4.18) are expressed in terms of y_2^* and v_2^*

$$\begin{aligned} \frac{\partial^2 h^*}{\partial z_1^{*2}} \left\{ 1 + \left(\frac{\partial h^*}{\partial z_1^*} \right)^2 \right\}^{-\frac{3}{2}} \gamma^* \left(\frac{\partial h^*}{\partial z_1^*} \right) + \left[(\lambda^* + 2\mu^*) \frac{\partial u_1^*}{\partial z_1^*} + \lambda^* \frac{\partial v_2^*}{\partial y_2^*} \right] \left(- \frac{\partial h^*}{\partial z_1^*} \right) \\ + \mu^* \left[\frac{\partial v_2^*}{\partial z_1^*} + \frac{\partial h^*}{\partial z_1^*} + \frac{\partial u_1^*}{\partial y_2^*} \right] = 0 \end{aligned} \quad (4.40)$$

and

$$\begin{aligned} \frac{\partial^2 h^*}{\partial z_1^{*2}} \left\{ 1 + \left(\frac{\partial h^*}{\partial z_1^*} \right)^2 \right\}^{-\frac{3}{2}} \gamma^* + \mu^* \left[\frac{\partial v_2^*}{\partial z_1^*} + \frac{\partial h^*}{\partial z_1^*} + \frac{\partial u_1^*}{\partial y_2^*} \right] \left(- \frac{\partial h^*}{\partial z_1^*} \right) \\ + \left[(\lambda^* + 2\mu^*) \frac{\partial v_2^*}{\partial y_2^*} + \lambda^* \frac{\partial u_1^*}{\partial z_1^*} \right] = 0 \end{aligned} \quad (4.41)$$

In terms of y_2^{**} and v_2^{**} , these become

$$\frac{\partial u_1^*}{\partial y_2^{**}} = 0 \quad (4.42)$$

and

$$\frac{\partial^2 h^*}{\partial z_1^{*2}} \gamma^* + \left\{ 1 + \left(\frac{\partial h^*}{\partial z_1^*} \right)^2 \right\}^{\frac{3}{2}} \left\{ -\mu^* \left(\frac{\partial h^*}{\partial z_1^*} \right)^2 + \left[(\lambda^* + 2\mu^*) \frac{\partial v_2^{**}}{\partial y_2^{**}} + \lambda^* \frac{\partial u_1^*}{\partial z_1^*} \right] \right\} = 0 \quad (4.43)$$

As y_2^{**} approaches infinity, the body force correction term will disappear and we also require that the inner solutions given as (4.38) and (4.39) should approach

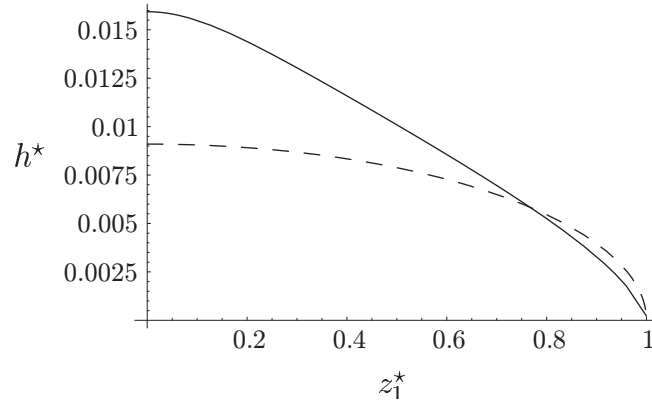


Fig. 21. Dimensionless crack configurations h^* (the solid curve) for $\delta^* = 0.02$ and $\delta^{**} = 2.50$. Here we have used $E = 100$ GPa, $\delta = 0.2$ nm (Israelachvili, 1973, 1991; Slattery et al., 2004), $a = 10$ nm, and $\mathcal{A} = 2\pi \times 10^{-20}$ J (Hough and White, 1980; Israelachvili, 1991; Slattery et al., 2004). The dash lines represent results from classical linear elastic fracture mechanics.

asymptotically the corresponding solutions in the outer region:

$$\text{as } y_2^{**} \rightarrow \infty : \quad u_1^* \rightarrow -\frac{\lambda^*}{2\mu^*(3\lambda^* + 2\mu^*)} \sigma_0^* z_1^* \quad (4.44)$$

$$T_{22}^* \rightarrow \sigma_0^* \quad (4.45)$$

$$\Phi^{**} \rightarrow 0 \quad (4.46)$$

In view of (4.42), (4.44), (4.45) and (4.46), we have

$$a(z_1^*) = 0 \quad (4.47)$$

$$b(z_1^*) = -\frac{\lambda^*}{2\mu^*(3\lambda^* + 2\mu^*)} \sigma_0^* z_1^* \quad (4.48)$$

$$f(z_1^*) = \sigma_0^* \left[1 + \frac{\lambda^{*2}}{2\mu^*(3\lambda^* + 2\mu^*)} \right] \quad (4.49)$$

so that the inner solutions given as (4.38) and (4.39) become

$$u_1^* = -\frac{\lambda^*}{2\mu^*(3\lambda^* + 2\mu^*)} \sigma_0^* z_1^* \quad (4.50)$$

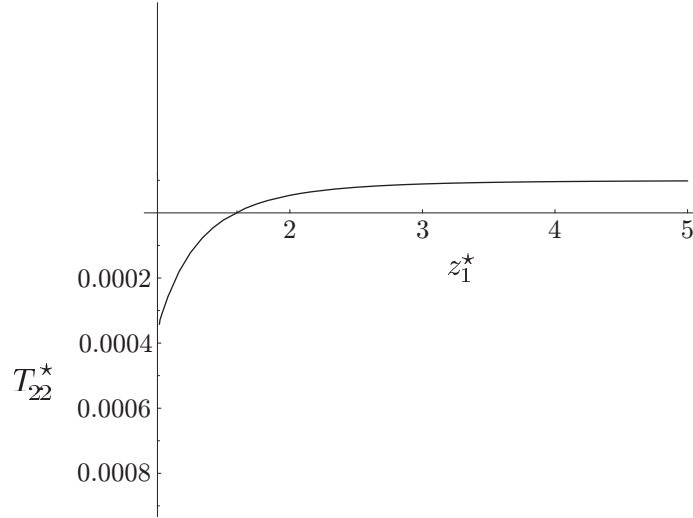


Fig. 22. Dimensionless stress distribution T_{22}^* on the fracture axis for $\delta^* = 0.02$ and $\delta^{**} = 2.50$. Here we have used $E = 100$ GPa, $\delta = 0.2$ nm (Israelachvili, 1973, 1991; Slattery et al., 2004), $a = 10$ nm, and $\mathcal{A} = 2\pi \times 10^{-20}$ J (Hough and White, 1980; Israelachvili, 1991; Slattery et al., 2004);

and

$$(\lambda^* + 2\mu^*)v_2^{**} = \int \Phi^{**} dy_2^{**} + \sigma_0^* \left[1 + \frac{\lambda^{*2}}{2\mu^*(3\lambda^* + 2\mu^*)} \right] y_2^{**} + g(z_1^*) \quad (4.51)$$

Using (4.50) and (4.51), we express the stress in inner region as

$$\begin{aligned} T_{22}^* &\equiv (\lambda^* + 2\mu^*) \frac{\partial v_2^{**}}{\partial y_2^{**}} + \lambda^* \frac{\partial u_1^*}{\partial z_1^*} \\ &= \Phi^{**} + \sigma_0^* \end{aligned} \quad (4.52)$$

Substituting (4.50) and (4.51) into (4.43), we will have

$$\frac{\partial^2 h^*}{\partial z_1^{*2}} \gamma^* + \left\{ 1 + \left(\frac{\partial h^*}{\partial z_1^*} \right)^2 \right\}^{\frac{3}{2}} \left\{ \sigma_0^* - \mu^* \left(\frac{\partial h^*}{\partial z_1^*} \right)^2 + \Phi^{**} \right\} = 0 \quad (4.53)$$

We can obtain configurations of crack surfaces from Equation (4.53). Since this is a

second-order differential equation, we need two boundary conditions as follows:

$$\text{at } z_1^* = 0 : \quad \frac{\partial h^*}{\partial z_1^*} = 0 \quad (4.54)$$

$$\text{at } z_1^* = 1 : \quad h^* = \delta^*/2 \quad (4.55)$$

The first reflects symmetry with respect to the crack surface. At the crack tip, there is only a separation distance between two crack surfaces.

E. Discussion

Figure 21 shows the dimensionless crack configuration for some given situation. Figure 22 shows the dimensionless stress distribution around the crack tip.

The results developed here are similar to those presented by Oh et al. (2005) with one important exception. Oh et al. (2005) show that the stress in the immediate neighborhood of the fracture tip is tensile, which is physically appealing. Figure 22 indicates that it is compressive. Oh et al. (2005) take the view that all of the correction of the long-range intermolecular forces are counted into variable surface energies. In this analysis, the correction of the long-range intermolecular forces are divided into constant surface energy and an additional correction.

The compressive stress distribution around crack tip leads us to compare the analysis with cohesive zone model. We consider that constant surface energy overestimate the contribution of intermolecular forces to cause the compressional stresses around crack tip.

Also, the assumption of constant surface energy gives us an advantage to compute energy release rate which follows the definition of Griffith (1921). Energy release rate is the partial derivative of the total potential energy with respect to the crack length.

In the future, we could study the interfacial crack problems possibly with com-

puting body force correction potential from molecular-based theories.

CHAPTER V

DISCUSSION OF RETARDED DISPERSION FORCES AND ITS APPLICATION
TO THE COALESCENCE PROBLEM

A. Retarded dispersion forces

Hamaker (1937) proposed explicit calculations of dispersion forces with assumption of pairwise additivity. But this simple theory fails at many situations, such as for condensed material. The continuum theory proposed by Lifshitz (1956) accounts many-body effects and predicts dispersion forces better for most systems. The difficulty for continuum theory is to employ methods of quantum electrodynamics and involve complicate numerical computations.

The most attractive feature of Hamaker's theory is the separation of the geometry and material property for potential which could be expressed as $\phi = f(r)g(\lambda)$. $f(r)$ represents the geometry and $g(\lambda)$ represents material property including wavelength, dielectric constant and so on.

To find a most suitable method for engineering applications, we need to consider accuracy, physical properties available and demand on computation. So, an approximation by using an effective Hamaker constant which is based on Lifshitz's continuum theory and Hamaker's geometric factor would meet the engineering requirement. Details could be found in Hough and White (1980) about how Hamaker constant includes all the material property. For many practical systems, Hamaker's approach is good enough when a calculated effective Hamaker constant based on Lifshitz' theory is applied.

As we described earlier, London van der Waals force is a function of $1/r^6$. But when the distance between two molecules is large enough, the time for electromagnetic

radiation to propagate between molecules becomes comparable to the lifetime of the fluctuating dipoles. The result is that the attraction is relatively weaker than it is at short distances and mathematically this results in a more rapid decrease with distance. This is called the retardation effect. Occasionally, it is called allowance for electromagnetic lag (Zimon, 1982).

Casimir and Polder (1948) are the first one to prescribe retardation effect with a monotonically decreasing correction factor. Hence, the attractive energy is ultimately a function of $1/r^{-7}$ instead of $1/r^{-6}$.

There are two different approaches to compute and introduce the retarded Hamaker constant in the use of Hamaker's theory.

Russel et al. (1989) and Mahanty and Ninham (1976) used same geometric factor $1/r^6$ as Hamaker did in non-retarded case while they proposed a different way to compute retarded Hamaker constant $A^{(eff)}$. The expression of $A^{(eff)}$ (Russel et al., 1989, p.154) includes a dimensionless correction factor which reflects that interaction energy decays more rapidly due to retardation effect. Hence, $A^{(eff)}$ has the same unit with non-retarded Hamaker constant in the context of this approach.

A different approach was proposed by Zimon (1982) and Görner and Pich (1989). Instead of using $1/r^6$ in non-retarded case, they used different geometric factor $1/r^7$ in retarded case. Görner and Pich (1989) stated that non-retarded Hamaker constant and retarded Hamaker constant have different units and gave the relationship between each other.

$$B_{(retarded)} = \frac{2.45A_{(non-retarded)}\lambda}{40\pi^2} \quad (5.1)$$

in which λ is the London wavelength of the material. In our analysis, it will be treated as an adjustable parameter.

In the following, we revisited the coalescence problem (Chen and Slattery, 1982; Chen et al., 1984; Hahn et al., 1985). While many researchers proclaim that retarded Hamaker constant is never truly constant but decreases progressively as distance increases, we have shown the agreement with experimental data that a constant could be used for computing retarded forces.

B. A review of coalescence

The rate at which drops or bubbles, suspended in a liquid, coalesce is important to the preparation and stability of emulsions, of foams, and of dispersions; to liquid–liquid extractions; to the formation of an oil bank during the displacement of oil from a reservoir rock; to mineral flotation.

On a smaller scale, when two drops (or bubbles) are forced to approach one another in a liquid phase or when a drop is driven through a liquid phase to another liquid surface, a thin liquid film forms between the two interfaces and begins to drain. As the thickness of the draining film becomes sufficiently small (about 100 nm), the effects of the correction for intermolecular forces and of electrostatic double-layer forces become significant. Depending upon the sign and the magnitude of the disjoining pressure attributable to the correction for intermolecular forces and the repulsive force of electrostatic double-layer forces, there may be a critical thickness at which the film becomes unstable, ruptures and coalescence occurs. (See Chapter III Section D for the definition of the disjoining pressure.) Ultimately we want to obtain the coalescence time at which the film thickness at the rim goes to zero.

Hartland (1969) developed a more detailed model for the evolution of the thinning film assuming that the shape of the drop beyond the rim did not change with time and that the configuration of the fluid–fluid interface at the center was a spherical

cap. He proposed that the initial film profile be taken directly from experimental data.

Hartland and Robinson (1977) assumed that the fluid–fluid interface consists of two parabolas, the radius of curvature at the apex varying with time in the central parabola and a constant in the peripheral parabola. *A priori* knowledge was required of the radial position outside the dimple rim at which the film pressure equaled the hydrostatic pressure.

For the case of a small spherical drop or bubble approaching a solid plane, the development of Lin and Slattery (1982b) is an improvement over those of Hartland (1969) and of Hartland and Robinson (1977).

Lin and Slattery (1982a) developed a more complete hydrodynamic theory for the thinning of a liquid film between a small, nearly spherical drop and a fluid–fluid interface that included an *a priori* estimate of the initial profile. Their theory is in reasonable agreement with data of Woods and Burrill (1972), Burrill and Woods (1973b), and Liem and Woods (1974) for the early stage of thinning in which any effects of London–van der Waals forces and of electrostatic forces generally can be neglected.

When the thickness of the draining film becomes sufficiently small (about 1000 \AA), the effects of the London–van der Waals forces and of electrostatic double-layer forces become significant. Depending upon the properties of the system and the thickness of the film on the solid, the London–van der Waals forces can contribute either a positive or negative component to the disjoining pressure (Dzyaloshinskii et al., 1961; Sonntag and Strenge, 1972; Blake, 1975). A positive disjoining pressure will slow the rate of thinning at the rim and stabilize the thinning film. A negative disjoining pressure will enhance the rate of thinning at the rim and destabilize the film. At this moment, we neglect electrostatic double-layer forces.

When London–van der Waals forces were dominant, with time the film either ruptures or becomes flat. Platikanov (1964) and Blake (1975) showed experimentally that a positive London–van der Waals disjoining pressure can be responsible for the formation of a flat, equilibrium wetting film on a solid surface.

When the contribution to the disjoining pressure of the London–van der Waals forces negative, the dimpled film always ruptures, and the rupture thickness decreases with increasing electrolyte concentration (Blake and Kitchener, 1972; Aronson and Princen, 1975; Schulze, 1975).

Jain and Ruckenstein (1976, Ruckenstein and Jain, 1974) studied the stability of an unbounded, stagnant, plane, liquid film. Jain and Ivanov (1980) considered a ring-shaped film. Their results suggest that the critical thickness decreases as the rim radius increases and as the width of the ring decreases. Blake and Kitchener (1972) found experimentally that films of smaller diameter were more stable to ambient vibrations than larger films.

Williams and Davis (1982) included the effects of the London–van der Waals forces in studying the evolution of an unbounded static film subjected to sinusoidal initial disturbances.

Buevich and Lipkina (1978) have extended their results for a dimpled thinning film to include the effects of London–van der Waals forces. They studied the thinning rate only at the rim. They found that the rim thickness can reach zero in a finite time. Although they did not mention it explicitly, this is true only for a negative disjoining pressure.

Chen and Slattery (1982) have extended the development of Lin and Slattery (1982b) for dimpled films to include the effects of the London–van der Waals forces as a small spherical drop or bubble approaches a solid plane. When the disjoining pressure is negative, there is a critical film thickness at the rim at which the film begins to

thin rapidly, leading to the rupture of the film and coalescence. Unfortunately, there are no experimental data with which to compare their predicted coalescence time, the time during which a small drop or bubble appears to rest at a phase interface before it coalesces under the influence of London–van der Waals forces. The inclusion of a positive disjoining pressure results in better descriptions of the film profiles measured by Platikanov (1964) for air bubbles pressed against glass plates.

Li and Slattery (1991) have extended these developments to the problem of attachment (coalescence) of a solid sphere to a bubble, including the effects of electrostatic forces as well as London–van der Waals forces. This is the central problem in mineral flotation (Evans, 1954; Laskowski and Kitchener, 1969; Derjaguin et al., 1984; Fuerstenau and Urbina, 1987).

For a drop or bubble forced to approach its homophase, the contribution of the London–van der Waals forces to the disjoining pressure is always negative. The effect is to enhance the rate of thinning at the rim and destabilize the film. This effect becomes significant, when the film thickness is of the order of 100 nm and increases with decreasing film thickness. When the film thickness at the rim is sufficiently small, the magnitude of the disjoining pressure becomes sufficiently large that the film ruptures at the rim.

Burrill and Woods (1973b,a) studied experimentally the coalescence of small oil drops at an interface between oil and aqueous solution of sodium lauryl sulfate and KCl. They observed that nearly all of the films ruptured at the rim and that the rim thickness at which rupture occurred was between 30 and 50 nm (Burrill and Woods, 1973b).

For a single-component system (clean or in the absence of surfactant), the coalescence times were very short. With the addition of a small amount of surfactant, the coalescence time normally increased dramatically. Under these conditions, the

interface could be expected to be less mobile as the result of the effect of either interfacial tension gradients or the interfacial viscosities. Alternatively, an ionic surfactant system could add a positive component to the disjoining pressure. Variations on this theme might be attributable to adsorption competition between species in a mixed surfactant system (Kitamura et al., 1988), to a complex adsorbed film of mixed surfactants (Becher, 1966; Davis and Smith, 1976), to interfacial turbulence (Lee and Tadros, 1982), or to an alteration of the disjoining pressure by the reagent system as the result of a pH change.

The effect of drop size on the coalescence time has been studied by many researchers, most of them found that the rest time increased with drop size.

Chen et al. (1984) have followed Buevich and Lipkina (1978) to obtain an expression for the rate of thinning at the rim as a bubble or drop approaches a fluid–fluid interface. For a bubble or drop approaching its homophase, the London–van der Waals disjoining pressure will be negative, leading to the development of an instability, rupture, and coalescence. Motivated by the experimental observation that rupture occurs off-center, (Charles and Mason, 1960; Burrill and Woods, 1973b), Chen et al. (1984) have constructed a linear stability analysis of this thinning equation to predict the rest time or coalescence time for a bubble at a fluid–fluid interface.

Hahn et al. (1985) have extended the development of Lin and Slattery (1982a) in providing a more complete description for the effects of the London–van der Waals forces as a small spherical drop or bubble approaches a fluid–fluid interface. The general trends predicted agree with those derived from the more approximate theory of Chen et al. (1984): the coalescence time increases as the bubble or drop diameter increases, as the viscosity of the draining film increases, as the interfacial tension decreases, as the strength of the London–van der Waals forces decreases, and as the density difference between the two phases increases. Their predicted coalescence

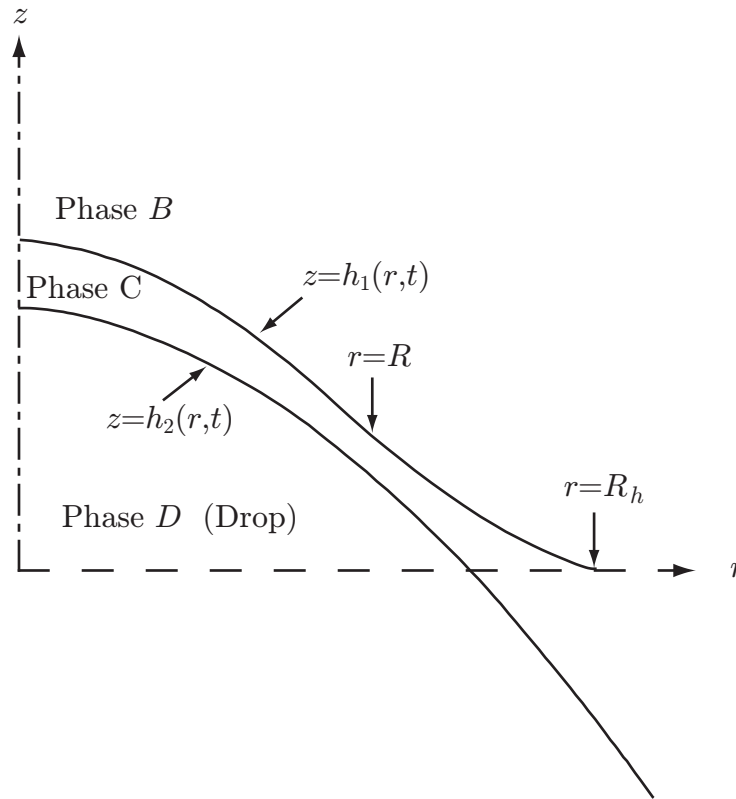


Fig. 23. A symmetric bubble (phase D) moves through a liquid (phase C) as it approaches a fluid–fluid interface (between phases C and B). The configuration of the bubble–fluid interface is given by $z = h_2(r, t)$; that of the fluid–gas interface by $z = h_1(r, t)$

times are upper bounds in the sense that they do not allow for the development of asymmetric drainage and of instabilities leading to premature rupture as observed by some experimentalists. This is also true in the observation of our own experiments. We will explain experimental results in a separate section.

C. Coalescence time

Figure 23 shows the liquid film formed as a small bubble approaches a fluid–gas interface. Our objective is to determine the coalescence time.

We make a number of assumptions.

i) Viewed in the cylindrical coordinate system of Fig. 23, the two interfaces bounding the draining liquid film are axisymmetric ($i = 1, 2$):

$$z = h_i(r, t) \quad (5.2)$$

ii) The dependence of h_i ($i = 1, 2$) upon r is sufficiently weak that

$$\left(\frac{\partial h_i}{\partial r}\right)^2 \ll 1 \quad (5.3)$$

iii) Introducing

$$h = h(r, t) \equiv h_1 - h_2 \quad (5.4)$$

let R be the rim radius of the bubble such that

$$\text{at } r = R = R(t) : \frac{\partial h}{\partial r} = 0 \quad (5.5)$$

The Reynolds lubrication theory approximation applies in the sense that, if

$$h_o \equiv h(0, 0) \quad (5.6)$$

and

$$R_o \equiv R(0) \quad (5.7)$$

we will require

$$\left(\frac{h_o}{R_o}\right)^2 \ll 1 \quad (5.8)$$

iv) There is surfactant present in both interfaces. The resulting interfacial tension gradients are sufficiently large that the tangential components of velocity \mathbf{v} are zero ($i = 1, 2$)

$$\text{at } z = h_i : \mathbf{P} \cdot \mathbf{v} = 0 \quad (5.9)$$

Here \mathbf{P} is the projection tensor that transforms every vector on an interface into its tangential components. The interfacial tension gradient required to create such an **immobile** interface is very small (Lin and Slattery, 1982b,a; Hahn et al., 1985). We will consequently assume that at the same radial positions the interfacial tensions in the two interfaces are equal. In this limit, the results developed will apply to a gas bubble approaching a gas–liquid interface, since all circulation within phases B and D in Figure 23 is suppressed.

v) The effect of mass transfer is neglected.

vi) The pressures within phases B and D are assumed to be constants.

vii) Phase C is an incompressible, Newtonian fluid, the viscosity of which is a constant.

viii) All inertial effects are neglected.

ix) The effects of gravity and of electrostatic double-layer forces are neglected within the draining film.

x) The pressure within the draining film approaches its local hydrostatic value beyond the rim where the Reynolds lubrication theory approximation (assumption iii) is still valid. At this point, ($r = R_h$), the two principal curvatures of the bubble are constants independent of time,

$$\text{at } r = R_h : \frac{\partial h}{\partial r} = \left(\frac{\partial h}{\partial r} \right)_{t=0} \quad (5.10)$$

$$\text{at } r = R_h : \frac{\partial^2 h}{\partial r^2} = \left(\frac{\partial^2 h}{\partial r^2} \right)_{t=0} \quad (5.11)$$

xii) The bubble is sufficiently small that it may be assumed to be spherical. Although it is not what we observe through the experiments, we make this assumption to reduce

mathematical difficulty. This is equivalent to assuming that the Bond number

$$N_{\text{Bo}} \equiv \frac{\Delta\rho g R_b^2}{\gamma_o} \ll 1 \quad (5.12)$$

Here

$$\Delta\rho \equiv \rho^{(B)} - \rho^{(C)} \quad (5.13)$$

is the magnitude of the density difference between the bubble phase B and the continuous phase C , g the magnitude of the acceleration of gravity, R_b the radius of the bubble, and γ_o the equilibrium interfacial tension.

xiii) Within each phase, the correction for long-range intermolecular forces is taken from Chapter III.

xiv) Because the critical film thicknesses measured or predicted by Allan et al. (1961), MacKay and Mason (1963), Vrij (1966), Ivanov et al. (1970), Burrill and Woods (1973b) are typically larger than 12 nm, we expect that the point-to-point forces are retarded as described in Section A .

In constructing this development, we will find it convenient to work in terms of these dimensionless variables:

$$\begin{aligned} r^* &\equiv \frac{r}{R_o}, & z^* &\equiv \frac{z}{h_o}, & h_i^* &\equiv \frac{h_i}{h_o}, & H_i^* &\equiv H_i R_o \quad (i = 1, 2) \\ h^* &\equiv h_1^* - h_2^*, & p^* &\equiv \frac{p^{(C)}}{\rho^{(C)} v_o^2}, & p_o^* &\equiv \frac{p_o}{\rho^{(C)} v_o^2}, & p_h^* &\equiv \frac{p_h}{\rho^{(C)} v_o^2} \\ v_r^* &\equiv \frac{v_r}{v_o}, & v_z^* &\equiv \frac{R_o v_z}{h_o v_o}, & t^* &\equiv \frac{t v_o}{R_o}, & \gamma^* &\equiv \frac{\gamma}{\gamma_o} \Phi^{(i,\text{corr})^*} \equiv \frac{\Phi^{(i,\text{corr})}}{\rho^{(C)} v_o^2} \quad i = A, B, C, \\ \mathcal{P}^* &\equiv \frac{p^{(C)} + \Phi^{(C,\text{corr})}}{\rho^{(C)} v_o^2} \mathcal{P}_o^* \equiv \frac{p_o + \Phi^{(B,\text{corr})}}{\rho^{(C)} v_o^2}, & \mathcal{P}_h^* &\equiv \frac{p_h + \Phi^{(A,\text{corr})}}{\rho^{(C)} v_o^2} \end{aligned} \quad (5.14)$$

and dimensionless Reynolds, Weber, and capillary numbers

$$N_{\text{Re}} \equiv \frac{\rho^{(C)} v_o R_o}{\mu} \quad N_{\text{We}} \equiv \frac{\rho^{(C)} v_o^2 R_o}{\gamma_o} \quad N_{\text{ca}} \equiv \frac{\mu v_o}{\gamma_o} \quad (5.15)$$

Here H_i ($i = 1, 2$) are the mean curvatures of the interfaces. The characteristic speed v_o will be defined later.

Equation (5.2) suggests that we seek a solution in which the velocity distribution takes the form

$$\begin{aligned} v_r^* &= v_r^*(r^*, z^*, t^*) \\ v_z^* &= v_z^*(r^*, z^*, t^*) \\ v_\theta^* &= 0 \end{aligned} \quad (5.16)$$

Under these circumstances, the differential mass balance for an incompressible fluid requires (Slattery, 1999, p. 50)

$$\frac{1}{r^*} \frac{\partial (r^* v_r^*)}{\partial r^*} + \frac{\partial v_z^*}{\partial z^*} = 0 \quad (5.17)$$

In the limit of assumption iii and viii, the r^* -, θ -, and z^* - components of the differential momentum balance for an incompressible, Newtonian fluid with a constant viscosity reduces to (Slattery, 1999, p. 52)

$$\frac{\partial \mathcal{P}^*}{\partial r^*} = \frac{1}{N_{\text{Re}}} \left(\frac{R_o}{h_o} \right)^2 \frac{\partial^2 v_r^*}{\partial z^{*2}} \quad (5.18)$$

$$\frac{\partial \mathcal{P}^*}{\partial \theta^*} = 0 \quad (5.19)$$

$$\frac{\partial \mathcal{P}^*}{\partial z^*} = \frac{1}{N_{\text{Re}}} \frac{\partial^2 v_z^*}{\partial z^{*2}} \quad (5.20)$$

Here we have neglected the effects of gravity within the draining liquid film (assumption ix), and we have represented the correction for long-range intermolecular forces

as described in assumption xiii. Equations (5.18) and (5.20) imply

$$\frac{\partial \mathcal{P}^*}{\partial z^*} \ll \frac{\partial \mathcal{P}^*}{\partial r^*} \quad (5.21)$$

and the dependence of \mathcal{P}^* upon z^* can be neglected. Note that the scaling argument used to neglect inertial effects (assumption viii) in arriving at (5.18) and (5.20) is presumed not to be the one ultimately used here. For this reason, we will regard the magnitude of N_{Re} and the definition of v_o to be as yet unspecified.

The jump mass balance is satisfied identically, since we define the position of the dividing surface by choosing $\rho^{(\sigma)} = 0$ and since the effect of mass transfer is neglected (assumption v).

With assumptions v and vi, the jump momentum balance for the interface between phases B and C reduces to

$$\nabla_{(\sigma)} \gamma + 2H_1 \gamma \boldsymbol{\xi} - (\mathbf{T} + p_h \mathbf{I}) \cdot \boldsymbol{\xi} = 0 \quad (5.22)$$

Here $\boldsymbol{\xi}$ is the unit normal to the interface pointing out of the liquid film. Under the conditions of assumptions ii and iii, the r - and z -components of (5.22) assume the forms at $z^* = h_1^*$

$$\frac{\partial \gamma^*}{\partial r^*} - 2 \frac{h_o}{R_o} H_1^* \gamma^* \frac{\partial h_1^*}{\partial r^*} - N_{\text{We}} \frac{h_o}{R_o} (p^* - p_h^*) \frac{\partial h_1^*}{\partial r^*} - N_{\text{ca}} \frac{R_o}{h_o} \frac{\partial v_r^*}{\partial z^*} = 0 \quad (5.23)$$

and

$$\frac{h_o}{R_o} \frac{\partial h_1^*}{\partial r^*} \frac{\partial \gamma^*}{\partial r^*} + 2H_1^* \gamma^* + N_{\text{We}} (p^* - p_h^*) - 2N_{\text{ca}} \frac{\partial v_z^*}{\partial z^*} + N_{\text{ca}} \frac{\partial v_r^*}{\partial z^*} \frac{\partial h_1^*}{\partial r^*} = 0 \quad (5.24)$$

The θ -component is satisfied identically. Adding $(h_o/R_o) (\partial h_1^*/\partial r^*)$ times (5.24) to (5.23) and recognizing assumptions ii and iii, we have

$$\text{at } z^* = h_1^* : \frac{\partial \gamma^*}{\partial r^*} - N_{\text{ca}} \frac{R_o}{h_o} \frac{\partial v_r^*}{\partial z^*} = 0 \quad (5.25)$$

so that (5.23) implies

$$\text{at } z^* = h_1^* : 2H_1^* \gamma^* + N_{\text{We}} (p^* - p_h^*) = 0 \quad (5.26)$$

In a similar fashion, we can also see that the jump momentum balance for the interface between phases C and A reduces to

$$\text{at } z^* = h_2^* : \frac{\partial \gamma^*}{\partial r^*} + N_{\text{ca}} \frac{R_o}{h_o} \frac{\partial v_r^*}{\partial z^*} = 0 \quad (5.27)$$

$$\text{at } z^* = h_2^* : 2H_2^* \gamma^* - N_{\text{We}} (p^* - p_o^*) = 0 \quad (5.28)$$

We will recognize assumptions iii and iv to say

$$\text{at } z^* = h_i^* : v_r^* = 0 \quad (i = 1, 2) \quad (5.29)$$

and we will employ (5.25) and (5.27) to calculate the interfacial tension gradient required to create the immobile interfaces assumed here.

Since we neglect the effect of mass transfer on the velocity distribution (assumption v),

$$\text{at } z^* = h_i^* : v_z^* = \frac{\partial h_i^*}{\partial t^*} + \frac{\partial h_i^*}{\partial r^*} v_r^* \quad (i = 1, 2) \quad (5.30)$$

Note that

$$\text{at } r^* = R^* : \frac{\partial h^*}{\partial r^*} = 0 \quad (5.31)$$

$$\text{at } r^* = 0 : \frac{\partial h^*}{\partial r^*} = \frac{\partial h_1^*}{\partial r^*} = 0 \quad (5.32)$$

and

$$\text{at } r^* = 0 : \frac{\partial p^*}{\partial r^*} = \frac{\partial \mathcal{P}^*}{\partial r^*} = 0 \quad (5.33)$$

Equations (5.26), (5.28), and (5.33) together with assumptions ii and iv imply

$$\begin{aligned} \text{at } r^* = 0 : \quad \frac{\partial(H_1^* - H_2^*)}{\partial r^*} &= \frac{1}{2} \frac{h_o}{R_o} \left(-\frac{1}{r^{*2}} \frac{\partial h^*}{\partial r^*} + \frac{1}{r^*} \frac{\partial^2 h^*}{\partial r^{*2}} + \frac{\partial^3 h^*}{\partial r^{*3}} \right) \\ &= 0 \end{aligned} \quad (5.34)$$

Solving for the third derivative and applying L'Hospital's rule shows us that

$$\text{at } r^* = 0 : \quad \frac{\partial^3 h^*}{\partial r^{*3}} = 0 \quad (5.35)$$

or alternatively

$$\text{at } r^* = 0 : \quad \frac{\partial^2 h^*}{\partial r^{*2}} = \frac{1}{r^*} \frac{\partial h^*}{\partial r^*} \quad (5.36)$$

According to assumption x, there is a point $r^* = R_h^* > R^*$ where the pressure p^* within the draining film approaches the local hydrostatic pressure in the neighborhood of the bubble and the effects of the London–van der Waals force disappear,

$$\text{at } r^* \rightarrow R_h^* : \quad p^* \rightarrow p_h^*, \quad h_1^* \rightarrow 0 \quad (5.37)$$

Assumption x also requires that

$$\text{at } r^* = R_h^* : \quad \frac{\partial h^*}{\partial r^*} = \left(\frac{\partial h^*}{\partial r^*} \right)_{t^*=0} \quad (5.38)$$

$$\text{at } r^* = R_h^* : \quad \frac{\partial^2 h^*}{\partial r^{*2}} = \left(\frac{\partial^2 h^*}{\partial r^{*2}} \right)_{t^*=0} \quad (5.39)$$

The initial time is to be chosen by requiring (assumption xi)

$$\text{at } t^* = 0 : \quad \frac{\partial h^*}{\partial t^*} = \text{const.} \quad (5.40)$$

Since the bubble is sufficiently small to be assumed spherical (assumption xii), the jump momentum balance requires [see (5.28)]

$$p_h^* - p_o^* = -\frac{2}{N_{We} R_b^*} \quad (5.41)$$

where R_b is the radius of the bubble. Because surface tension is assumed to be nearly independent of position by assumption iv, (5.27) implies that the effects of viscous forces can be neglected in the jump momentum balance.

An integral momentum balance for the bubble requires (for more details, see Lin and Slattery (1982b))

If

$$R_f \equiv \lim_{t \rightarrow \infty} R \quad (5.42)$$

we would expect from (5.26) and (5.28) that

$$\text{as } t^* \rightarrow \infty : p^* - p_o^* \rightarrow \frac{1}{2} (p_h^* - p_o^*) \text{ for } 0 \leq r^* \leq R_f^* \quad (5.43)$$

and from (5.37) that

$$\text{as } t^* \rightarrow \infty : p^* \rightarrow p_h^* \text{ for } r^* > R_f^* \quad (5.44)$$

Recognizing (5.41), (5.43), and (5.44), we find that (5.42) gives (Chappellear, 1961)

$$\text{as } t^* \rightarrow \infty : R^* \rightarrow R_f^* = \left(\frac{4 \Delta \rho g R_o^2}{3 \gamma_o} \right)^{1/2} R_b^{*2} \quad (5.45)$$

Given R_b , we determine R_f by requiring (5.45) to be satisfied (since R_o drops out of this equation). We identify $R_o = R_f/R_f^*$.

For the sake of simplicity, let us define our characteristic speed

$$v_o \equiv \frac{\mu}{\rho^{(C)} R_o} \quad (5.46)$$

which means

$$N_{\text{Re}} = 1, \quad N_{\text{We}} = N_{\text{ca}} = \frac{\mu^2}{\rho^{(C)} R_o \gamma_o} \quad (5.47)$$

Note that we have not used this definition for v_o or this definition for N_{Re} in scaling the Navier–Stokes equation to neglect inertial effects (assumption viii). The scaling

argument required to suggest *a priori* under what circumstances inertial effects can be ignored would be different, based perhaps on the initial speed of displacement of one of the fluid–fluid interfaces calculated at the center of the film.

Our objective in what follows is to obtain a solution to (5.17) and (5.18) consistent with (5.26), (5.28) through (5.32), (5.35) through (5.40), and the second portion of assumption xi. Given R_b , we determine R_f by requiring that, as $t^* \rightarrow \infty$ or just prior to the development of an instability and coalescence, (5.45) be satisfied; we identify $R_o = R_f/R_f^*$. Note that, in addition to physical properties, only one parameter R_b is required.

Integrating (5.18) twice consistent with (5.29), we find in view of (5.47)

$$v_r^* = \frac{1}{2} \left(\frac{h_o}{R_o} \right)^2 \frac{\partial \mathcal{P}^*}{\partial r^*} [z^{*2} - (h_1^* + h_2^*) z^* + h_1^* h_2^*] \quad (5.48)$$

Substituting (5.48) into (5.17) and integrating once, we have

$$\begin{aligned} v_z^* = & -\frac{1}{2} \left(\frac{h_o}{R_o} \right)^2 \left\{ \left[\frac{\partial^2 \mathcal{P}^*}{\partial r^{*2}} + \frac{1}{r^*} \frac{\partial \mathcal{P}^*}{\partial r^*} \right] \right. \\ & \times \left[\frac{z^{*3}}{3} - \frac{1}{2} (h_1^* + h_2^*) z^{*2} + h_1^* h_2^* z^* \right] \\ & + \frac{\partial \mathcal{P}^*}{\partial r^*} \left[- \left(\frac{\partial h_1^*}{\partial r^*} + \frac{\partial h_2^*}{\partial r^*} \right) \frac{z^{*2}}{2} \right. \\ & \left. \left. + \left(\frac{\partial h_1^*}{\partial r^*} h_2^* + h_1^* \frac{\partial h_2^*}{\partial r^*} \right) z^* \right] \right\} - C(r^*) \end{aligned} \quad (5.49)$$

in which $C(r^*)$ is an as yet undetermined function of r^* .

With (5.48) and (5.49), equation (5.30) tells us ($i = 1, 2$)

$$\begin{aligned}
-\frac{\partial h_i^*}{\partial t^*} = & \frac{1}{2} \left(\frac{h_o}{R_o} \right)^2 \left\{ \left[\frac{\partial^2 \mathcal{P}^*}{\partial r^{*2}} + \frac{1}{r^*} \frac{\partial \mathcal{P}^*}{\partial r^*} \right] \right. \\
& \times \left[\frac{1}{3} h_i^{*3} - \frac{1}{2} (h_i^* + h_2^*) h_i^{*2} + h_1^* h_2^* h_i^* \right] \\
& + \frac{\partial \mathcal{P}^*}{\partial r^*} \left[- \left(\frac{\partial h_1^*}{\partial r^*} + \frac{\partial h_2^*}{\partial r^*} \right) \frac{h_i^{*2}}{2} \right. \\
& \left. \left. + \left(\frac{\partial h_1^*}{\partial r^*} h_2^* + h_1^* \frac{\partial h_2^*}{\partial r^*} \right) h_i^* \right] \right\} - C(r^*) \quad (5.50)
\end{aligned}$$

and the difference of these two expressions gives

$$\frac{\partial h^*}{\partial t^*} = \left(\frac{h_o}{R_o} \right)^2 \left\{ \frac{1}{12} \left[\frac{\partial^2 \mathcal{P}^*}{\partial r^{*2}} + \frac{1}{r^*} \frac{\partial \mathcal{P}^*}{\partial r^*} \right] h^{*3} + \frac{1}{4} h^{*2} \frac{\partial h^*}{\partial r^*} \frac{\partial \mathcal{P}^*}{\partial r^*} \right\} \quad (5.51)$$

Taking the difference between (5.26) and (5.28), recognizing (5.41) and (5.47), and applying the appropriate expressions for the dimensionless mean curvatures H_i^* ($i = 1, 2$) as well as assumption ii, we see

$$\begin{aligned}
N_{ca}(p^* - p_o^*) + \frac{1}{R_b^*} \\
= N_{ca}(\mathcal{P}^* - \mathcal{P}_o^*) - N_{ca}[\Phi^{(C)*}(h_2^*) - \Phi^{(B)*}(h_2^*)] + \frac{1}{R_b^*} \\
= N_{ca}(\mathcal{P}^* - \mathcal{P}_o^*) + N_{ca}\Phi^{(B)*}(h_2^*) + \frac{1}{R_b^*} \\
= N_{ca}(\mathcal{P}^* - \mathcal{P}_o^*) - \frac{B^*}{h^{*4}} + \frac{1}{R_b^*} \\
= -\frac{1}{2} \frac{h_o}{R_o} \frac{1}{r^*} \frac{\partial}{\partial r^*} \left(r^* \frac{\partial h^*}{\partial r^*} \right) \quad (5.52)
\end{aligned}$$

In writing this, we have used the results of Section D in Chapter III in particular.

We have also taken $\gamma^* = 1$ by assumption xiv, and we have defined

$$B^* \equiv \frac{R_o B}{10\pi\gamma_o h_o^4} \quad (5.53)$$

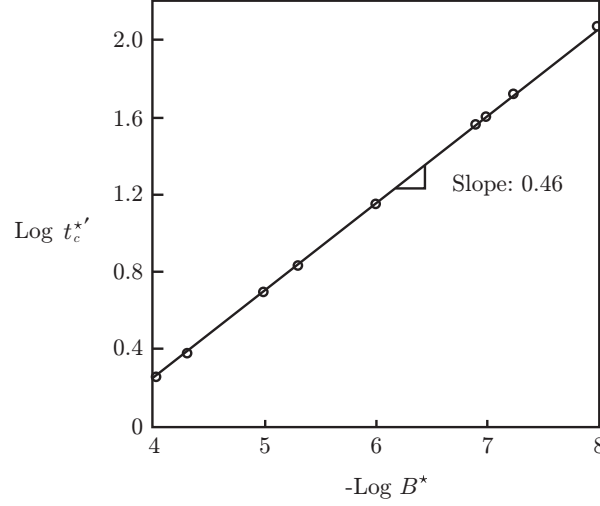


Fig. 24. Dependence of t_c^* on B^*

Where B is defined as a combination of retarded Hamaker constants

$$B \equiv (A^{(ACB)} - A^{(AC)} + A^{(CC)} - A^{(BC)}) \quad (5.54)$$

Inserting (5.52) into (5.51), we discover

$$\begin{aligned} -\frac{\partial h^*}{\partial t^*} = & \frac{1}{3} h^{*3} \left(\frac{1}{r^{*3}} \frac{\partial h^*}{\partial r^*} - \frac{1}{r^{*2}} \frac{\partial^2 h^*}{\partial r^{*2}} + \frac{2}{r^*} \frac{\partial^3 h^*}{\partial r^{*3}} + \frac{\partial^4 h^*}{\partial r^{*4}} \right) \\ & + h^{*2} \frac{\partial h^*}{\partial r^*} \left(-\frac{1}{r^{*2}} \frac{\partial h^*}{\partial r^*} + \frac{1}{r^*} \frac{\partial^2 h^*}{\partial r^{*2}} + \frac{\partial^3 h^*}{\partial r^{*3}} \right) \\ & + \frac{8}{3} B^* \left[\frac{1}{r^*} \frac{1}{h^*} \frac{\partial h^*}{\partial r^*} + \frac{1}{h^*} \frac{\partial^2 h^*}{\partial r^{*2}} - \frac{2}{h^{*3}} \left(\frac{\partial h^*}{\partial r^*} \right)^2 \right] \end{aligned} \quad (5.55)$$

where

$$t^* \equiv \frac{t\mu}{8\rho^{(C)} R_o^2 N_{ca}} \left(\frac{h_o}{R_o} \right)^3 \quad (5.56)$$

Hereafter, we have followed the computation of Hahn et al. (1985) .

Numerical computations give the graphical relationship between dimensionless coalescence time t_c^* and dimensionless Hamaker constant B^* shown in Figure 24.

Alternatively, we can express this relationship as

$$t_c^* = 2.5 \times 10^{-2} B^{*-0.46} \quad (5.57)$$

We recommend that from boundary conditions

$$R_o = \frac{R_f}{1.1} = 1.05 \left(\frac{\Delta \rho g}{\gamma_o} \right)^{1/2} R_b^2 \quad (5.58)$$

The dimensionless mean curvature at $r^* = R_h^*$ was generated in our computation to be 12.58. This together with (5.58) fix the initial film thickness at the center:

$$h_o = 0.175 \frac{\Delta \rho g R_b^3}{\gamma_o} \quad (5.59)$$

In view of (5.56), (5.58), and (5.59), equation (5.57) may be rearranged as

$$t_c = 0.79 \frac{\mu (R_b)^{4.06} (\Delta \rho g)^{0.84}}{\gamma_o^{1.38} B^{0.46}} \quad (5.60)$$

D. Comparison with experimental results

Hexadecane(99%), an alkane hydrocarbon, is obtained from the Sigma-Aldrich, Inc (St. Louis, USA). The density is 0.773 g/cm^3 , viscosity is $3.34 \text{ g/m} \cdot \text{s}$

The air bubble is released from the bottom of the liquid Hexadecane, then the bubble rises up through the liquid and form the thin film while it approaches the liquid-gas interface. We measure the coalescence time at which the film thickness at the rim goes to zero.

For Hexadecane, $\gamma_o = 27.6 \times 10^{-3} \text{ N/m}$. We show the coalescence time for three different radiuses R_b in Table IV.

Computational results from Equation (5.60) are shown in Table V. We have used Equation (5.1) to compute retarded Hamaker constant B . Non-retarded Hamaker constant $A = 0.80 \times 10^{-20}$ is taken from Hough and White (1980). λ is used as an

adjustable parameter. In getting Table V, we choose $\lambda = 9.17 \times 10^{-5}m$.

Table IV.: Experimental results for three different sizes of the bubble.

Radius (mm)	Time (Sec)	Radius (mm)	Time (Sec)	Radius (mm)	Time (Sec)
0.38	4.42	0.50	11.49	0.55	19.05
0.38	4.08	0.50	13.52	0.55	18.98
0.38	4.08	0.50	12.27	0.55	17.75
0.38	4.52	0.50	13.18	0.55	16.07
0.38	3.89	0.50	13.30	0.55	19.37
Average	4.20		12.75		18.24

We have noticed that the computational result is within 10% error range of the average of experimental results.

Table V.: Computational results from Equation (5.60).

Radius = 0.38mm	Coalescence Time = 3.91 Seconds
Radius = 0.50mm	Coalescence Time = 12.56 Seconds
Radius = 0.55mm	Coalescence Time = 18.50 Seconds

E. Discussion

As we understand, this is the first time to use the approach of Görner and Pich (1989) in the computation of retarded dispersion forces and compare with experimental results. While many researchers proclaim that retarded Hamaker constant is never truly constant but decreases progressively as distance increases, we have shown

the agreement with experimental data that a constant could be used for computing retarded forces.

To get a full speculation of retarded dispersion forces with this approach, more experiments are needed. With more experimental data on different materials, we don't have to set up λ as the adjustable parameter.

CHAPTER VI

CONCLUSION

In the context of continuum mechanics, nanoscale problems always involve the immediate neighborhood of a phase interface or the immediate neighborhood of a three-phase line of contact or common line. A general theory extending continuum mechanics to the nanoscale is described in details. The discussion of intermolecular forces correction is based upon a long history of important developments beginning with that of Hamaker (1937).

Four successful applications appeared in this dissertation

1. We analyzed the supercritical adsorption of argon, krypton, and methane on impermeable carbon spheres. Their comparisons with previously reported experimental observations are significantly better than the results of previously reported alternative theories.
2. A variety of static contact angles $\Theta^{(\text{stat})}$ have been predicted with no adjustable parameters. At least for the systems studied and the experimental data reported, (3.87) is superior to previous theories. The results for the contact angle analysis also provide a successful test of a previously derived form of Young's equation for the true, rather than apparent, common line.
3. It is observed that the incorporation of these long-range intermolecular forces removes the square-root stress singularity predicted by linear elastic fracture mechanics. We also provide insight on bridging different methods of modelling crack tip for either one material or bi-material.
4. We included retardation effects in the discussion of intermolecular force corrections and revisited coalescence problem. As we understand, this is the first

time to use the approach of Görner and Pich (1989) in the computation of retarded dispersion forces and compare with experimental results. While many researchers proclaim that retarded Hamaker constant is never truly constant but decreases progressively as distance increases, we have shown the agreement with experimental data that a constant could be used for computing retarded forces.

While we are experiencing the success of this general theory, we also realize its limitations. The idea of including intermolecular forces correction into differential balances is tested successfully. But the improvement of the computation of body force correction and more interactions with other molecular-based theories are needed.

NOTATION

Roman Letters

a	crack length in Figure 19
a_c	area of unit cell on the lattice plane
$A^{(AB)}$	Hamaker constant between phases A and B
$A^{(ACB)}$	Hamaker constant for species A and B interacting across a phase C
A^*	dimensionless Hamaker constant
$\mathbf{b}^{(A,corr)}$	body force per unit volume at a point in phase A . This is introduced to correct for the use of bulk material behavior in the interfacial region
$\mathbf{b}^{(A,corr)\infty}$	body force per unit volume at a point in phase A . This is introduced to correct for the use of constant surface tension on a dividing surface
$B_{(retarded)}$	retarded Hamaker constant
B^*	dimensionless retarded Hamaker constant
$c^{(f)}$	molar density of supercritical fluid, equal to $n^{(f)}/N$
$c^{(f,bulk)}$	molar density of supercritical fluid that would exist in the absence of the crystalline solid
$C^{(AB)}$	London dispersion force coefficient between phases A and B
E	Young's modulus
$\mathbf{f}^{(A,B)}$	force per unit volume of phase A per unit volume of phase B
g	magnitude of acceleration of gravity

h	configuration of the $A - C$ interface
h_0	film thickness at $t = 0$ and $r = 0$
h_1	configuration of the fluid-gas interface
h_2	configuration of the drop-fluid interface
H	mean curvature of a dividing surface
$M^{(C)}$	molecular weight of material C
$n^{(A)}$	number density at the specified point in phase A
$n^{(A,bulk)}$	number density that would exist in phase A , if phase B were not present
n_c	number of atoms in the unit cell on the lattice plane
n_u	number of repeating units in the molecule
N	Avogadro's number
N_{Re}	Renolds number
N_{ca}	capillary number defined by (5.47)
P	thermodynamic pressure
\mathcal{P}	modified pressure defined in (3.49)
\mathbf{P}	projection tensor (Slattery, 1990, p. 1085)
R_b	radius of the drop
R_0	rim radius of the drop at $t = 0$
$R_{(A)}$	region occupied by phase A
\mathbf{S}	extra stress defined in (3.48)
t_c^*	dimensionless coalescence time
t_c	coalescence time at which film ruptures
T_c	critical temperature
$\mathbf{T}^{(I)}$	stress tensor using real description of material behavior

$\mathbf{T}^{(I,bulk)}$	stress tensor using bulk description of material behavior, corrected for intermolecular forces from the adjoining phase
$\mathbf{T}^{(\sigma)}$	surface stress tensor, stress tensor on a dividing surface
$\mathbf{v}^{(I)}$	velocity using real description of material behavior
$\mathbf{v}^{(I,bulk)}$	velocity using bulk description of material behavior, corrected for intermolecular forces from the adjoining phase
$\mathbf{v}^{(\sigma)}$	surface velocity, velocity on a dividing surface

Greek Letters

γ_0	equilibrium interfacial tension
$\gamma^{(AC)}$	surface tension between phases A and C
γ^∞	surface tension (or energy) that corresponds to static, unbounded dividing surfaces
$\Gamma^{(\sigma)}$	surface excess moles per unit area defined by (2.11)
$\delta^{(AB)}$	separation distance between phases A and B
Δ	distance between lattice planes
$\epsilon^{(A,B)}$	well depth for two molecules A and B in (2.3)
Θ_0	contact angle at the true common line
$\Theta^{(stat)}$	static contact angle at the apparent common line
λ	distance measured along the normal to the dividing surface (Chapter III)
λ	London wavelength of the material (Chapter V)
λ, μ	Lamé constant (Chapter IV)
μ	bulk viscosity of the liquid film (Chapter V)
$\xi^{(\alpha)}$	unit normal to the interface pointing into phase α

$\Delta\rho$	density difference between liquid film and the drop
$\rho^{(I)}$	bulk density using real description of material behavior
$\rho^{(I,bulk)}$	bulk density using bulk description of material behavior, corrected for intermolecular forces from the adjoining phase
$\rho^{(\sigma)}$	surface density, density on a dividing surface
σ_0	external stress
$\sigma^{(A,B)}$	collision diameter for two molecules A and B in (2.3)
$\phi^{(AC)}$	Lennard-Jones potential for two molecules A and C separated by a distance
$\Phi^{(A,corr)}$	correction for intermolecular potential at a point in phase A
$\Phi^{(A,corr)\infty}$	correction for intermolecular potential at a point in phase A when the surface tension is introduced to the dividing surface

REFERENCES

- Abraham, F. F., 2001. The atomic dynamic of fracture. *J. Mech. Phys. Solids* 49, 2095–2111.
- Abraham, F. F., Brodbeck, D., Rudge, W. E., Broughton, J. Q., Schneider, D., Land, B., Lifka, D., Gerner, J., Rosenkrantz, M., Skovira, J., Gao, H., 1998. *Ab Initio* dynamics of rapid fracture. *Modelling Simul. Sci. Eng.* 6, 639–670.
- Abraham, F. F., Brodbeck, D., Rudge, W. E., Xu, X., 1997. A molecular dynamics investigation of rapid fracture mechanics. *J. Mech. Phys. Solids* 45 (8), 1595–1619.
- Abraham, F. F., Gao, H., 2000. How fast can cracks propagate? *Phys. Rev. Lett.* 84 (14), 3113–3116.
- Abraham, F. F., Singh, Y., 1978. Comment on “the structure of a hard sphere fluid in contact with a soft repulsive wall”. *J. Chem. Phys.* 68, 4767–4768.
- Adamson, A. W., 1976. *Physical Chemistry of Surfaces*, 3rd Edition. John Wiley, New York.
- Allan, R. S., Charles, G. E., Mason, S. G., 1961. The approach of gas bubbles to a gas/liquid interface. *J. Colloid Sci.* 16, 150–165.
- Aranovich, G. L., Donohue, M. D., 1996. Adsorption of supercritical fluids. *J. Coll. Inter. Sci.* 180, 537–541.
- Ari, N., Eringen, A. C., 1983. Nonlocal stress field at Griffith crack. *Cryst. Latt. Def. Amorph. Mat.* 10, 33–38.

- Aronson, M. P., Princen, H. M., 1975. Destabilization of aqueous films on silica by nonionic surfactant. *J. Coll. Inter. Sci.* 52, 345–355.
- Astala, R., Kaukonen, M., Nieminen, R., Heine, T., 2000. Nanoindentation of silicon surfaces: Molecular-dynamics simulations of atomic force microscopy. *Physical Review B* 61 (4), 2973–2980.
- Baier, R. E., Meyer, A. E., 1992. Surface analysis of fouling-resistant marine coatings. *Biofouling* 6, 165–180.
- Barenblatt, G. I., 1962. The mathematical theory of equilibrium cracks in brittle fracture. *Adv. Appl. Mech.* VII, 55–129.
- Becher, P., 1966. *Emulsions: Theory and Practice*, 2nd Edition. Reinhold, New York.
- Benner Jr., R. E., Scriven, L. E., Davis, H. T., 1982. Structure and stress in the gas-liquid solid contact region. *Faraday Symposium, The Royal Soc. Chem.* 16, 169–190.
- Berry, M. V., 1974. Simple fluids near rigid solids—statistical-mechanics of density and contact angle. *J. Phys. A: Math., Nucl. Gen.* 7, 231–245.
- Bird, R. B., Stewart, W. E., Lightfoot, E. N., 2002. *Transport Phenomena*, 2nd Edition. John Wiley, New York.
- Blake, T. D., 1975. Investigation of equilibrium wetting films of n-alkanes on alpha-alumina. *J. Chem. Soc. Faraday Trans.* 71, 192–208.
- Blake, T. D., Kitchener, J. A., 1972. Stability of aqueous films on hydrophobic methylated silica. *J. Chem. Soc. Faraday Trans.* 68, 1435–1442.

- Blumel, S., Koster, F., Findenegg, G. H., 1982. Physical adsorption of krypton on graphite over a wide density range. *J. Chem. Soc. Faraday Trans. 2* 78, 1753–1764.
- Bowen, W. R., Jenner, F., 1995. The calculation of dispersion forces for engineering applications. *Advances in Colloid and Interface Science* 56, 201–243.
- Bowers, R. C., Zisman, W. A., 1964. Surface properties. In: Baer, E. (Ed.), *Engineering Design for Plastics*. Van Nostrand Reinhold Co., New York, pp. 689–741.
- Buevich, Y. A., Lipkina, E. K., 1978. Disruption of thin liquid-films. *Kolloid Zh.* 40, 167–171.
- Burrill, K. A., Woods, D. R., 1973a. Film shapes for deformable drops at liquid-liquid interfaces. 3. drop rest-times. *J. Coll. Inter. Sci.* 42, 35–51.
- Burrill, K. A., Woods, D. R., 1973b. Film shapes for deformable drops at liquid-liquid interfaces. 2. mechanisms of film drainage. *J. Coll. Inter. Sci.* 42, 15–34.
- Bush, A. W., 1992. *Perturbation Methods for Engineers and Scientists*. CRC Press, Boca Raton, FL.
- Cao, D., Wang, W., Duan, X., 2002. Grand canonical Monte Carlo simulation for determination of optimum parameters for adsorption of supercritical methane in pillared layered pores. *J. Coll. Inter. Sci.* 254, 1–7.
- Casimir, H., Polder, D., 1948. The influence of retardation on the London-van der Waals forces. *Physical Review* 73 (4), 360–372.
- Chappelear, D. C., 1961. Models of a liquid drop approaching an interface. *J. Colloid Sci.* 16, 186–197.

- Charles, G. E., Mason, S. G., 1960. The coalescence of liquid drops with flat liquid/liquid interfaces. *J. Colloid Sci.* 15, 236.
- Chaudhury, M. K., Whitesides, G. M., 1991. Direct measurement of interfacial interactions between semispherical lenses and flat sheets of polydimethylsiloxane and their chemical derivatives. *Langmuir* 7, 1013–1025.
- Chen, J. D., Hahn, P. S., Slattery, J. C., 1984. Coalescence time for a small drop or bubble at a fluid-fluid interface. *AIChE J.* 30, 622–630.
- Chen, J. D., Slattery, J. C., 1982. Effects of London-van der Waals forces on the thinning of a dimpled liquid-film as a small drop or bubble approaches a horizontal solid plane. *AIChE J.* 28, 955–963.
- Costanzo, F., Allen, D. H., 1995. A continuum thermodynamic analysis of cohesive zone models. *International Journal of Engineering Science* 33, 2197–2219.
- Costanzo, F., Walton, J. R., 1997. A study of dynamic crack growth in elastic materials using a cohesive zone model. *International Journal of Engineering Science* 35, 1085–1114.
- Davis, S. S., Smith, A., 1976. Stability of hydrocarbon oil droplets at surfactant-oil interface. *Colloid Polym. Sci.* 254, 82–98.
- Derjaguin, B. V., Dukhin, S. S., Rulyov, N. N., 1984. Kinetic theory of small particles. In: Matijevic, E., Good, R. J. (Eds.), *Surface Colloid Science*. Vol. 13. Plenum Press, New York, pp. 71–144.
- Drummond, C. J., Chan, D. Y. C., 1997. van der Waals interaction, surface free energies, and contact angles: dispersive polymers and liquids. *Langmuir* 13, 3890–3895.

- Dugas, R., 1955. *A History of Mechanics*. Éditions Du Griffon, Neuchatel-Switzerland.
- Dugdale, D. S., 1960. Yielding in steel sheets containing slits. *J. Mech. Phys. Solid* 8, 100–104.
- Dussan V, E. B., 1979. Spreading of liquids on solid-surfaces - static and dynamic contact lines. *Ann. Rev. Fluid Mech.* 11, 371–400.
- Dzyaloshinskii, I. E., Lifshitz, E. M., Pitaevskii, L. P., 1960. van der Waals forces in liquid films. *Soviet Physics JETP* 37, 161–170.
- Dzyaloshinskii, I. E., Lifshitz, E. M., Pitaevskii, L. P., 1961. The general theory of van der Waals forces. *Adv. Phys.* 10, 165–209.
- Egorov, S. A., 2001. Adsorption of supercritical fluids and fluid mixtures: inhomogeneous integral equation study. *J. Phys. Chem. B* 105, 6583–6591.
- Eringen, A. C., 1967. *Mechanics of Continua*. John Wiley & Sons, New York.
- Eringen, A. C., 1972. Linear theory of nonlocal elasticity and dispersion of plane waves. *Int. J. Engng Sci.* 10, 425–435.
- Eringen, A. C., 1981. On the nature of boundary conditions for crack tip stress. *Arch. Mech.* 33 (6), 937–945.
- Eringen, A. C., Speziale, C. G., Kim, B. S., 1977. Crack-tip problem in non-local elasticity. *J. Mech. Phys. Solids* 25, 339–355.
- Evans, L. F., 1954. Bubble-mineral attachment in flotation. *Ind. Eng. Chem.* 46, 2420–2424.

- Findenegg, G. H., Fischer, J., 1975. Adsorption of fluids: Simple theories for the density profile in a fluid near an adsorbing surface. *Faraday Disc. Chem. Soc.* 59, 38–45.
- Fineberg, J., Gross, S. P., Marder, M., Swinney, H. L., 1991. Instability in dynamic fracture. *Phy. Rev. Lett.* 67 (4), 457–460.
- Fischer, J., 1977. Three-dimensional virial expansions in physical adsorption. *Molecular Physics* 34, 1237–1245.
- Fischer, J., 1978. Physical adsorption at high pressures and high temperatures: The density profile of the gas. *J. Chem. Phys.* 68, 3947–3948.
- Fox, H. W., Zisman, W. A., 1950. The spreading of liquids on low energy surfaces. i. polytetrafluoroethylene. *J. Colloid Sci.* 5, 514–531.
- Fu, K., Robinson, R. L., Slattery, J. C., 2004. An analysis of supercritical adsorption in the context of continuum mechanics. *Chemical Engineering Science* 59, 801–808.
- Fuerstenau, D. W., Urbina, R. H., 1987. Flotation fundamentals. In: Somasundaran, P., Moudgil, B. M. (Eds.), *Reagents in Mineral Technology*. Marcel Dekker, New York, pp. 1–38.
- Girifalco, L. A., Good, R. J., 1957. A theory for the estimation of surface and interfacial energies. I. derivation and application to interfacial tension. *J. Phys. Chem.* 61, 904–909.
- Görner, P., Pich, J., 1989. Generalized theory of dispersion forces. *Journal of Aerosol Science* 20 (7), 735–747.
- Griffith, A. A., 1921. The phenomena of rupture and flow in solids. *Phil. Trans. Royal Soc. London A221*, 163–197.

- Gurtin, M. E., 1979. Thermodynamics and cohesive zone in fracture. *Zeitschrift Fur Angewandte Mathematik Und Physik* 30 (6), 991–1003.
- Gusev, V. Y., OBrien, J. A., Seaton, N. A., 1997. A self-consistent method for characterization of activated carbons using supercritical adsorption and grand canonical Monte Carlo simulations. *Langmuir* 13 (10), 2815–2821.
- Hahn, P. S., Chen, J. D., Slattery, J. C., 1985. Effects of London-van der waals forces on the thinning and rupture of a dimpled liquid-film as a small drop or bubble approaches a fluid-fluid interface. *AIChE J.* 31, 2026–2038.
- Hamaker, H. C., 1937. The London-van der Waals attraction between spherical particles. *Physica* 4, 1058–1072.
- Hartland, S., 1969. The profile of the draining film beneath a liquid drop approaching a plane interface. *Chem. Eng. Prog. Symp. Ser.* 65 (91), 82–89.
- Hartland, S., Robinson, J. D., 1977. Model for an axisymmetric dimpled draining film. *J. Coll. Inter. Sci.* 60, 72–81.
- Hein, P., 1914. Untersuchungen über den kritischen Zustand. *Z. Phys. Chem. (Munich)* 86, 385–410.
- Hirschfelder, J. O., Curtiss, C., Bird, R. B., 1954. *Molecular Theory of Gases and Liquids*. Wiley, New York, corrected with notes added 1964.
- Holland, D., Marder, M. P., 1998. Ideal brittle fracture of silicon studied with molecular dynamics. *Phys. Rev. Lett.* 80 (4), 746–749.
- Hough, D. B., White, L. R., 1980. The calculation of Hamaker constants from Lifshitz theory with applications to wetting phenomena. *Adv. Colloid Interface Sci.* 14, 3–41.

- Hui, C. Y., Lagoudas, D. C., Ruina, A., 1987. Constitutive modeling for nontraditional materials. In: Stokes, V. K., Krajcinovic, D. (Eds.), *Constitutive models for crazes and their effects on crack growth in glassy polymers*. Vol. 85. ASME, pp. 87–115.
- Irwin, G. R., 1958. *Handbuch der Physik*. Vol. VI. Springer-Verlag, Berlin.
- Irwin, G. R., 1961. Plastic zone near a crack and fracture toughness. *Sagamore Research Conference Proceedings* 4, 1605–1619.
- Israelachvili, J. N., 1973. van der Waals dispersion force contribution to works of adhesion and contact angles on basis of macroscopic theory. *J. Chem. Soc. Faraday Trans. II* 69, 1729–1738.
- Israelachvili, J. N., 1991. *Intermolecular and Surface Forces*, 2nd Edition. Academic Press, New York.
- Ivanov, I. B., Radoev, B., Manev, E., A. Sheludko, 1970. Theory of critical thickness of rupture of thin liquid films. *Trans. Faraday Soc.* 66, 1262–1280.
- Jain, R. K., Ivanov, I. B., 1980. Thinning and rupture of ring-shaped films. *J. Chem. Soc. Faraday Trans.* 76, 250–266.
- Jain, R. K., Ruckenstein, E., 1976. Stability of stagnant viscous films on a solid-surface. *J. Coll. Inter. Sci.* 54, 108–116.
- Jameson, G. J., del Cerro, M. C. G., 1976. Theory for equilibrium contact-angle between a gas, a liquid and a solid. *J. Chem. Faraday Trans.* 72, 883–895.
- Jasper, J. J., Kring, E. V., 1955. Thermodynamic properties of surfaces of a n-alkane series. *J. Phys. Chem.* 59, 1019–1021.

- Joanny, J. F., deGennes, P. G., 1984. A model for contact-angle hysteresis. *J. Chem. Phys.* 81, 552–562.
- Joanny, J. F., deGennes, P. G., 1986. Role of long-range forces in heterogeneous nucleation. *J. Coll. Inter. Sci.* 111, 94–101.
- Kevorkian, J., Cole, J. D., 1981. *Perturbation Methods in Applied Mathematics.* Springer-Verlag, New York.
- Kitamura, Y., Ohta, T., Takahashi, T., 1988. Coalescence of drops at oil-surfactant-aqueous alcohol solution interface(in Japanese). *Sekiyu Gakkaishi* 31, 244–249.
- Knauss, W. G., 1993. Time dependent fracture and cohesive zones. *Journal of Engineering Materials and Technology* 115, 262–267.
- Laskowski, J., Kitchener, J. A., 1969. Hydrophilic-hydrophobic transition on silica. *J. Coll. Inter. Sci.* 29, 670.
- Lee, G. W. J., Tadros, T. F., 1982. Formation and stability of emulsions reduced by dilution of emulsifiable concentrates.1. an investigation of the dispersion on dilution of emulsifiable concentrates containing cationic and non-ionic surfactants. *Colloids Surfaces* 5, 105–115.
- Lennard-Jones, J., Dent, B. M., 1928. Cohesion at a crystal surface. *Transactions of the Faraday Society* 24, 92–108.
- Li, D., Slattery, J. C., 1991. Analysis of the moving apparent common line and dynamic contact angle formed by a draining film. *J. Colloid Interface Sci.* 143(2), 382–396.
- Liem, A. J. S., Woods, D. R., 1974. Application of parallel disk model for uneven film thinning. *Can. J. Chem. Eng.* 52, 222–227.

- Lifshitz, E. M., 1956. The theory of molecular attractive forces between solids. Soviet Physics, JETP (Engl. Transl.) 2, 73.
- Lin, C. Y., Slattery, J. C., 1982a. Thinning of a liquid film as a small drop or bubble approaches a fluid-fluid interface. AICHE J. 28, 786–792.
- Lin, C. Y., Slattery, J. C., 1982b. Thinning of a liquid film as a small drop or bubble approaches a solid plane. AICHE J. 28, 147–156.
- Love, A. E. H., 1944. A Treatise on the Mathematical Theory of Elasticity, 4th Edition. Dover, New York.
- Lozano-Castelló, D., Cazorla-Amorós, D., Linares-Solano, A. Quinn, D. F., 2002. Micropore size distributions of activated carbons and carbon molecular sieves assessed by high-pressure methane and carbon dioxide adsorption isotherms. J. Phys. Chem. B 106, 9372–9379.
- Maass, O., 1938. Changes in the liquid state in the critical temperature region. Chem. Rev. 23, 17–28.
- MacKay, G. D. M., Mason, S. G., 1963. The gravity approach and coalescence of fluid drops at liquid interfaces. Can. J. Chem. Eng. 41, 203–212.
- Mahanty, J., Ninham, B. W., 1976. Dispersion Forces. Academic Press, New York.
- Marder, M., Gross, S., 1995. Origin of crack tip instabilities. J. Mech. Phys. Solids 43 (1), 1–48.
- Martynov, G. A., Starov, V. M., Churaev, N. V., 1977. Hysteresis of contact-angle at homogeneous surfaces. Colloid J. USSR 39, 406–417.

- McIntosh, R. L., Dacey, J. R., Maass, O., 1939. Pressure, volume, temperature relations of ethylene in the critical region. II. *Can. J. Res., Sect. B* 17, 241–250.
- Michels, A., Wijker, H., Wijker, H., 1949. Isotherms of argon between 0°C and 150°C and pressures up to 2900 atmospheres. *Physica* 7, 627–633.
- Miller, C. A., Ruckenstein, E., 1974. Origin of flow during wetting of solids. *J. Coll. Inter. Sci.* 48, 368–373.
- Miller, R., Shenoy, V., 2000. Size-dependent elastic properties of nanosized structural elements. *Nanotechnology* 11 (3), 139–147.
- Miyawaki, J., Kanda, T., Suzuki, T., Okui, T., Maeda, Y., Kaneko, K., 1998. Macroscopic evidence of enhanced formation of methane nanohydrates in hydrophobic nanospaces. *J. Phys. Chem. B* 102, 2187–2192.
- Murata, K., Kaneko, K., 2001. The general equation of supercritical gas adsorption isotherm. *J. Phys. Chem. B* 105, 8498–8503.
- Neimark, A. V., Ravikovitch, P. I., 1997. Calibration of pore volume in adsorption experiments and theoretical models. *Langmuir* 13 (19), 5148–5160.
- Oh, E.-S., Slattery, J. C., Walton, J. R., 2005. A theory of fracture based upon an extension of continuum mechanics to the nanoscale. Submitted to *Journal of Applied Mechanics*.
- Ohkubo, T., Miyawaki, J., Kaneko, K., Ryoo, R., Seaton, N. A., 2002. Adsorption properties of templated mesoporous carbon (CMK-1) for nitrogen and supercritical methane— experiment and GCMC simulation. *J. Phys. Chem. B* 106, 6523–6528.

- Ono, S., Kondo, S., 1960. Molecular theory of surface tension in liquids. In: Flugge, S. (Ed.), *Encyclopedia of Physics, Structure of Liquids*. Vol. 10. Springer-Verlag, Berlin, p. 134.
- Owens, D. K., Wendt, R. C., 1969. Estimation of the surface free energy of polymers. *Journal of Applied Polymer Science* 13, 1741–1747.
- Padday, J. F., Uffindell, N. D., 1968. Calculation of cohesive and adhesive energies from intermolecular forces at a surface. *J. Phys. Chem.* 72, 1407–1414.
- Pethica, J., Hutchings, R., Oliver, W., 1983. Hardness measurement at penetration depths as small as 20 nm. *Phil. Mag. A* 48 (4), 593–606.
- Platikanov, D., 1964. Experimental investigation on the 'dimpling' of thin liquid films. *J. Phys. Chem.* 68, 3619–3624.
- Rangarajan, B., Lira, C. T., Subramanian, R., 1995. Simplified local density model for adsorption over large pressure ranges. *AIChE J.* 41, 838–845.
- Rayleigh, L., 1890. On the theory of surface forces. *Phil. Mag.* 30, 285–298.
- Roco, M. C., Williams, R. S., Alivisatos, P., 2000. *Nanotechnology Research Directions*. Kluwer Academic Publishers, Boston.
- Rowlinson, J. S., 2002. *Cohesion: A Scientific History of Intermolecular Forces*. Cambridge University Press, Cambridge.
- Ruckenstein, E., Jain, R. K., 1974. Spontaneous rupture of thin liquid-films. *J. Chem. Soc. Faraday Trans.* 70, 132–147.
- Russel, W. B., Saville, D. A., Schowalter, W. R., 1989. *Colloidal Dispersions*. Cambridge University Press, Cambridge.

- Salvetat, J., Briggs, G., Bonard, J., Bacsá, R., Kulik, A., Stockli, T., Burnham, N., Forro, L., 1999. Elastic and shear moduli of single-walled carbon nanotube ropes. *Physical Review Letters* 82 (5), 944–947.
- Saville, G., 1978. Computer simulation of liquid-solid-vapor contact-angle. *J. Chem. Soc. Faraday Trans.* 73, 1122–1132.
- Schapery, R. A., 1975. A theory of crack initiation and growth in viscoelastic media. I. theoretical development. *International Journal of Fracture* 11, 141–159.
- Schulze, H. J., 1975. Rupture of thin liquid-films on solid-surfaces. *Colloid Polym. Sci.* 253, 730–737.
- Slattery, J. C., 1990. *Interfacial Transport Phenomena*. Springer-Verlag, New York.
- Slattery, J. C., 1999. *Advanced Transport Phenomena*. Cambridge University Press, Cambridge.
- Slattery, J. C., Oh, E.-S., Fu, K., 2004. Extension of continuum mechanics to the nanoscale. *Chem. Eng. Sci.* 59, 4621–4635.
- Slepyan, L. I., Ayzenberg-Stepanenko, M. V., Dempsey, J. P., 1999. A lattice model for viscoelastic fracture. *Mech. Time-Dep. Mater.* 3, 159–203.
- Smith, G., Tadmor, E., Bernstein, N., Kaxiras, E., 2001. Multiscale simulations of silicon nanoindentation. *Acta Materialia* 49 (19), 4089–4101.
- Sokolowski, S., 1982. Quantitative description of the adsorption of gases on graphite at high temperatures. *J. Chem. Soc. Faraday Trans.* 2 78, 255–264.
- Sonntag, H., Strenge, K., 1972. *Coagulation and Stability of Disperse Systems*. Halsted Press, New York.

- Soutas-Little, R. W., 1973. *Elasticity*. Dover Publications, Mineola, New York.
- Specovius, J., Findenegg, G. H., 1978. Physical adsorption of gases at high pressures: Argon and methane onto graphitized carbon black. *Ber. Bunsenges. Phys. Chem.* 82, 174–180.
- Steele, W. A., 1973. The physical interaction of gases with crystalline solids. *Surf. Sci.* 36, 317–352.
- Steele, W. A., 1974. *The Interaction of Gases with Solid Surfaces*. Pergamon Press, New York.
- Steele, W. A., 1978. The interaction of rare gas atoms with graphitized carbon black. *J. Phys. Chem.* 82, 817–821.
- Swadener, J. G., Baskes, M. I., Nastasi, M., 2002. Molecular dynamics simulation of brittle fracture in silicon. *Phys. Rev. Lett.* 89 (8).
- Tan, Z., Gubbins, K. E., 1990. Adsorption in carbon micropores at supercritical temperatures. *J. Phys. Chem.* 94, 6061–6069.
- Timoshenko, S. P., 1953. *History of Strength of Materials*. McGraw-Hill, New York.
- Trappeniers, N. J., Wassenaar, T., Abels, J. C., 1979. Isotherms and thermodynamic properties of methane at temperatures between 0°C and 150°C and at densities up to 570 amagat. *Physica* 98A, 289–297.
- Trappeniers, N. J., Wassenaar, T., Abels, J. C., 1980. Erratum isotherms and thermodynamic properties of methane at temperatures between 0°C and 150°C and at densities up to 570 amagat. *Physica* 100A, 660.

- Trappeniers, N. J., Wassenaar, T., Wolkers, G. J., 1966. Isotherms and thermodynamic properties of krypton at temperatures between 0°C and 150°C and at densities up to 620 amagat. *Physica* 32, 1503–1520.
- Truesdell, C., 1966. *The Elements of Continuum Mechanics*. Springer-Verlag, New York.
- Truesdell, C., 1968. *Essays in the History of Mechanics*. Springer-Verlag, New York.
- Truesdell, C., Noll, W., 1965. The non-linear field theories of mechanics. In: Flügge, S. (Ed.), *Handbuch der Physik*, vol. 3/3. Springer-Verlag, Berlin, pp. 1–579.
- Truesdell, C., Toupin, R. A., 1960. The classical field theories. In: Flügge, S. (Ed.), *Handbuch der Physik*, vol. 3/1. Springer-Verlag, Berlin, pp. 226–793.
- Vrij, A., 1966. Possible mechanism for spontaneous rupture of thin free liquid films. *Discuss. Faraday Soc.* 42, 23–33.
- Wayner, P. C., 1980. Interfacial profile in the contact line region of a finite contact-angle system. *J. Coll. Inter. Sci.* 77, 495–500.
- Wayner, P. C., 1982. The interfacial profile in the contact line region and Young-Dupre equation. *J. Coll. Inter. Sci.* 88, 294–295.
- Westergaard, H. M., 1939. Bearing pressures and cracks. *J. Appl. Mech.* 6, A.49–A.53.
- Williams, M. B., Davis, S. H., 1982. Non-linear theory of film rupture. *J. Coll. Inter. Sci.* 90, 220–228.
- Williams, M. L., 1957. On the stress distribution at the base of a stationary crack. *J. App. Mech.* 24, 109–114.

- Winkler, C. A., Maass, O., 1933. Density discontinuities at the critical temperature. *Can. J. Phys.* 9, 613–629.
- Woods, D. R., Burrill, K. A., 1972. Stability of emulsions. *J. Electroanal. Chem.* 37, 191–213.
- Young, T., 1805. An essay on the cohesion of fluids. *Philos. Trans. R. Soc. London* 95, 65–87.
- Zhou, L., Zhou, Y., Li, M., Chen, P., Wang, Y., 2000. Experimental and modeling study of the adsorption of supercritical methane on a high surface activated carbon. *Langmuir* 16, 5955–5959.
- Zimon, A. D., 1982. *Adhesion of Dust and Powder*, 2nd Edition. Consultants Bureau, New York.
- Zisman, W. A., 1962. Constitutional effects on adhesion and abhesion. In: Weiss, P. (Ed.), *Adhesion and Cohesion: Proceedings of the symposium on adhesion and cohesion*. Elsevier, Amsterdam, pp. 176–208.
- Zisman, W. A., 1964. Contact angle, wettability, and adhesion. No. 43 in *Advances in Chemistry Services*. American Chemical Society, Washington DC.

VITA

Personal Data

- Citizenship: China
- Date of Birth: July 23, 1977
- Family: Wife–Jihong, Children–David(09/2003), Daniel(02/2005)

Contact Information

- Tel: (979)739-1102
- Email: kaibinfu@gmail.com
- Permanent Address: People's South St. BL.4 # 13 Chengdu, Sichuan
610041 P.R. China

Education

- **B.A.** in Scientific Editing, Tsinghua University, Beijing, China 1999
- **B.En.** in Engineering Mechanics, Tsinghua University, Beijing, China
1998

Publications

- **K. Fu**, R. L. Robinson, J. C. Slattery 2004, "An analysis of supercritical adsorption in the context of continuum mechanics" *Chemical Engineering Science*, 59(4), 801-808
- J. C. Slattery, E-S. Oh, **K. Fu** 2004, "Extension of continuum mechanics to the nanoscale" *Chemical Engineering Science*, 59(21), 4621-4635